NONLINEAR SIGNAL PROCESSING TECHNIQUES FOR UWB IMPULSE RADIOS

by

Aidong Yang

Submitted in partial fulfillment of the requirements for
the degree of Doctor of Philosophy

at

Dalhousie University
Halifax, Nova Scotia
August, 2017

TABLE OF CONTENTS

LIST OF FIGURES

ABSTRACT

Impulse Radio (IR) Ultra-wideband (UWB) communication is an attractive potential technology for low-power, low-complexity, and high-speed communications in short range links. One of the main challenges it faces is the highly frequency-selective multipath channel, which generates hundreds of overlapped copies of the transmitted pulse with different delays and amplitudes. In collecting the energy of these multipath components, conventional Rake receivers suffer from high implementation and computational costs due to channel estimation. To circumvent the problem, several non-coherent receivers, energy detection (ED) based receivers, are proposed; however, they come at the cost of degraded performance when narrowband interferences (NBIs) are present.

In this dissertation, we present low-complexity, high-performance, non-coherent receiver designs that *i*) avoid the expensive channel estimation; *ii*) lower the hardware implement complexity with the use of nonlinear signal processing techniques; and *iii*) improve the error performance by considering practical imperfections.

Firstly, we propose a Kurtosis Detection (KD) operator to replace the square operator in conventional ED; without high sampling rates, the KD based receiver achieves better performances.

Secondly, we propose another nonlinear signal processing technique, variance detection (VD), to mitigate NBI effect on the ED-based IR-UWB systems. The lognormal distribution model is introduced and used for derivation of the analytical BER of the VD-based receiver.

Thirdly, we propose a unified framework, generalized nonlinear detection (GND), to generalize existing nonlinear detection technologies and further optimize the performances. Our results show that the GND-based receivers have better system performance and stronger ability to resist NBIs than the existing nonlinear detection algorithms.

Finally, a blind NBI mitigation technique with a square law (SL) device is presented to mitigate the NBI effects. Our results show that the SL technique can significantly improve the signal-to-interference ratio of the received UWB signal without any prior knowledge of the NBI, and can be implemented in hardware easily; therefore, the proposed SL technique is an implementable and highly effective blind NBI mitigation technique for ED-based IR-UWB systems.

LIST OF ABBREVIATIONS

BER	Bit Error Rate
UWB	Ultra-wideband
IR	Impulse Radio
NBI	Narrowband Interference
AWGN	Additive White Gaussian Noise
FCC	Federal Communications Commission
PPM	Pulse Position Modulation
MPCs	Multipath Components
FSR	Frequency-shifted Reference
CSR	Code-shifted Reference
DCSR	Differential Code-shifted Reference
FD	Fourth-order Detection
TKO	Teager-Kaiser operator
SL	Square Law
BPF	Band Pass Filter
PDF	Probability Density Function
IFI	Inter-Frame-Interference
IPI	Inter-Symbol-Interference
β	*S*ystem Parameter of the Generalized Nonlinear Detector
Γ	Channel Parameter of the Multipath Effects
Ψ	Square Law Operator
ξ	Zero-mean Independent Normal Random Variables
ω	Gaussian Noise and Interference

ACKNOWLEDGEMENTS

I would like to express my appreciation to my supervisor Dr. Zhizhang (David) Chen and co-supervisor Dr. Hong Nie, who brought me into the fascinating ultra-wideband communication fields and guide me with their continuous patience in my research. This thesis would not have been completed without their expert advice and unfailing patience. I do really appreciate for their guidance and support for my PhD study.

I would express my special appreciation to Dr. Zhimeng Xu, who gave valuable comments and suggestions for my thesis. Without his patient guidance, I cannot finish this thesis. I also wish to thank the rest of my thesis committee: Dr. Jacek Ilow and Dr. William Philips, for their useful suggestions and comments for this thesis.

I would also extend to thank my colleagues, Dr. Wei Fan, Wan Peng, Jiacheng Guo, Dr. Colin O' Flynn, Dr. Farid Jolani, and other group members for their kind help during my Ph. D study.

Finally, I am grateful to my friends in Halifax, for your help, understanding and encouragement during my stay in Halifax. I cannot list all your names here, but you are all in my mind.

CHAPTER 1 INTRODUCTION

This thesis mainly focuses on investigation of the properties of the Impulse Radio Ultra-wideband (IR-UWB) nonlinear signal processing technologies and improvement the Bit-Error-Rate (BER) performance of conventional Energy Detection (ED) based IR-UWB systems. This chapter introduces the research background of the thesis, and then reviews the state-of-art IR-UWB nonlinear signal processing technologies. Research objectives, contributions, and organization of this thesis are also presented.

1.1 MOTIVATIONS

IR-UWB communications use a very large bandwidth to transmit signals at a very low power spectral density. According to the definition from the Federal Communications Commission (FCC) in the United States, the bandwidth of a UWB communication occupies at least 500 MHz or a fractional bandwidth exceeding 20% [1]. The huge signaling bandwidth reveals several attractive features of UWB communications, including the potential high-data-rate communications, the fine resolution ranging, and the possibility of low-complexity devices. Due to these merits, UWB communications have wide interest as an enabling technique that provides low-power and low-complexity UWB transmissions in a huge unlicensed band [2]. For example, IEEE Standard 802.15.4a-2007 [3] has regulated UWB communications with maximum 27.24 Mbps transmission within 10 meters in a single UWB channel, and IEEE Standard 802.15.4g-2012 [4] makes it an ideal candidate for low cost, low power consumption and low data rate applications in wireless body area networks.

By transmitting ultra-short pulses at a very low-power spectral density, the IR-UWB is one of the most popular signals in UWB communications. However, transmitting short duration pulses introduces a challenge in the receiver design. In a multipath environment, received IR UWB signals may consist of a large amount of resolvable multipath components (MPCs) that need to be tracked and estimated [1]. Using the well-known Rake receiver [5] to process those MPCs often leads to an unacceptably high system complexity.

To address the issue and to capture signal energy from more MPCs with low system complexity, in recent years, a group of energy detection based transceiver technologies have been proposed. These include an on-off keying transceiver [6], pulse position modulation (PPM) ED transceiver [7] frequency-shifted reference (FSR) transceiver [8], code-shifted reference (CSR) transceiver [9], and differential CSR (DCSR) transceiver [10]. Unlike the Rake receiver that detects specific waveforms from the received IR UWB signals, the ED based receivers detect energy from the received IR-UWB signals. Hence, they do not need to track and estimate MPCs.

However, the ED based receivers cannot distinguish noise and interferences from the desired IR-UWB signals. Energy of noise and interferences is also collected and considered as signal energy. Consequently, compared with the Rake receiver, the ED based receivers are more vulnerable to noise and interferences [11] [12]. Meanwhile, due to the wide bandwidth of IR-UWB systems, the received IR-UWB signals are typically corrupted by wideband Additive White Gaussian Noise (AWGN) or strong narrowband interferences (NBIs). Therefore, advanced signal processing technologies must be applied in conjunction with the ED based receivers to mitigate destructive effects of AWGN and NBIs.

Most present signal processing technologies proposed for IR-UWB receivers, such as digital interference cancelation techniques [13] and analog notch filter bank [14], are straightforward derivatives of those developed for narrowband wireless transceivers. Those

technologies neither take advantages of the wideband feature of IR-UWB signals nor have low complexity that comes with potential uses of carrier-less UWB impulses. Thus, the present UWB signal processing technologies can hardly be employed in the ED based receivers with low complexity and low power consumption.

To overcome this problem, non-traditional signal processing technologies, which can fully utilize the special characteristics of IR-UWB signals, need to be explored. To this end, nonlinear signal processing technologies have emerged as promising techniques.

To the best of our knowledge, the initial attempt to employ a nonlinear signal processing technology in ED based IR-UWB receivers was proposed in [15], where two nonlinear devices, called Fourth-order detection (FD) and kurtosis detector (KD), are used to replace the second-order operator in conventional ED with the forth-order operator. The simulation results in [15] show the FD and KD based receivers have a superior BER performance than that of the conventional ED-based receivers. This feature makes the FD or KD technology well suitable for processing IR-UWB signals. Although the FD and the KD based receivers do not require explicit channel estimation and enable simple receiver structures, they exhibit considerable error performance degradation when NBIs present in the received IR-UWB signals.

To achieve dynamic NBI mitigation with a low system complexity, we propose the use of another nonlinear signal processing technique, variance detector (VD) [16] to improve the system performance of IR-UWB receivers. The effects of NBI on the performance of the proposed VD-based receivers are assessed through computer simulations. The simulation results validate that VD receiver has an inherent robustness to NBI existing in IR-UWB signals. Furthermore, the proposed VD receiver does not require high sampling rates and there is only a slight increase in receiver complexity as compared to conventional ED-based receivers. Therefore, the VD-based receiver is another preferred nonlinear

detection technology for IR-UWB systems. However, because of the difficulties in analyzing stochastic processes involving nonlinearity, no systematical approaches have been developed to characterize the NBI mitigation performance of the VD based detection technology [16].

Other attempts to employ a nonlinear signal processing technology in ED based IR-UWB receivers have also been proposed in recent years, such as Teager-Kaiser operator (TKO) [17], Square Law (SL) technology [18]. As shown in [17] and [18], when a signal with a frequency band between f_1 and f_2 is sent into a TKO or SL, the frequency band of the output signal falls in between DC and $f_2 - f_1$. A NBI is then shifted to a frequency band close to DC and hence can be removed easily with a high pass filter (HPF) in TKO or band pass filter (BPF) in SL. Further work has been carried out to identify the limitations of the TKO or SL technology and improve its performance [19] [20].

In all, motivated by the observations above, we see that presently most signal processing technologies employed in impulse radio UWB transceivers are straightforward derivatives of those designed for conventional wireless narrowband transceivers. They appear not to take full advantage of some special features offered by the impulse radio UWB transceivers, such as ultra-wide bandwidth and very short duration pulses. To move beyond this shortcoming, in this thesis, nonlinear signal processing technologies, in particular, the Kurtosis detector, TK operator, the SL operator and variance detector, are employed and studied. It is found that nonlinear signal processing technologies can mitigate destructive effects caused by both narrowband interferences and wideband noises and hence can significantly improve the BER performance. In other words, the use of nonlinear signal processing technologies is a ground-breaking innovation and presents a potentially new horizon for research and development of UWB systems. This thesis is

intended to move along this direction and is expected to make original contributions in the area.

1.2 OBJECTIVES

The goal of this thesis is to solve the above-mentioned problems present in the conventional energy detection based impulse radio UWB systems. More specifically, the objectives are given as follows:

a) Avoid the stringent channel estimation by exploiting non-coherent detection;
b) Maintain the simple hardware structure of the non-coherent receivers;
c) Lower the computational and hardware complexity of the existing detectors by employing nonlinear signal processing techniques; and
d) Improve the error performance of the non-coherent receivers by taking account of practical imperfections, e.g., channel multipath effects, and narrowband interference.

1.3 ORGANIZATION

The rest of the dissertation is organized as follows:

Chapter 2 gives a brief introduction to UWB communications and presents the existing UWB receiver designs and their complexity-performance trade-offs.

Chapter 3 proposes a kurtosis detector with low complexity and a better performance.

Chapter 4 shows another new nonlinear detector, variance detector, and develops a log-normal stochastic model to analyze its BER performance with and without NBIs.

Chapter 5 develops a unified framework, denoted as generalized nonlinear detection, to encompass existing nonlinear detection technologies as well as further optimize the performance of nonlinear detection for IR-UWB receivers.

Chapter 6 studies a square-law based energy detector for impulse radio UWB systems to improve the IR-UWB system performance and NBI mitigation ability.

Chapter 7 concludes the dissertation and proposes some future research topics.

CHAPTER 2 BACKGROUND

The background information of UWB communications and the existing work on UWB receiver designs are presented in this chapter. Specifically, the Section 2.1 describes the main characteristics of UWB communications, which have great impacts on UWB receiver designs. A brief literature reviews of the existing receiver designs and their complexity-performance trade-off is given in Section 2.2 and Section 2.3.

2.1 OVERVIEW OF UWB COMMUNICATIONS

IR-UWB has emerged as a strong candidate solution for low power and low complexity applications, such as the IEEE 802.15.4a and IEEE 802.15.6 standard wireless personal area networks [3] [4]. This rather new technology is assigned the frequency band of 3.1 GHz to 10.6 GHz by the FCC, where it is permitted to coexist with the other wireless communication systems without requiring a license. However, as a result of the very large bandwidth of UWB communications, the spectrum of UWB systems inevitably overlays those of the existing narrowband or wideband signals, e.g., GSM, GPS, and WiFi, resulting in interference. To avoid the mutual interference with the existing signals, the transmission power of UWB communications has to be limited at a very low level (usually at the noise floor). As shown in Fig. 1, the FCC spectral mask for indoor UWB commercial systems, which allows the operation of UWB systems over an up to 7.5 GHz bandwidth, is limited less than the noise floor (-40 dBm/MHz).

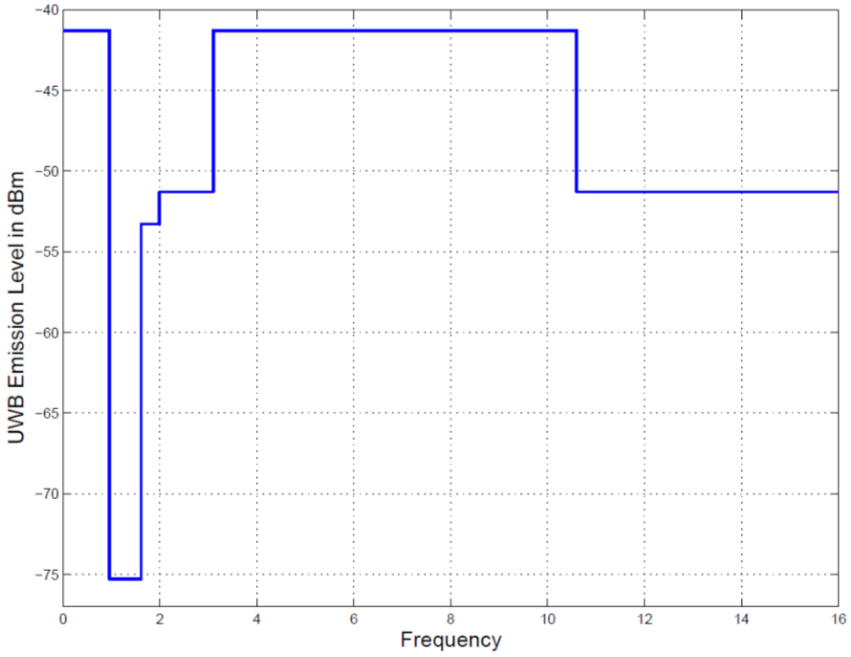

Figure 1 The FCC spectral mask for indoor UWB communications

To exploit the large bandwidth of UWB communications with a low complexity, IR-UWB transmits the users' information with low-power ultra-short pulses. Since the transmitted pulses are low power, each information symbol is conveyed over N_f pulses such that the receiver can collect enough energy. Each pulse is transmitted within a frame with duration $T_f \gg T_P$. A pulse position modulation (PPM) is applied for each pulse in each frame to carry the information of the desired symbol. For a binary IR-UWB transmission with a sequence of information symbols $d_j \in \{0,1\}$, the transmitted signal is

$$s(t) = \sqrt{E_s} \sum_{i=-\infty}^{\infty} \sum_{j=0}^{N_f-1} p(t - iT_s - jT_f - d_j\delta) \tag{2.1}$$

where $p(t)$ is an energy normalized UWB pulse with a duration of T_p, a center frequency f_c and a bandwidth BW. E_s is the transmitted energy per frame. The starting time of the j^{th} transmitted pulse is either at jT_f where $d_j = 0$ or $jT_f + \delta$ where $d_j = 1$, and each symbol

duration, T_s, N_f pulses are transmitted so $T_s = N_f T_f$. For the sake of simplification, in this thesis, we make $N_f = 1$. Furthermore, to eliminate inter-frame-interference (IFI) and to maintain the orthogonality of the received symbols, the frame duration is chosen such that $T_f > \delta + T_p + T_m$, where δ is the PPM time offset and T_m is the maximum excess delay of the channel.

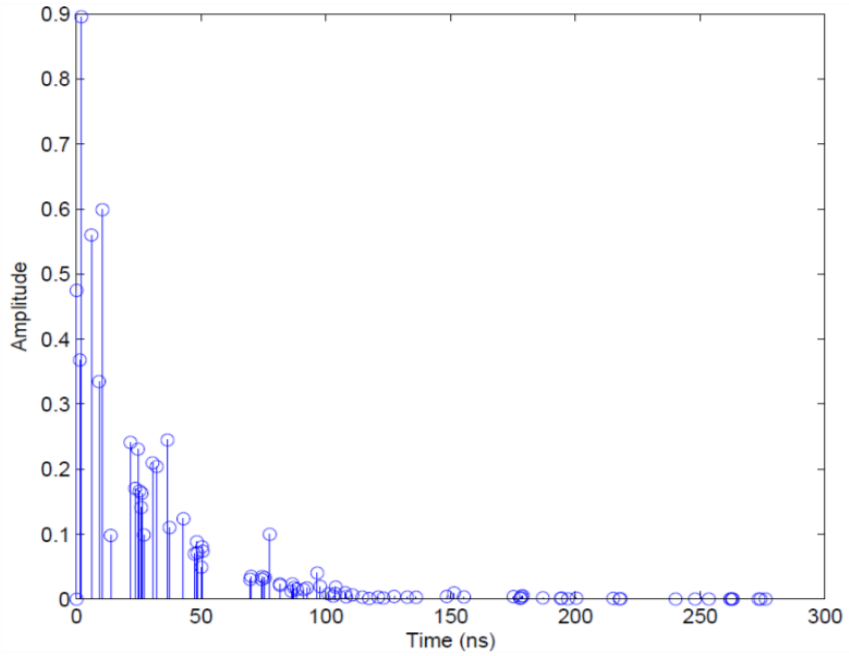

Figure 2 A realization of the channel impulse response of the IEEE802.15.4a CM1 channel model

After the signal is transmitted, the receiver will obtain the signal that is mainly distorted by two effects: *i*) the high frequency-selective UWB fading channel; and *ii*) the AWGN. Because of the large bandwidth of the transmitted pulse, the UWB channel is high frequency selective, where the receiver can observe hundreds of overlapped copies of the transmitted pulse with different delays and amplitudes. The delays and amplitudes of these

MPCs can be well characterized by the well-known Saleh-Valenzuela (S-V) channel model in which the channel impulse response is modeled as

$$h(t) = \sum_{l=0}^{L} \alpha_l \delta(t - \tau_l), \tag{2.2}$$

where L is the total number of multipath components, and $\delta(t)$ is a Dirac Delta function. Each multipath component is with gain α_l and delay τ_l. Fig. 2 depicts a realization of the IEEE802.15.4a channel impulse response [3] based on the S-V channel model. From Fig. 2, we observe hundreds of MPCs and that the maximum excess delay T_m can be up to 300ns.

2.2 EXISTING RECEIVER DESIGNS

This section gives a brief overview of the existing UWB receiver designs and their complexity-performance trade-offs. We use the transmission model in Eq. (2.1), the channel model in Eq. (2.2), and the corresponding received signal model as

$$\begin{aligned} r(t) &= [s(t) * h(t) + n(t) + i(t)] * h_f(t) \\ &= \sum_{i=-\infty}^{\infty} \sum_{j=0}^{N_f - 1} q\left(t - iT_s - jT_f - d_j \delta\right) + \omega(t), \end{aligned} \tag{2.3}$$

where $h_f(t)$ is an ideal band-pass filter with bandwidth BW at radio frequency front in the receiver, $q(t) = \sqrt{E_s}\, p(t) * h(t) * h_f(t)$ is the received UWB pulse, and $n(t)$ and $i(t)$ stand for the AWGN with zero mean and two-sided power spectral density (PSD) $N_0/2$, and interferences passing through the BPF, respectively. Note that $\omega(t) = [n(t) + i(t)] * h_f(t)$ is the sum of noises and interference; when no interferences are present, $\omega(t) = n(t) * h_f(t)$.

2.2.1 Coherent Receiver

After passing through the multipath channel, as shown in Fig. 3, the received IR UWB signals may consist of a large amount of resolvable MPCs, which makes the receiver design suffer a challenge due to the completed channel impulse response that needs to be tracked and estimated.

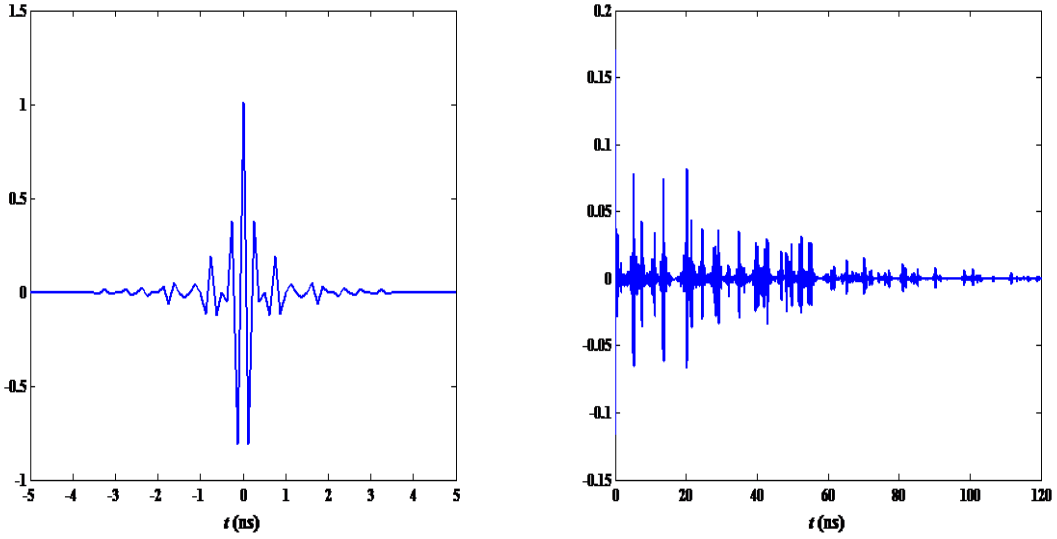

(a) The transmitted IR-UWB pulse (b) The received IR-UWB pulse

Figure 3 The received impulse radio UWB signals consisting of many multipath components.

The well-known Rake receiver [5] applies a perfect match filter, which has a full channel information, $q(t)$ to collect all the energies of the MPCs and estimates the i^{th} information symbol within the j^{th} frame period as

$$r_i[j] = \mathrm{sgn}\left(\int_0^{T_f} q(t)r(t)dt\right) . \tag{2.4}$$

Although the ideal Rake receiver achieves the optimal error performance, the Rake receiver faces several challenges in practice: *i*) The Rake receiver requires perfect channel state information, which incurs an extremely high sampling rate and the intensive computational cost for estimating the amplitudes and delays of the MPCs. *ii*) The Rake receiver may suffer from error performance degradation because of the channel estimation error [21]. *iii*) As shown in Fig. 4, the Rake receiver requires high implementation cost on many Rake fingers constructed $q(t)$.

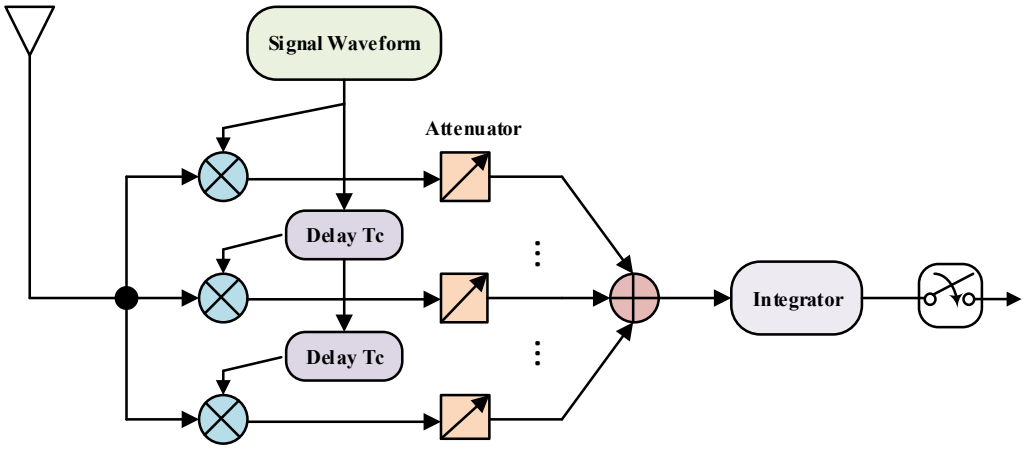

Figure 4 Rake receiver model for processing the multipath components of impulse radio UWB signal.

2.2.2 Non-coherent Receiver

Unlike coherent receivers, which detect specific waveforms from the received IR UWB signals, non-coherent receivers detect signal energy from the received IR-UWB signals. It does not need to track and estimate channel MPCs, so non-coherent receivers have a low complexity and low cost system structure. For IR-UWB systems, non-coherent reception schemes can be divided into two types: autocorrelation and energy detection.

• ***Transmitted Reference Receiver***

The typical autocorrelation reception scheme is Transmitted Reference (TR) [22], which is shown in Fig. 5. The TR receiver sends a reference pulse along with the data-modulated pulse for each frame as

$$s(t) = \sum_{i=-\infty}^{\infty} \sum_{j=0}^{N_f-1} p(t - iT_s - jT_f) + (-1)^{d_j} p(t - iT_s - jT_f - T_d), \tag{2.5}$$

where the first pulse is used to generate a noisy channel template and the second pulse is delayed with T_d. To avoid inter-pulse interference (IPI), $T_d > T_m + T_p$ and $T_f > T_d + T_m + T_p$ must be set. The corresponding received signal for a TR transmission is given by

$$r(t) = \sum_{i=-\infty}^{\infty} \sum_{j=0}^{N_f-1} q(t - iT_s - jT_f) + (-1)^{d_j} q(t - iT_s - jT_f - T_d) + \omega(t). \tag{2.6}$$

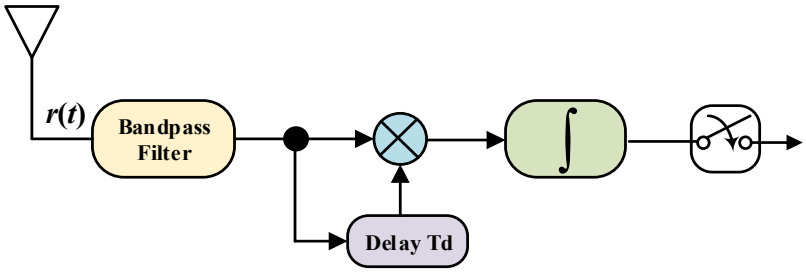

Figure 5 The transmitted reference receiver.

At the receiver, the TR receiver is simply an autocorrelation receiver, which estimates the i^{th} information symbol within the j^{th} frame period by correlating the reference signals with the data-modulated pulses as

$$r_i[j] = \mathrm{sgn}\left(\int_0^{T_r} r(t) r(t - T_d) dt \right), \tag{2.7}$$

where $0 < T_r < T_f$ denotes integration interval. Note that, since two pulses are transmitted in one frame and T_d is set smaller than the multipath channel coherence time, these two pulses can be viewed as passing through a same channel multipath fading at the receiver. Furthermore, the perfect channel template $q(t)$ for the ideal Rake receiver in Eq. (2.4) is replaced by the noisy channel template $r(t-T_d)$ for TR transmission, therefore, TR receiver does not require any channel estimation and has a much lower system complexity.

Although the TR receiver does not require explicit channel estimation, compared to the ideal Rake receiver, the TR method exhibits several drawbacks: *i*) The TR method requires two pulses per frame, which increases transmission power and decreases data rate, yielding lower spectral efficiency. *ii*) The error performance of the TR receiver is severely degraded by the noisy channel template. *iii*) It requires a delay element with ultra-wide bandwidth to provide the delayed version of the IR-UWB signals, which is very difficult to realize in the low complexity and low power IR-UWB systems, especially at the integrated circuit level.

• ***Frequency Shifted Reference***

To remove the delay element in the TR-UWB receiver, a slight frequency shifted reference (FSR) UWB scheme was proposed to deal with the issue of TR-UWB. The FSR UWB scheme separates the reference signal and data signal in the frequency domain rather than in the time domain, in which the transmitted signal is given by

$$s(t) = \sum_{i=-\infty}^{\infty} \sum_{j=0}^{N_f-1} p\left(t - iT_s - jT_f\right) + \left(-1\right)^{d_j} p\left(t - iT_s - jT_f\right) cos(2\pi f_0 t), \qquad (2.8)$$

where $f_0 = 1/T_s$ is the frequency shift of the data signal relative to the reference. To make the reference and data sequence pulses experience the same distortion channel, the

frequency offset between them needs to be smaller than the channel coherent bandwidth [8] [23]. The corresponding received signal for a FSR transmission is

$$s(t)=\sum_{i=-\infty}^{\infty}\sum_{j=0}^{N_f-1} q\left(t-iT_s-jT_f\right)+\left(-1\right)^{d_j} q\left(t-iT_s-jT_f\right)cos(2\pi f_0 t)+\omega\left(t\right). \qquad (2.9)$$

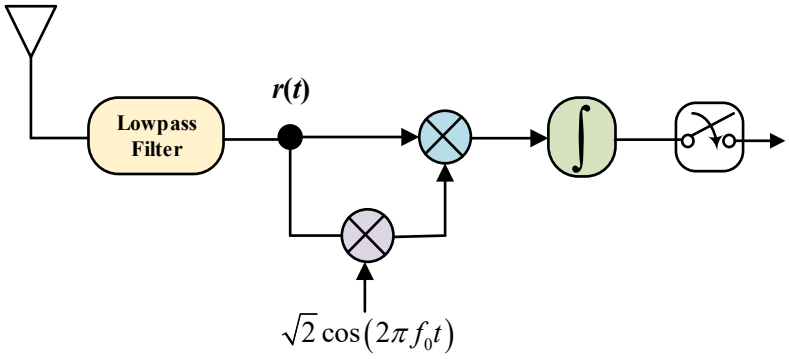

Figure 6 The frequency-shifted receiver.

In the receiver side, as shown in Fig 6, the reference pulse sequence is shifted by the same set of frequency tones to detect the information bits from the data pulse sequences within the j^{th} frame period as

$$r_i[j]=sgn\left(\int_0^{T_r} r^2(t)cos(2\pi f_0 t)\right), \qquad (2.10)$$

where $0 < T_r < T_f$ denotes integration interval. Since the separation of the reference pulse sequence and the data pulse sequences is implemented in frequency domain instead of time domain, the FSR UWB receiver does not require any delay element.

However, because analog frequency tones are employed to shift the IR-UWB signals, not only the complexity to implement the FSR UWB system is relatively high, but also its performance is affected by frequency errors caused by oscillator mismatch, phase errors caused by multipath fading, and amplitude errors caused by nonlinear amplifiers [9].

• ***Conventional Energy Detection Receiver***

ED is another popular non-coherent reception technology [24]- [26]. As shown in Fig. 7, the ED- based receiver consists of a low pass noise amplifier, a BPF to limit the noise and the adjacent-channel interference, and a square law device followed by an integrator. The ED measures the energy associated with the received signal over a specified time duration and bandwidth. This measurement is then compared with an appropriately selected threshold to decide the presence or the absence of the IR-UWB pulse with j^{th} frame period,

$$r_i[j] = \int_0^{T_I} r^2(t)dt\,, \tag{2.11}$$

where $r(t)$ is the received signal in Eq. (2.3) for the i^{th} information symbol within the j^{th} frame period, and T_I is the integration window over the specified time duration.

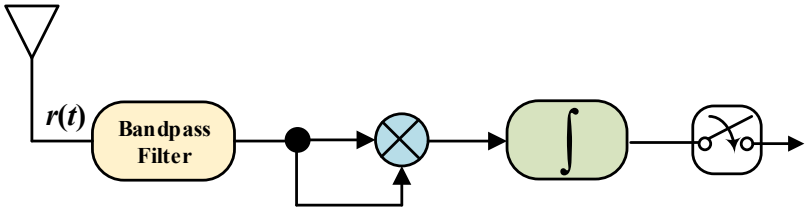

Figure 7 Conventional energy detection receiver model.

Note that, the ED technology does not require any channel estimation, time delay element or frequency shifted operator, so the ED based receiver has a simple structure and a low implement complexity. Since the integration time is usually fixed at the pulse repeat period T_f, it has a much lower sampling rate, usually, it is just in MHz level. These features make the ED technology well suitable for the low-cost applications.

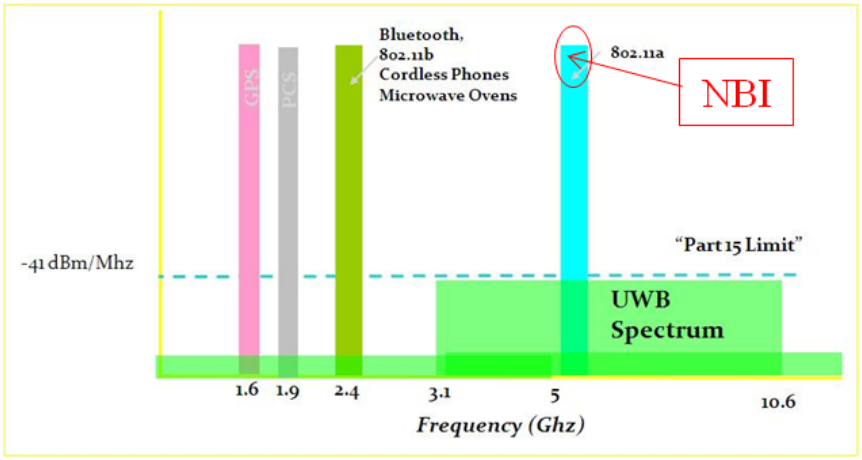

Figure 8 UWB power spectral corrupted by strong narrowband interference

However, the ED technology exhibits considerable error performance degradation compared to the coherent receiver. First, the ED technology cannot distinguish noise and interferences from the desired IR-UWB signals. Energy of noise and interferences is also collected and considered as signal energy, which makes the ED based receivers more vulnerable to noise and interferences [11] [12]. Furthermore, due to the wide bandwidth of IR-UWB systems, the received IR-UWB signals are typically corrupted by wideband AWGN or NBIs, shown in Figure 8. Typically, the power of these NBIs can be up to a few tens of dBs [1]. More significantly, in carrier modulated wideband systems, the received signal is down-converted to the baseband and sampled above the Nyquist rate, which allows numerous efficient NBI suppression algorithms based on the digital signal processing techniques. However, in IR-UWB, sampling the received signal at the Nyquist rate requires an extremely high sampling frequency, which is not possible with the existing technology. In addition to the high sampling rate, the ADC must support a very large dynamic range to resolve the signal from the strong NBIs. Currently, such ADCs are far from practical. Thus, many of the NBI suppression techniques applied to other wideband

systems are either not applicable for IR-UWB, or complexities of these methods are too great for the IR-UWB receiver requirements.

2.3 Receiver Designs based on Nonlinear Signal Processing Technology

To overcome these problems of the ED based receivers, in recent years, some researchers tried to get a better system performance by improving the RF analog signal processing circuit, and proposed some new receivers, such as FD [15], KD [15] and TKO [17]. The common feature of these technologies is the slightly added analog signal processing units which keep the advantages of simple structure in the conventional ED based receivers. Since the added analog signal processing circuits are nonlinear devices, these new IR-UWB technologies are denoted as nonlinear signal processing technologies in this thesis.

2.3.1 Four-order Detection-based Receiver

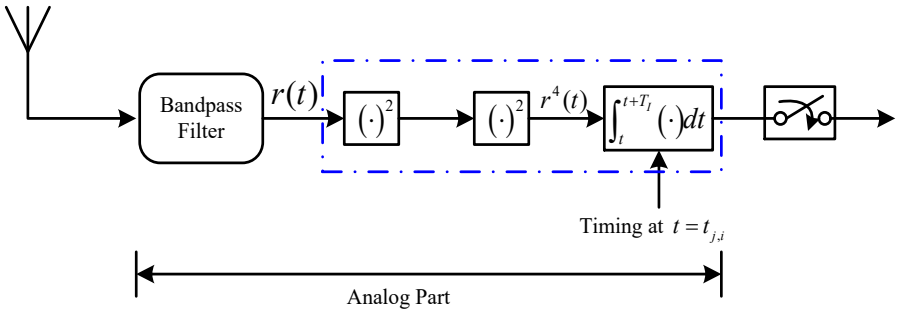

Figure 9 The FD based receiver for IR-UWB systems

In order to improve the system performance of the conventional ED based receiver, [27] proposed an improved energy detection based receiver by replacing the square law device in ED with an arbitrary positive *p*-order operator; and [15] proposed another FD based receiver. As shown in Fig. 9, it is seen that the FD based receiver has a similar structure with the ED based receiver. In the FD based receiver, first, the receiver signal is sent to two square law devices, after passing the BPF at the RF front, to get the four-order signal, $r^4(t)$, and then integrated by an integrator over a specified time duration to get the four-order statistics. Finally, the data is recovered by comparing the statistics with a decision threshold.

2.3.2 Kurtosis Detection-based Receiver

Kurtosis, also known as kurtosis coefficient, is used to characterize the peak value at the location of mean in the statistical probability density distribution curve. In the communication signal processing, by use of kurtosis the signal can be divided into three types: Gaussian signal, Super-Gaussian and Sub-Gaussian signals [28]. For a real signal $x(t)$, its kurtosis is defined as [28]

$$K(x) = \mathrm{E}\left[x^4\right] - 3\left(\mathrm{E}[x^2]\right)^2 , \tag{2.12}$$

or

$$K(x) = \frac{\mathrm{E}[x^4]}{\left(\mathrm{E}[x^2]\right)^2} - 3 . \tag{2.13}$$

Using the definition above, a signal with the kurtosis of zero is a Gaussian signal; a signal with the positive kurtosis is a super-Gaussian signal; and a signal with a negative kurtosis is the sub-Gaussian signal. Compared with the probability density function (PDF)

of Gaussian signal, the PDF of the super-Gaussian signal has a higher and narrower peak; while the sub-Gaussian signal PDF has a lower and wider peak.

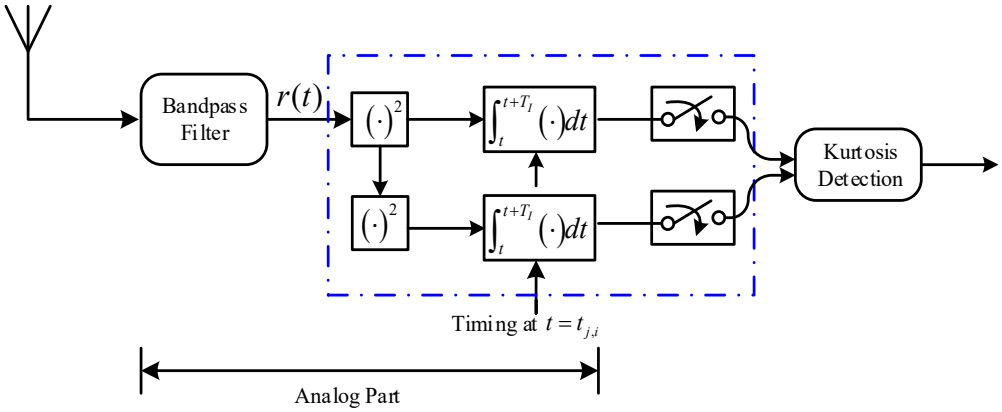

Figure 10 The KD based receiver for IR-UWB systems

Since the IR-UWB signal is an impulse signal, it has a positive kurtosis, while noise signal has a zero-kurtosis value. Motivated by this observation, the kurtosis is proposed to detect IR-UWB signal in [15], and the KD based receiver is shown in Fig. 10. From Fig. 10, it is seen that the KD based receiver consists of two branches: the upper branch and the lower branch. The upper branch has a similar structure to the ED based receiver, it measures the signal energy; while the lower branch is similar to FD, which measures the four-order statistics of signal. By using Eq. (2.12), the kurtosis of signal can be obtained with a specified time duration to recover the transmitted bits.

CHAPTER 3 KURTOSIS DETECTOR FOR IMPULSE RADIO UWB SIGNALS

IR-UWB receivers based on KD can achieve much better performance than those based on ED. However, when NBIs are present, the existing KD- based receivers have serious performance degradation. In this chapter, a modified KD (MKD) is proposed to improve the NBI mitigation ability of the receiver. Computer simulation results show that although the BER performances of the MKD-based receiver are marginally lower than those of the KD-based receiver when no NBI is present, the MKD-based receiver can achieve much better BER performance when NBIs are present.

3.1 INTRODUCTION

ED is a non-coherent detector to detect IR-UWB signals, which utilizes a square law device followed by an integrator to capture the energy of received IR-UWB pulses for bit information detection [29]. The complexity of ED-based receivers is much lower than that of Rake receivers, but the performance of ED-based receivers is inferior as well, because the ED cannot distinguish the energy of noise and interferences from that of IR-UWB signals [30]. Recently, another non-coherent detector, denoted as KD, is proposed to improve the BER performance of ED-based receivers [15]. In a KD-based receiver, the square law device is replaced by a nonlinear kurtosis operator. Simulation results in [15] showed that KD-based receivers have a better BER performance than ED-based receivers in AWGN Channel.

However, none of the existing research on KD-based receivers have considered the destructive effects of NBIs. In the real world, due to their ultra-wide bandwidth, IR-UWB systems have to coexist with many narrowband wireless systems, such as IEEE 802.11a wireless local area network (WLAN) [31]. Thus, with a high probability, NBIs exist in received IR-UWB signals. Those NBIs can seriously degrade the performance of KD-based receivers. In order to improve the NBI mitigation ability of KD-based receivers, in this chapter, a MKD is proposed, which allows KD-based receivers achieving much better BER performance when strong NBIs are present.

The organization of the chapter is as follows. In section 3.2, the signal model of an IR-UWB system with binary PPM is presented. Then the receiver structures of the ED-, KD- and MKD-based receivers are described. In section 3.3, the performances of the three receivers are evaluated through computer simulations and the simulation results are discussed. Finally, conclusions are given in section 3.4.

3.2 System Model and Receiver Structure

In an IR-UWB system with BPPM, the transmitted UWB signal can be expressed as

$$s(t) = \sqrt{E_s} \sum_{j=-\infty}^{\infty} p(t - jT_s - d_j \delta), \tag{3.1}$$

where $p(t)$ is a normalized UWB pulse with a duration of T_p, E_s is the transmitted energy per symbol, T_s is the symbol duration, and $\delta = T_s / 2$ is the BPPM shift to differentiate 0 and 1. In the same equation, $d_j \in \{0,1\}$ is the information bit transmitted in the j^{th} symbol, which determines the starting time of the transmitted pulse either at jT_s or $jT_s + \delta$. The received UWB signal can be expressed as

$$r(t) = \sqrt{E_s} \sum_{j=-\infty}^{\infty} q(t - jT_f - d_j\delta) + n(t) + i(t), \tag{3.2}$$

where $n(t)$ is an AWGN with a two-side power spectral density $S_n(f) = N_0/2$, $i(t)$ is NBI, and $q(t)$ is the received UWB pulse given by $q(t) = p(t) * h(t)$. Here $h(t)$ presents multipath channels and * is linear convolution. In this chapter, we assume that no inter-pulse-interference (IPI) exists, *i.e.* the duration of $q(t)$ is less than δ.

In IR-UWB receivers, the received UWB signal is first filtered by a BPF to remove out-of-band noise and interferences. We denote the signal after passing through the BPF as $\tilde{r}(t)$.

3.2.1 Energy Detector

In an ED-based receiver, the decision variables are obtained as follows

$$Z_{ed,j0} = \int_{jT_s}^{jT_s+T_m} \tilde{r}^2(t)\, dt, \tag{3.3}$$

$$Z_{ed,j1} = \int_{jT_s+\delta}^{jT_s+\delta+T_m} \tilde{r}^2(t)\, dt, \tag{3.4}$$

where the sub-indices "*ed,j0*" and "*ed,j1*" denote signal energy collected from the first and the second integration interval, respectively. The length of the integration interval, T_m, varies from T_p in an AWGN channel to $T_s/2$ in a severe multipath channel.

The bit detection in an ED-based receiver is made in comparison to the energy collected over two integration intervals, *i.e.*,

$$\tilde{b}_j = \begin{cases} 0, & Z_{ed,j0} > Z_{ed,j1}, \\ 1, & Z_{ed,j0} \le Z_{ed,j1}. \end{cases} \tag{3.5}$$

3.2.2 Kurtosis Detector

A kurtosis detector based receiver is shown in Fig. 10 where kurtosis is a statistical quantity indicating the non-Gaussian characteristic of a random variable [32]. The kurtosis definition used is given by [15]:

$$kurt(x) = E\{x^4\} - 3\left[E\{x^2\}\right]^2 , \tag{3.6}$$

where $E(\cdot)$ denotes the expected value of a variable.

Correspondingly, as shown in Fig. 10, the decision variables in a KD-based receiver are calculated as follows:

$$Z_{kd,j0} = \frac{1}{T_m}\int_{jT_s}^{jT_s+T_m} \tilde{r}^4(t)\, dt - \frac{3}{T_m^2}\left(\int_{jT_s}^{jT_s+T_m} \tilde{r}^2(t)\, dt\right)^2 , \tag{3.7}$$

$$Z_{kd,j1} = \frac{1}{T_m}\int_{jT_s+\delta}^{jT_s+\delta+T_m} \tilde{r}^4(t)\, dt - \frac{3}{T_m^2}\left(\int_{jT_s+\delta}^{jT_s+\delta+T_m} \tilde{r}^2(t)\, dt\right)^2 . \tag{3.8}$$

Similar to ED-based receivers, the bit detection of a KD-based receiver is made by comparing $Z_{kd,j0}$ with $Z_{kd,j1}$:

$$\tilde{b}_j = \begin{cases} 0, & Z_{kd,j0} > Z_{kd,j1} , \\ 1, & Z_{kd,j0} \le Z_{kd,j1} . \end{cases} \tag{3.9}$$

3.2.3 The Proposed Modified Kurtosis Detector

Computer simulations shown in the following section indicate that when strong NBIs are present, the KD-based receivers as shown in Fig. 10 have serious performance degradation. In order to improve the NBI mitigation ability of KD-based receivers, we propose to use another definition for kurtosis:

$$kurt(x) = E\{x^4\} \Big/ \left[E\{x^2\}\right]^2 \tag{3.10}$$

With this new definition, we have modified the KD to calculate the decision variables as follows:

$$Z_{mkd,j0} = \left[\frac{1}{T_m}\int_{jT_s}^{jT_s+T_m} \tilde{r}^4(t)\,dt\right] \Big/ \left[\frac{1}{T_m^2}\left(\int_{jT_s}^{jT_s+T_m} \tilde{r}^2(t)\,dt\right)^2\right], \tag{3.11}$$

$$Z_{mkd,j1} = \left[\frac{1}{T_m}\int_{jT_s+\delta}^{jT_s+\delta+T_m} \tilde{r}^4(t)\,dt\right] \Big/ \left[\frac{1}{T_m^2}\left(\int_{jT_s+\delta}^{jT_s+\delta+T_m} \tilde{r}^2(t)\,dt\right)^2\right]. \tag{3.12}$$

3.3 Performance Evaluation and Discussions

In order to thoroughly investigate the NBI mitigation ability of the MKD, the ED-, KD-, and MKD-based receivers were simulated over AWGN channel in with-NBI and without-NBI scenarios. The system parameters for the computer simulations were set to be $T_p = 20ns$, $T_s = 100ns$, $T_m = 50ns$, and $\delta = 50ns$. Moreover, the bandwidth of NBI was set at 6MHz and the central frequency was set at 5GHz.

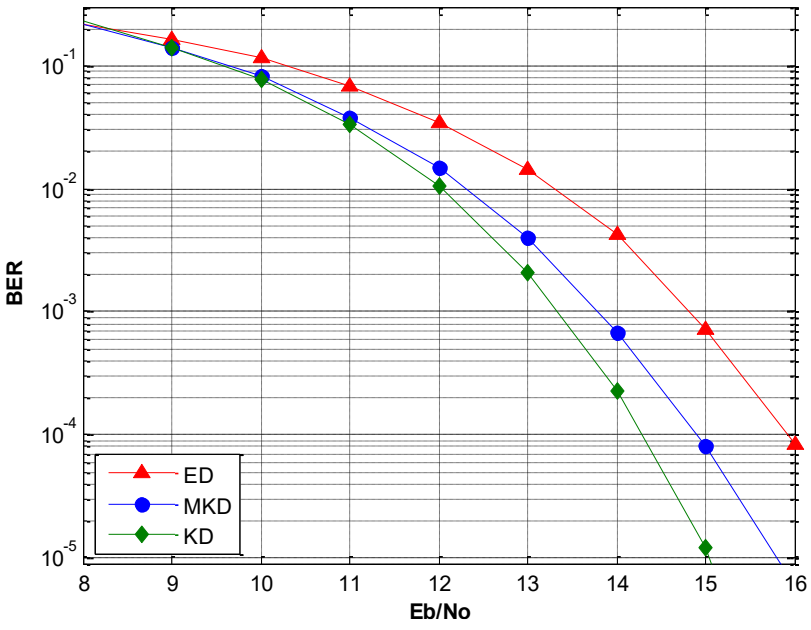

Figure 11 BERs of ED-, KD-, and MKD-based receivers for IR-UWB signals without NBI

First, when no NBI is present, the BER performances of the ED-, KD-, and MKD-based receivers have been evaluated through computer simulations, and the results are shown in Fig. 11. Obviously, both the KD- and MKD-based receivers can achieve better BER performances than the ED-based receiver. The higher the signal-to-noise ratio (SNR), *i.e.*, E_b/N_0, the larger the performance improvement. In comparison with the KD-based receiver, the MKD-based receiver has a marginal performance degradation.

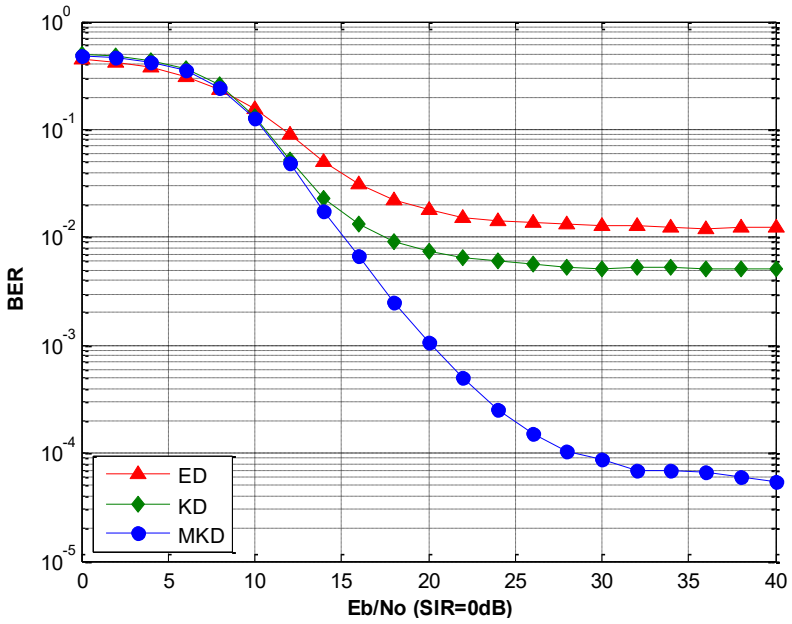

Figure 12 BERs of ED-, KD- and MKD-based receivers with a strong NBI (SIR = 0dB).

Second, we have investigated the NBI mitigation ability of the three receivers. As shown in Fig. 12, when a strong NBI is present, for example, the signal-to-interference rate (SIR) is equal to 0dB, error floor of the ED-based receiver occurs at 1.2×10^{-2}, that of the KD-based receiver occurs at 5.0×10^{-3}, and that of the MDK-based receiver occurs at 5.0×10^{-5}. The MKD-based receiver has a much lower error floor than the other two receivers. From Fig. 13, it can be seen that regardless of the SIR value, the MKD-based receiver can

always achieve a considerable performance improvement over the ED- and KD-based receivers. In other words, the MKD-based receiver has an inherent ability to mitigate the destructive effects caused by NBI.

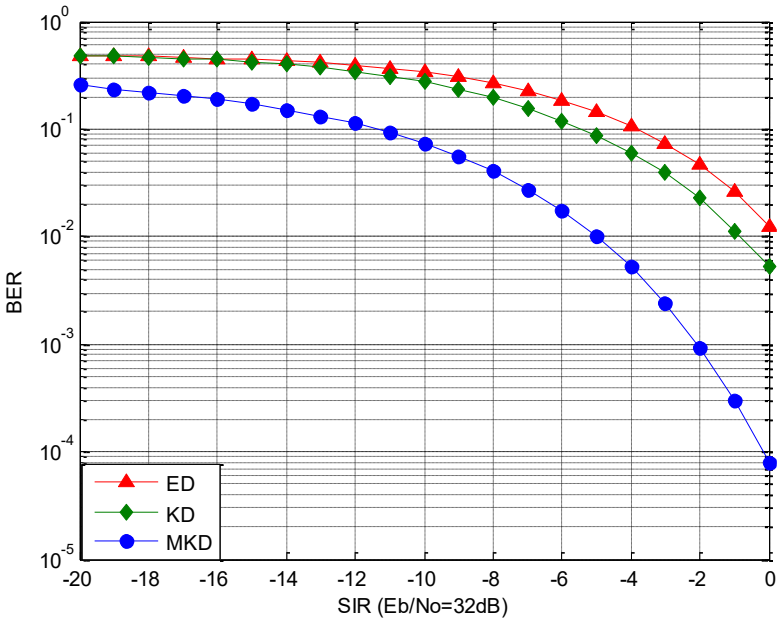

Figure 13 BERs of ED-, KD- and MKD-based receivers versus SIR (E_b/N_0 = 32dB).

3.4 CONCLUSION

NBIs can seriously degrade the performance of ED- and KD-based IR-UWB receivers. In this chapter, a new MKD-based receiver is proposed to mitigate destructive effects caused by NBIs. Simulation results show that although the BER performances of the MKD-based receiver are marginally lower than those of the KD-based receiver when no NBI is present, the MKD-based receiver can achieve much better BER performance when NBIs are present. Therefore, the MKD-based receiver is a preferred detection technology for IR-UWB systems.

CHAPTER 4 ON THE VARIANCE-BASED DETECTION FOR IMPULSE RADIO UWB SYSTEMS

A variance detection (VD)[1] based IR-UWB system has a potential of mitigating NBI, even in multipath environments. However, as a highly nonlinear system which involves fourth-order multiplications, comprehensive analysis and evaluations of its performances have not been seen so far. In this chapter, we address the issues by developing a log-normal random distribution model for the VD-based IR-UWB receiver and deriving the analytical bit-error-rate formulas for the system in both AWGN and CM1 multipath channels with and without NBIs for the first time. Furthermore, through both theoretical analysis and simulations, we show that the presented VD-based receivers can outperform the conventional energy-detection based and the fourth-order detection based receivers and have a stronger inherent ability to mitigate destructive performance degradation caused by strong NBIs. This makes the VD-based IR-UWB system a good candidate as a non-coherent IR-UWB receiver for low power and low complexity applications.

4.1 INTRODUCTION

An appealing characteristic of impulse radio ultra-wideband (IR-UWB) systems is that they can utilize a very large frequency bandwidth (greater than 500MHz) without a license as long as transmitted IR-UWB pulses have a very low power spectrum density (not higher

[1] This chapter is mainly based on our published papers [33] and [16], which are A. Yang, Z. Xu, H. Nie, Z. Chen, "On the Variance-based Detection for Impulse Radio UWB systems," published on *IEEE transaction on Wireless communication*, vol. 15, no.12, pp. 8249-8259, Dec., 2016, and A. Yang, H. Nie, Z. Xu and Z. Chen, "Variance detection for non-coherent impulse radio UWB receivers," in *IEEE Computing, Networking, and Communications Conference*, pp. 529-533, Feb. 2014.

than -41.3dBm/MHz). Furthermore, IR-UWB pulses can be radiated with or without a carrier, which simplifies the IR-UWB system structure and makes it a strong candidate for low power and low complexity applications, such as the IEEE 802.15.4a wireless personal area network [3] and IEEE 802.15.6 standard wireless personal area network [4]. However, transmitting very short duration IR-UWB pulses presents a couple of challenges at the receiver end due to the fact that the received IR-UWB signals, after going through a UWB channel, may have a large number of resolvable multipath components [34].

To tackle the above problem, various receiver structures for the IR-UWB systems have been proposed. Among them are the coherent receivers [24] such as Rake receivers (which are optimum receivers in theory). With the coherent receivers, overall UWB channel responses need to be accurately estimated. However, channel estimation is a non-trivial task in IR-UWB systems as it involves intensive signal with a sampling rate at Gigahertz (GHz) level [21] [35]. As an alternative to the coherent receivers, non-coherent energy-detection (ED) based transceivers have emerged for low complexity and low power applications; they include on-off keying transceiver [36], pulse position modulation ED (PPM-ED) transceiver [7], frequency-shifted reference transceiver [37], code-shifted reference transceiver [38], and differential code-shifted reference transceiver [39]. These ED-based transceivers detect the presence of a signal by measuring its energy and comparing the measured energy with a predetermined or reference threshold. The measurement and comparison requires no channel information; therefore, the ED-based transceivers can be of simple structures with much lower sampling rates than those with the coherent receivers.

However, in comparison with the coherent receivers, the ED-based receivers do encounter a few problems. Due to the large transmission bandwidth of IR-UWB systems that span across the frequency bands of other existing narrowband wireless systems, the ED-

based receivers take in the narrowband signals from the existing wireless systems and have them as narrowband interferences (NBIs). These NBIs, together with noises, can corrupt the received IR-UWB signals and lead to serious performance degradation for the ED-based receivers. To mitigate this destructive effect, various techniques have then been developed; they include use of notch filters in the receiver [14], digital interference cancellation [13], and weighted energy detection [40]. While these techniques can improve performance of the ED-based receivers, they come at the expense of added complexities undesirable for practical systems, such as a large number of integrators, high sampling rates, and large power consumptions.

To circumvent the above problems and achieve good performances with low system complexity, researchers tried to replace the square operation in conventional ED-based receivers with a higher order operation, such as fourth-order detection (FD) [15], and variance-detection (VD) [16]. The VD recovers information bits by measuring the variance of the squared received signal. In a VD system, the NBI is shifted to a frequency band close to DC through the square operation; and then suppressed by a "DC-remover" operator, resulting in improved the system performance. The computer simulations in our previous research show that the VD-based receivers can achieve a much better performance than the conventional ED-based and FD-based receivers with and without the presences of NBIs [16]. Since the VD-based technique does not need any prior knowledge of NBI, it can meet the requirement of low complexity and low power consumption for the IR-UWB system.

However, as the VD-based receiver is a highly nonlinear system which uses a fourth-order multiplication, the theoretical analysis of system performance, especially with NBIs, becomes quite challenging due to the unknown of the probability density function (PDF) of the statistics. The conventional Gaussian distribution model, which is usually used in non-

coherent IR-UWB system analysis, becomes inaccurate for the four-order statistics within a limit integration time. In [41] a Generalized Extreme Value (GEV) distribution model with three parameters is proposed for approximating the four-order statistics, and simulations show the GEV model fits the PDF well, but the parameter estimation is challenging. In [42], a Gamma distribution with two parameters is used for a high-order statistic; however, the simulation results show a larger approximation error as the signal-to-noise ratio (SNR) becomes high. Furthermore, both models do not consider NBI.

In this chapter, we resolve the above issues by developing a log-normal stochastic distribution model for the statistics of VD-based detector. With the model, we derive the theoretical bit-error-rate formula for the VD-based receiver in both AWGN and multipath channels with and without NBIs, and we then verify the validity of the theoretical analysis with computer simulations.

The original contributions of this chapter are in three aspects. Firstly, by developing a log-normal random distribution model and exploiting a discrete signal analysis approach, a systematic theoretical framework of analyzing the system performance for the VD-based receiver is proposed; it presents an efficient way to evaluate the performance of the VD-based receivers and other nonlinear receivers. Secondly, the analytical BER formulas for the VD-based receivers are derived for both AWGN and dense multipath channel conditions with and without NBIs for the first time. Last but not the least, the mechanism and performance of VD technology are studied and clarified; they prove the effectiveness of the VD-based IR-UWB systems in mitigating the negative impacts of the NBIs.

The organization of the chapter is as follows. Section 4.2 describes the system structure of the proposed VD-based receiver. Section 4.3 presents the VD-based detection algorithm and the log-normal model we develop. Section 4.4 analyzes the theoretical performances of

the proposed VD-based receiver. Section 4.5 presents various simulation results to verify the validity of theoretical analysis as well as evaluate the overall BER performance. Finally, the conclusions of this paper are given in Section 4.6.

4.2 THE PROPOSED VARIANCE-DETECTION BASED RECEIVER

In this section, we first present the IR-UWB signal and the channel model considered by this chapter, and then the structure of the VD based IR-UWB receiver.

4.2.1 The UWB Signal and Channel Model Used

Without loss of generality, a single-user binary pulse position modulated (BPPM) IR-UWB signaling system [7] is considered as an example. The transmitted BPPM IR-UWB signal $s(t)$, which is in the frequency band of 3.1GHz to 10.6GHz, can be written as:

$$s(t) = \sqrt{E_s} \sum_{j=-\infty}^{\infty} p(t - jT_f - d_j T_f / 2), \tag{4.1}$$

where $d_j \in \{0,1\}$ are independent binary information symbols, $p(t)$ is a normalized UWB pulse with a duration of T_p, a center frequency f_c and a bandwidth BW. T_f is the pulse repetition interval or frame time, and E_s is the transmitted energy per frame. The starting time of the j^{th} transmitted pulse is either at jT_f where d_j=0 or $jT_f + T_f/2$ where d_j=1.

The CM1 multipath channels defined by IEEE 802.15.4a [43] are considered in this paper and the associated impulse response $h(t)$ is given by:

$$h(t) = \sum_{l=0}^{L-1} \alpha_l \delta(t - \tau_l), \tag{4.2}$$

where L is the total number of multipath components, and $\delta(t)$ is a Dirac Delta function. Each multipath component is with gain α_l and delay τ_l. To prevent the inter-symbol interference and to maintain the orthogonality of the received symbols, we set the PPM offset larger than the maximum delay spread of the channel [7], *i.e.* $T_f/2 > T_p + \tau_{L-1}$.

4.2.2 The VD-based Receiver Structure

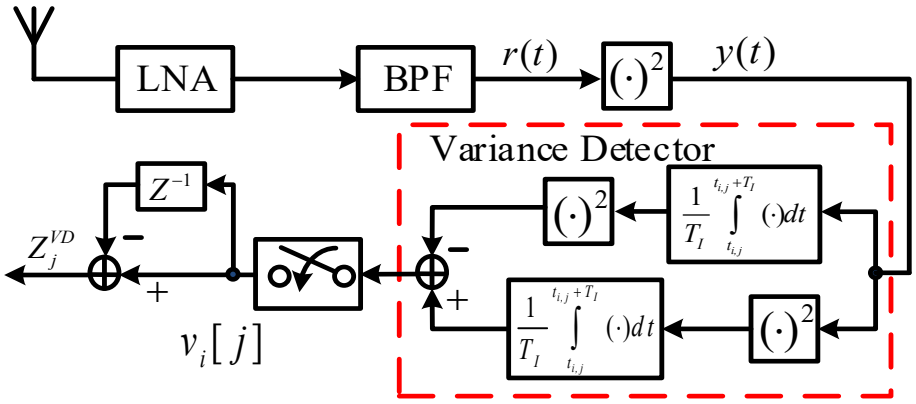

Figure 14 The proposed VD-based receiver for a BPPM IR-UWB system. Two samples are detected over the j^{th} symbol time: the first sample $v_0[j]$ is measured from $t_{0,j} = jT_f + \tau_0$ to $t_{0,j} + T_I$ within the first half of the j^{th} symbol frame time; while the second sample $v_1[j]$ is measured from $t_{1,j} = jT_f + T_f/2 + \tau_0$ to $t_{1,j} + T_I$ within the second half of the j^{th} symbol frame time. τ_0 is the delay of the first received pulse component.

Fig. 14 shows the structure of the proposed VD-based IR-UWB receiver. As usual, a low-noise amplifier (LNA) followed by a band-pass filter (BPF) in cascade is placed at the front end of the receiver to amplify the weak signal and then remove unwanted out-of-band signals, noises and interferences. Denote the combined impulse response of the amplifier and the filter as $h_f(t)$. After passing through the multipath channel, the LNA, and the BPF, the filtered signal, $r(t)$, can be expressed as:

$$r(t) = \sum_{j=-\infty}^{\infty} q(t - jT_f - d_j T_f/2) + n(t) + i(t) \\ = \sum_{j=-\infty}^{\infty} q(t - jT_f - d_j T_f/2) + w(t), \tag{4.3}$$

where $n(t)$ and $i(t)$ are noises and interferences passing through the BPF, and $q(t)=\sqrt{E_b}$ $p(t)*h(t)*h_f(t)$. The filtered signal $r(t)$ is sent to a square law device to generate the squared IR-UWB signal $y(t)=r^2(t)$. Note that $w(t)=n(t)+i(t)$ is the sum of noises and interference; when no interferences are present, $w(t)=n(t)$.

$y(t)$ is then sent to the proposed variance detector to measure two "variance" samples over the j time frame:

$$v_i[j] = \frac{1}{T_I} \int_{t_{i,j}}^{t_{i,j}+T_I} y^2(t)\,dt - \left[\frac{1}{T_I} \int_{t_{i,j}}^{t_{i,j}+T_I} y(t)\,dt \right]^2, \quad i = 0,1. \tag{4.4}$$

For the first sample $v_0[j]$, $t_{0,j} = jT_f + \tau_0$, (within the first half of the j^{th} frame time) and for the second sample $v_1[j]$, $t_{1,j} = jT_f + T_f/2 + \tau_0$ (within the second half of the j^{th} frame time). Here τ_0 is the delay of wireless channel, and T_I is the integration time, which varies from T_p (when an AWGN channel is considered) to $T_f/2$ (when a multipath fading channel with severe delay spread is considered).

Finally, with the two samples, the j^{th} information bit is recovered according to the following measurement:

$$\hat{d}_j = \begin{cases} 0, & \text{when } Z_j^{VD} = v_1[j] - v_0[j] < 0, \\ 1, & \text{when } Z_j^{VD} = v_1[j] - v_0[j] \geq 0. \end{cases} \tag{4.5}$$

4.3 NONLINEAR DETECTION ALGORITHMS AND COMPARISONS

In this section, we will present the VD-based detection algorithm and its comparison with the other nonlinear detection algorithms, then the stochastic model for $v_i[j]$, which is the variance detection output of the proposed receiver.

Without loss of generality, we assume a transmission with perfect synchronization of the integration window, no ISI and no IPI. Moreover, assume that the j^{th} information bit is one, i.e. $d_j = 1$. Thus, the UWB pulse is at the second half of the j^{th} frame time. Then, based on (4.3), the received signal, $r(t)$, within the first half of the j^{th} frame time (between $jT_f + \tau_0$ to $jT_f + \tau_0 + T_l$), can then be expressed as

$$r_{j0}(t) = w_{j0}(t), \tag{4.6}$$

where $r_{j0}(t)$ is the notation of $r(t)$ within the first half of the j^{th} frame time, and $w_{j0}(t)$ is the received noise and interferences within the same time period. Then $r_{j0}(t)$ is sent to the squared device and becomes $y_{j0}(t)$:

$$y_{j0}(t) = r_{j0}^2(t) = w_{j0}^2(t), \tag{4.7}$$

where $y_{j0}(t)$ is the notation of $y(t)$ within the first half of the j^{th} frame time.

In a similar way, the received signal, $r(t)$, within the second half the j^{th} frame time (between $jT_f + T_f/2 + \tau_0$ and $jT_f + T_f/2 + \tau_0 + T_l$) can be expressed as:

$$r_{j1}(t) = q_{j1}(t) + w_{j1}(t), \tag{4.8}$$

where $r_{j1}(t)$ is the notation of $r(t)$ within the second half the j^{th} frame time, and $w_{j1}(t)$ is the received noises and interferences and $q_{j1}(t)$ is the received UWB pulse in the same time period. Correspondingly, $y(t)$ within the second half of the j^{th} frame time can be obtained as follows:

$$y_{j1}(t) = r_{j1}^2(t) = q_{j1}^2(t) + w_{j1}^2(t) + 2q_{j1}(t)w_{j1}(t), \tag{4.9}$$

where $y_{j1}(t)$ is the notation of $y(t)$ within the second half of the j^{th} frame time.

In the above equations, $q_{j1}^2(t)$ is the UWB term, $2q_{j1}(t)w_{j1}(t)$ is the cross-term, and $w_{j1}^2(t)$ is the noise/interference term, in which $w_{ji}(t)$ with i=0,1 is given by:

$$w_{ji}(t) = n(t) + i_{ji}(t). \tag{4.10}$$

When no interferences are present, $i_{ji}(t) = 0$.

4.4.1 ED-based Detection Algorithm

In order to detect the UWB pulse in the received signal, the ED-based detection algorithm measures the "mean" of the squared signal $y(t)$, *i.e.* the energy of $r(t)$, as follows,

$$Z_{ji} = \frac{1}{T_I}\int_{t_{i,j}}^{t_{i,j}+T_I} y(t)dt = \frac{1}{T_I}\int_{t_{i,j}}^{t_{i,j}+T_I} y_{ji}(t)dt, \quad i = 0,1, \tag{4.11}$$

and the j^{th} information bits is then recovered according to the following rule:

$$\hat{d}_j = \begin{cases} 0, & \text{when } Z_j = Z_{j1} - Z_{j0} < 0, \\ 1, & \text{when } Z_j = Z_{j1} - Z_{j0} \geq 0. \end{cases} \tag{4.12}$$

4.4.2 FD-based Detection Algorithm

By replacing the "mean" operator in ED-based detection algorithm, the FD-based detection algorithm measures the "energy" of the squared signal $y(t)$, i.e. the four-order power of $r(t)$, as follows,

$$Z_{ji} = \frac{1}{T_I} \int_{t_{i,j}}^{t_{i,j}+T_I} y^2(t)dt = \frac{1}{T_I} \int_{t_{i,j}}^{t_{i,j}+T_I} y_{ji}^2(t)dt, \quad i = 0,1, \tag{4.13}$$

and recovers the information bits as the same rule in (4.12).

4.4.3 The Proposed VD-based Detection Algorithm

While in the VD-based detection algorithm, instead of measuring the "mean" or the "energy" of the squared signal $y(t)$, the signal "variance", as shown in Fig. 14, is measured as follows,

$$\begin{aligned} V_{ji} &= \frac{1}{T_I} \int_{t_{i,j}}^{t_{i,j}+T_I} y^2(t)dt - \left[\frac{1}{T_I} \int_{t_{i,j}}^{t_{i,j}+T_I} y(t)dt \right]^2 \\ &= \frac{1}{T_I} \int_0^{T_I} y_{ji}^2(t)dt - \left[\frac{1}{T_I} \int_0^{T_I} y_{ji}(t)dt \right]^2, \quad i = 0,1, \end{aligned} \tag{4.14}$$

where V_{ji} is the notation of $v_i[j]$ (i.e. Eq. (4.4)). From (4.14), we can see that, unlike the FD-based detection algorithm of (4.13), the VD-based detection algorithm of (4.14) has the second term of DC, $\left[\frac{1}{T_I}\int_0^{T_I} y_{ji}(t)dt\right]^2$, on the right-hand side which is substracted or removed, further improving the system performance.

In order to explore the rationale behind the proposed VD-based detectors, we first present the power spectrums of the received signal $r(t)$ and the squared signal $y(t)$ as depicted in Fig. 15. The squared signal $y(t)$ of (4.9) consists of three terms: the UWB term, the cross-term and the noise/interference term. In frequency domain, the UWB term is located in $[0, BW]$ and $[2f_c - BW, 2f_c + BW]$, the NBI term is in $[0, BW_I]$ and $[2f_I - BW_I, 2f_I + BW_I]$, the noise term is in $[0, BW]$ and $[2f_c - BW, 2f_c + BW]$, and the cross-terms are in $[0, |f_c - f_I| + (BW + BW_I)/2]$, $[0, BW]$, $[f_c + f_I - (BW + BW_I)/2, f_c + f_I + (BW + BW_I)/2]$ and $[2f_c -$

$BW, 2f_c + BW$]. Here f_I is the NBI center frequency and BW_I is its bandwidth. It should be noted that $y(t)$ has a strong DC component of NBI/noise, which is generated by noise/NBI term in (4.9). It degrades the system performance.

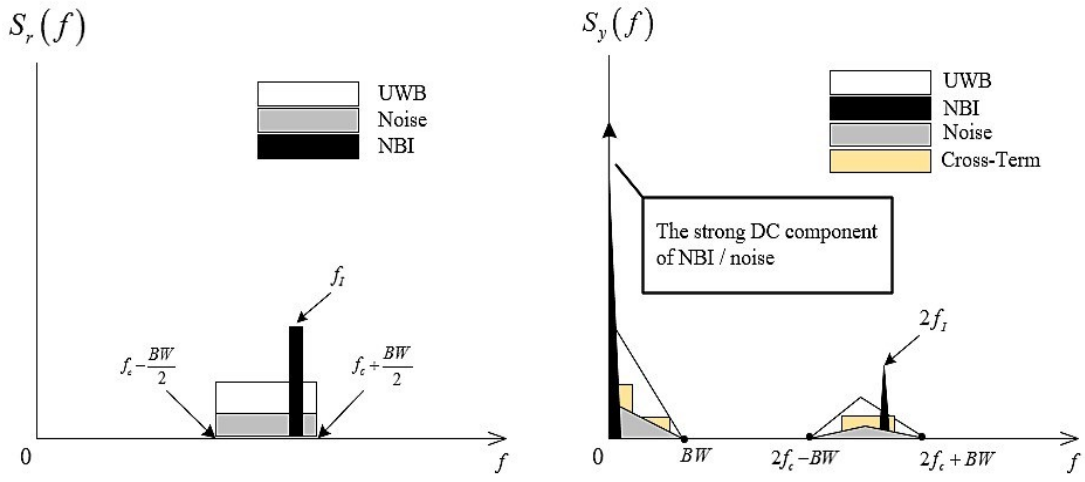

Figure 15 Power spectrums of the received signal r(t) (left) and the squared signal y(t) (right) in VD-based receivers.

With the above observation, we have the further notes on the VD operations.

(i) The proposed VD-based detector has an inherent ability to mitigate NBI and noise. With the help of "DC-remover", the proposed VD-based detector can mitigate the strong DC component of noise/NBI, and improve system performance. It is quite different from the ED-based detection. The ED-based detection algorithms detect the DC component, i.e. the mean in (4.11), while the FD-based detection algorithms detect all the energy of $y(t)$ including DC component.

(ii) The DC-remover in the VD-based detector suppresses NBI blindly regardless of its center frequency location. As shown in Fig. 15, after passing through a square operator, the strong NBI component in received signal $r(t)$ is moved from its center

frequency, f_I, to DC, and then is removed by the DC-remover without any prior information.

(iii) The complexity increase to measure the variance instead of the mean of $y(t)$ is not significant. As shown in Fig. 14, the upper signal flow in the VD is to measure the mean of $y(t)$, which is needed by every ED-based receiver, and only the lower signal flow is the added signal processing unit to measure the variance of $y(t)$. Luckily, this added unit can be easily implemented with an analog square law device and an integrator, and the integration output only needs to be sampled at symbol rate.

4.3.4 The Stochastic Model for the VD Output

In order to derive a theoretical formula for the BER performance of the VD-based receivers, the stochastic characteristics of the samples outputted by the VD must be analyzed first. In most existing ED-based receivers, the samples outputted by the ED are approximated with a Gaussian random distribution. However, because fourth-order multiplications are involved for manipulating the received IR-UWB signal in the proposed VD, approximating the VD output with a Gaussian random distribution becomes inaccurate. We investigated, through empirical simulations, a group of random distributions that can be fully determined with their mean and variance for the proposed VD-based receiver. The empirical results are shown in Fig. 16 for the cumulative distribution function (CDF) of the two variances, V_{j0} and V_{j1}, in the AWGN channel and a multipath channel.

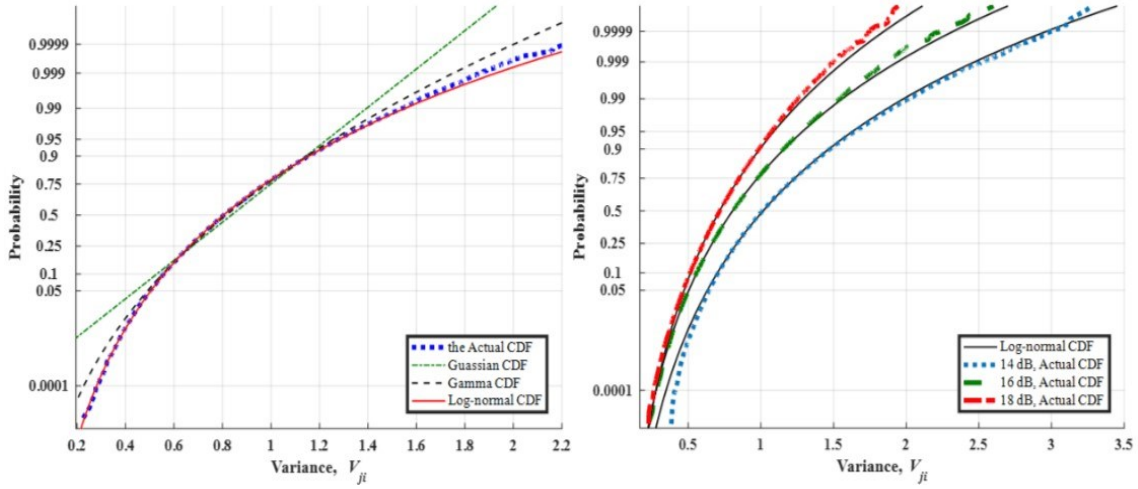

(a) AWGN

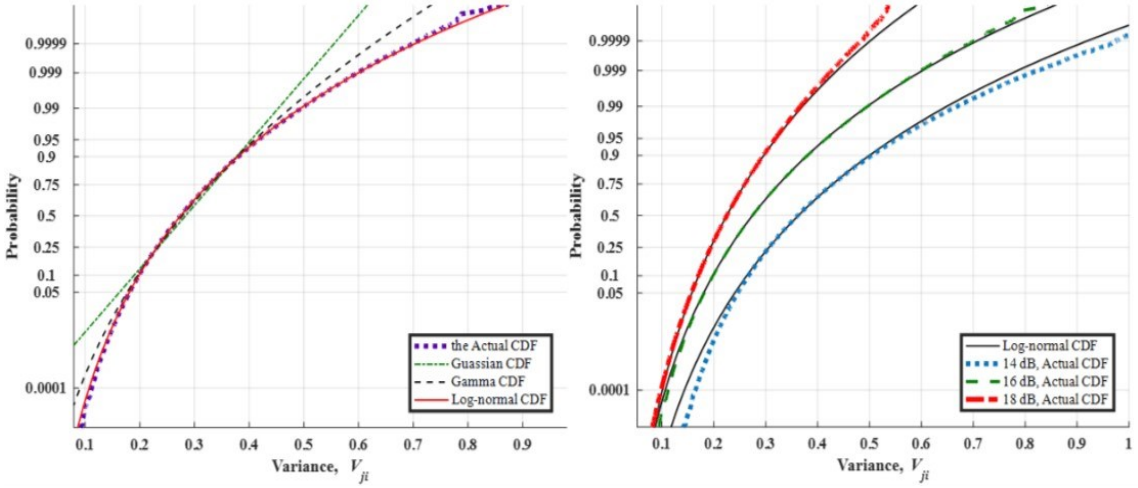

(b) CM 1

Figure 16 Probability plots for the cumulative distribution functions (CDF) obtained by simulations with (a) the AWGN channel and (b) CM1 channel and their comparisons with other known distributions. BW = 2 GHz, E_b/N_0 = 16 dB (left), and T_I = 200 ns.

It is clear that approximating V_{ji}(i = 0 or 1) with a Gaussian distribution will have large discrepancy either in the head portion (small values) or the tail portion (large values) of V_{ji}. Alternatively, the Gamma distribution can better approximate V_{ji} in the head portion of V_{ji}; however, in the tail portion of V_{ji}, the Gamma distribution will have large deviation. On

the other hand, the Log-normal distribution can accurately approximate V_{ji} in a wide probability range from 0.0001 to 0.9999, and the approximated error becomes smaller as signal-to-noise ratio increases. Therefore, the stochastic model of the variances can be established to be of the log-normal distribution, which is expressed as:

$$f_V(\upsilon) = \frac{1}{\upsilon\beta\sqrt{2\pi}} \exp\left[\frac{-(\ln\upsilon - \alpha)^2}{2\beta^2}\right], \quad \upsilon>0, \tag{4.15}$$

where α and β, respectively, refer to the location and scale parameters of the log-normal distribution.

Eq. (4.15) lays the foundations for further performance analysis of the VD-based IR-UWB transceiver systems. In the next section, it is used to find the bit-error-rate of the proposed VD-based receiver.

4.4 BIT-ERROR-RATE OF THE VD-BASED RECEIVER

In this section, the performance of the proposed VD-based UWB receiver is evaluated. Based on the definitions in Section 4.3, the conditional error probability $P_{e|h(t)}$ of VD-based receivers for a given propagation channel $h(t)$ is given by

$$\begin{aligned} P_{e|h(t)} = {} & P(0)P\left(V_{j1} \geq V_{j0} \mid d_j = 0, h(t)\right) \\ & + P(1)P\left(V_{j1} < V_{j0} \mid d_j = 1, h(t)\right) \end{aligned}, \tag{4.16}$$

where $P(V_{j1} \geq V_{j0}|d_j = 0,h(t))$ is the probability that $V_{j1} \geq V_{j0}$ when 0 is sent in the j^{th} frame, and $P(V_{j1} < V_{j0}|d_j = 1,h(t))$ is the probability that $V_{j1} < V_{j0}$ when 1 is sent in the j^{th} frame.

As $d_j \in \{0,1\}$ are equiprobable binary information bits and $P(V_{j1} \geq V_{j0}|d_j = 0, h(t))$=$P(V_{j1} < V_{j0}|d_j = 1, h(t))$ for a symmetry binary communication system, the (4.16) can be simplified as

$$P_{e|h(t)} = P\left(V_{j1} < V_{j0} \mid d_j = 1, h(t)\right), \tag{4.17}$$

where V_{j1} and V_{j0} can be approximated with the Log-normal distribution, derived from (4.15), $\ln(V_{j1})$ and $\ln(V_{j0})$ will be of Gaussian distribution. Therefore, the change-of-variable technique described in [44] can be applied and (4.17) can be reformulated as:

$$\begin{aligned} P_{e|h(t)} &= P\left[\ln\left(V_{j,1}\right) < \ln\left(V_{j,0}\right) \mid d_j = 1, h(\mathrm{t})\right] \\ &= P\left[G_j^{VD} < 0 \mid d_j = 1, h(\mathrm{t})\right], \end{aligned} \tag{4.18}$$

where

$$G_j^{VD} = \ln\left(V_{j1}\right) - \ln\left(V_{j0}\right). \tag{4.19}$$

Since $\ln(V_{j1})$ and $\ln(V_{j0})$ can be approximated as Gaussian distribution, G_j^{VD} will be of Gaussian distribution. Therefore, the PDF of G_j^{VD} can be expressed as:

$$f_{G_j^{VD}|d_{j=1},h(\mathrm{t})}\left(x, m_g, \sigma_g\right) = \frac{1}{\sigma_g\sqrt{2\pi}} e^{-\frac{\left(x-m_g\right)^2}{2\sigma_g^2}}, \tag{4.20}$$

where m_g is the expectation of G_j^{VD}, as shown in Appendix I, m_g can be approximated by

$$m_g = E\left(G_j^{VD}\right) \approx \ln\left[E\left(V_{j1}\right)/E\left(V_{j0}\right)\right], \tag{4.21}$$

and σ_g^2 is the variance of G_j^{VD} with

$$\sigma_g^2 = Var\left(G_j^{VD}\right) = Var\left(\ln\left(V_{j1}\right)\right) + Var\left(\ln\left(V_{j0}\right)\right). \tag{4.22}$$

To compute (4.22), the following approximation for a random variable X is applied [56]:

$$\mathrm{Var}\left[f(X)\right] \approx \left(\frac{df\left(\mathrm{E}[X]\right)}{dX}\right)^2 \mathrm{Var}[X], \tag{4.23}$$

where $f(X)$ is a second-order differentiable function with its expectation, $E[X]$, and variance, $Var[X]$, being finite.

Application of (4.23) to (4.22) reads

$$\sigma_g^2 \approx Var\left(V_{j,1}\right)/E^2\left(V_{j,1}\right) + Var\left(V_{j,0}\right)/E^2\left(V_{j,0}\right). \tag{4.24}$$

Finally, combining (4.20), (4.21) and (4.24), $P_{e|h(t)}$ can be given by

$$\begin{aligned} P_{e|h(t)} &= P\left(G_j^{VD} < 0 \mid d_j = 1, h(\mathrm{t})\right) \\ &= \int_{-\infty}^{0} f_{G_j^{VD}|d_{j=1},h(\mathrm{t})}\left(x, m_g, \sigma_g\right) dx \\ &\approx Q\left(\frac{\ln\left[E\left(V_{j1}\right)/E\left(V_{j0}\right)\right]}{\sqrt{Var\left(V_{j1}\right)/E^2\left(V_{j1}\right) + Var\left(V_{j0}\right)/E^2\left(V_{j0}\right)}}\right), \end{aligned} \tag{4.25}$$

where $Q(.)$ is the Q-function defined in [22] that are applicable to both AWGN and CM1 channels.

As seen from (4.7), (4.9) and (4.14), V_{ji} involves up to fourth order moment of a random signal $r_{ji}(t)$. Therefore, derivation of $E\{V_{ji}\}$ and $Var\{V_{ji}\}$ become very challenging. By exploiting a discrete signal analysis approach, $E\{V_{ji}\}$ and $Var\{V_{ji}\}$ are derived with a series of painstaking but tractable stochastic analysis as follow.

Assume that the bandwidth of $y(t)$ is BW_y which covers from DC to BW. For an IR-UWB signal, typically $L=T_I \times BW_y >>1$. With sampling theorem, $y(t)$ is then expressed as

$$y(t) = \sum_{k=-\infty}^{\infty} y_k \phi(t - kT_s), \tag{4.26}$$

where $y_k = y(kT_s)$ is the sample of $y(t)$ at time $t=kT_s$, $T_s = \frac{1}{2BW_y}$ is the digital sampling period, and $\phi(t) = sin(\pi t/T_s)/(\pi t/T_s)$. Substituting (4.26) to (4.14), V_{ji} can be approximated by

$$\begin{aligned} V_{ji} &\approx \frac{1}{N}\sum_{k=0}^{N-1} y_{ji}^2(kT_s) - \frac{1}{N^2}\left(\sum_{k=0}^{N-1} y_{ji}(kT_s)\right)^2 \\ &= \frac{1}{N}\sum_{k=0}^{N-1} r_{ji}^4(kT_s) - \frac{1}{N^2}\left(\sum_{k=0}^{N-1} r_{ji}^2(kT_s)\right)^2 \\ &= \frac{1}{N}\sum_{k=0}^{N-1} r_{jik}^4 - \frac{1}{N^2}\left(\sum_{k=0}^{N-1} r_{jik}^2\right)^2, \end{aligned} \tag{4.27}$$

where $N = T_I/T_s$ is the number of the samples taken within the integration time interval T_I. $r_{jik} \triangleq r_{ji}(kT_s)$ is the notation of $r_{ji}(t)$ at sampling time $t = kT_s$.

4.4.1 The Derivation of Expectation, $E[V_{ji}]$

From (4.27), the expectation of V_{ji} is given by

$$\begin{aligned} E\{V_{ji}\} &= \frac{1}{N}E\left\{\sum_{k=0}^{M-1} r_{jik}^4 + \sum_{k=M}^{N-1} w_{jik}^4\right\} - \frac{1}{N^2}E\left\{\left(\sum_{k=0}^{M-1} r_{jik}^2 + \sum_{k=M}^{N-1} w_{jik}^2\right)^2\right\} \\ &= \frac{1}{N}E\left\{\sum_{k=0}^{M-1} r_{jik}^4 + \sum_{k=M}^{N-1} w_{jik}^4\right\} \\ &\quad - \frac{1}{N^2}E\left\{\sum_{k=0}^{M-1}\sum_{l=0}^{M-1} r_{jik}^2 r_{jil}^2 + \sum_{k=M}^{N-1}\sum_{l=M}^{N-1} w_{jik}^2 w_{jil}^2 + 2\sum_{k=0}^{M-1}\sum_{l=M}^{N-1} r_{jik}^2 w_{jil}^2\right\}, \end{aligned} \tag{4.28}$$

where $w_{jik} \equiv w_{ji}(kT_s)$ is the sampled value of $w_{ji}(t)$ at the sampled time $t = kT_s$ and $M = (T_p + \tau_{L-1})/T_s$ is the number of the samples of the received pulse $q_{ji}(t)$. Since T_I is chosen to be larger than the pulse duration $T_p + \tau_{L-1}$, it is clear that $M \le N$. In addition, $r_{ji1} = w_{ji1}$ for $M < k < N - 1$ since it falls outside the duration of symbol $q_{ji}(t)$.

By using the Appendix B, $E[V_{ji}]$ in (4.28) can be found as

$$E\{V_{ji}\} = \frac{M(3N-M-2)}{N^2}\sigma_{ri}^4 - \frac{2M(N-M)}{N^2}\sigma_{ri}^2\sigma_w^2 + \frac{(N-M)(M+2N-2)}{N^2}\sigma_w^4. \quad (4.29)$$

In the above equations, $\sigma_{r1}^2 = \sigma_q^2 + \sigma_w^2$ where $\sigma_q^2 = \frac{1}{T_q}\int_0^{T_q}[p(t) * h(t) * h_f(t)]^2\, dt$ is the variance of the received signal $q_{j1}(t)$ (*i.e.* the received signal power at receiver) and $\sigma_{r0}^2 = \sigma_w^2$ because of no signal presents (*i.e.* $q_{j0}(t) = 0$). $\sigma_w^2 = \sigma_n^2 + \sigma_i^2$ with $\sigma_n^2 = N_0 BW$ being the variance of the noises $n(t)$ and $\sigma_i^2 = P_I$ being the variance of the interference $i(t)$ with a power of P_I.

4.4.2 The Derivation of Variance, $Var[V_{ji}]$

The variance $Var\{V_{ji}\}$ can be expressed as

$$Var\{V_{ji}\} = E\{V_{ji}^2\} - E^2\{V_{ji}\}, \quad (4.30)$$

where $E\{V_{ji}\}$ has been found as (4.29) and $E\{V_{ji}^2\}$ is derived by:

$$\begin{aligned} E\{V_{ji}^2\} = {} & \frac{1}{N^2}E\left\{\left(\sum_{k=0}^{M-1} r_{jik}^4 + \sum_{k=M}^{N-1} w_{jik}^4\right)^2\right\} + \frac{1}{N^4}E\left\{\left(\sum_{k=0}^{M-1} r_{jik}^2 + \sum_{k=M}^{N-1} w_{jik}^2\right)^4\right\} \\ & - \frac{2}{N^3}E\left\{\left(\sum_{k=0}^{M-1} r_{jik}^4 + \sum_{k=M}^{N-1} w_{jik}^4\right)\left(\sum_{k=0}^{M-1} r_{jik}^2 + \sum_{k=M}^{N-1} w_{jik}^2\right)^2\right\}. \end{aligned} \quad (4.31)$$

By using the method shown in Appendix C and the moment theorem [23], we get the variance in (4.30) as follows,

$$
\begin{aligned}
Var\left\{V_{ji}\right\} &= E\left\{V_{ji}^2\right\} - E^2\left\{V_{ji}\right\} \\
&= \frac{1}{N^4}\Big(6M^3N - 18M^2N^2 + 18MN^3 - 6N^4 - 5M^3 - 60N^3 \\
&\quad - 108M^2N + 216MN^2 + 53M^2 + 60N^2 + 48M\Big)\cdot\sigma_{ri}^8 \\
&\quad + \frac{16}{N^4}M(N-M)(M-3N+2)\cdot\sigma_{ri}^6\sigma_w^2 \\
&\quad + \frac{8}{N^4}M(N-M)(N+2)\cdot\sigma_{ri}^4\sigma_w^4 \\
&\quad - \frac{16}{N^4}M(N-M)(M+2N-2)\cdot\sigma_{ri}^2\sigma_w^6 \\
&\quad + \frac{1}{N^4}\Big((N-M)(6M^2N - 12MN^2 + 6N^3 \\
&\quad - 5M^2 - 2MN + 103N^2 - 53M + 53N + 48)\Big)\cdot\sigma_w^8 , \quad i = 0,1 .
\end{aligned}
\tag{4.32}
$$

Based on (4.29) and (4.32), the analytical BER formula in (4.25) of the proposed VD-based IR UWB system can be obtained. The theoretical results presented in this paper can be used in the scenarios of NBI present and not present. If NBI is not present, the BER can be simply computed analytically by setting $P_I = 0$.

4.5 PERFORMANCE EVALUATION

In order to thoroughly assess the performance of the proposed VD-based receiver and validate the analytical results derived in the previous section, Monte Carlo simulations were employed to evaluate the BER performance and NBI mitigation ability of the proposed VD-based detector in both with- and without-NBI scenarios. Performance comparisons with the other nonlinear detection based receivers, conventional ED-based detector, and the FD-based detector [15] as well as with Rake receiver (which is the ideal receiver) are also given in this section.

In the following simulations, a BPPM IR-UWB modulation scheme is used as an example. The transmitted signal as defined by (4.1) contains a UWB pulse $p(t)$ which is compliant with IEEE 802.15.4a proposed standard and has the shape

$$p(t) = \frac{\sin(\pi t / T_p)}{\pi t / T_p} \cdot K(t,\eta) \cdot \cos(2\pi f_c t) \tag{4.33}$$

where $K(t,\eta)$ is the Kaiser window with a parameter η = 5.44. The pulse has a duration of T_p=20ns, a bandwidth of 2GHz, and a center frequency of f_c=4.1GHz.

The duration of the BPPM frame, T_f, is set as 400ns, and the integration interval, T_I, is set at 200ns at the receiver unless otherwise specified. In addition, an NBI is considered to have a bandwidth of 20MHz and a center frequency 3.5GHz, and a perfect synchronization is assumed.

4.5.1 In the Absence of NBI

When no NBI is present (i.e. P_I = 0), the BER improvement offered by the VD based receiver was thoroughly computed in AWGN channel and IEEE 802.15.4a CM1 multipath channels [43], respectively.

First, we investigate the effect of $h(t)$ on the BER performance of the VD-based receivers. The channel multipath phenomenon does influence the performance. To clearly explain the influence, we define a channel parameter as follows:

$$\Gamma = \frac{\frac{1}{T_I}\int_0^{T_I} h^4(t)dt - \left(\frac{1}{T_I}\int_0^{T_I} h^2(t)dt\right)^2}{\frac{1}{T_I}\int_0^{T_I} h_{\text{awgn}}^4(t)dt - \left(\frac{1}{T_I}\int_0^{T_I} h_{\text{awgn}}^2(t)dt\right)^2} \propto \frac{L}{L-1}\sum_{l=1}^{L}\alpha_l^4 - \frac{1}{L-1}\left(\sum_{l=1}^{L}\alpha_l^2\right)^2, \tag{4.34}$$

where $h(t)$ is a normalized impulse response of the multipath channel, given by (4.2), with gain α_l and total multipath number L. For the AWGN channel $h_{awgn}(t)$, the gain α_l is set as $\alpha_0 = 1$ and $\alpha_l = 0$, $l \in \{1,2,...,L-1\}$. In the VD-based system, the parameter is the ratio of the variance of $h^2(t)$ to the variance of $h^2_{awgn}(t)$, which measures the proportion of the power of strong multipath components in $h^2(t)$. As seen from (4.34), $0 < \Gamma < 1$ for multipath channels and $\Gamma = 1$ for AWGN channel.

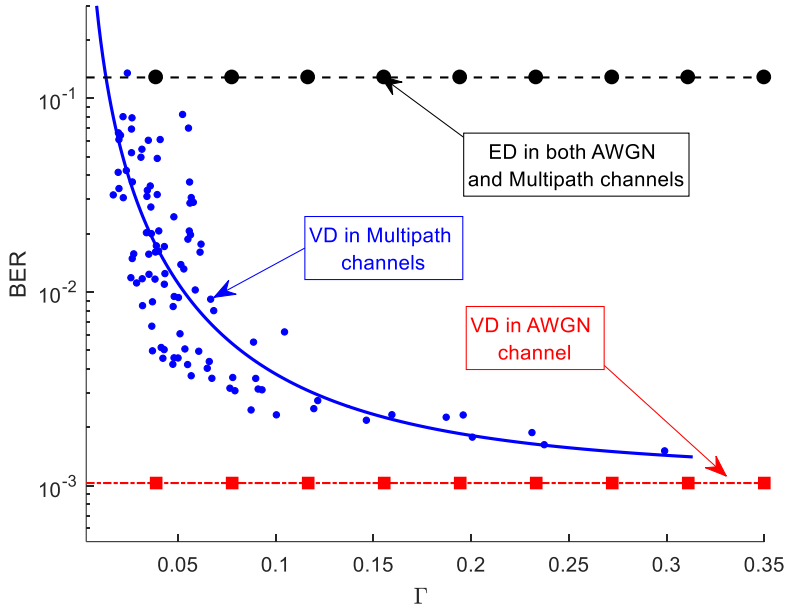

Figure 17 The multipath effect on BER performances of VD- and ED- based receivers. $E_b/N_0 = 15$ dB.

Fig. 17 shows the BER performance under different multipath conditions from IEEE 802.15.4a CM1 channel model. The multipath does degrade the BER performance. The larger Γ (less multipath), the better BER performance; when $\Gamma = 1$ (i.e. AWGN channel), VD gets the best performance. The larger Γ means that the received pulse power is more concentrated on a few strong multipath components. The VD can detect this better by measuring its variance than ED (since ED detects the total multipath energy which is

constant for all the difference channels). Therefore, the VD-based receiver has a better performance than ED in both AWGN and multipath channel conditions.

Next, we investigate the effect of $h(t)$ on our proposed theoretical analysis. Fig. 18 shows the theoretical and simulation results of BER in different multipath channels. As shown in the figure, the theoretical results match the simulation results well. The approximated error decreases as E_b/N_0 increases; this is because the cross-term of signal by noise/interference in (4.9) becomes smaller with the increasing of E_b/N_0 and the actual distribution of V_{ji} moves closer towards log-normal distribution as shown in Fig. 16. Furthermore, in comparisons with the ED- based receiver, the VD- based receiver has a E_b/N_0 improvement of 2 ~ 5dB at the BER=10^{-4} in different multipath channels. The larger Γ, the better performance improvement.

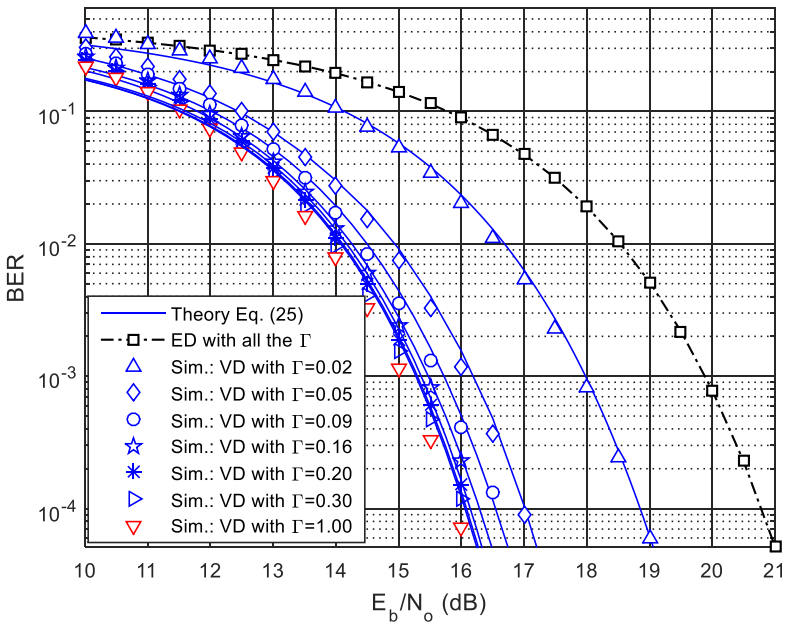

Figure 18 BER performances for the VD- and ED- based receivers with different multipath channel conditions.

4.5.2 In the Presence of NBI

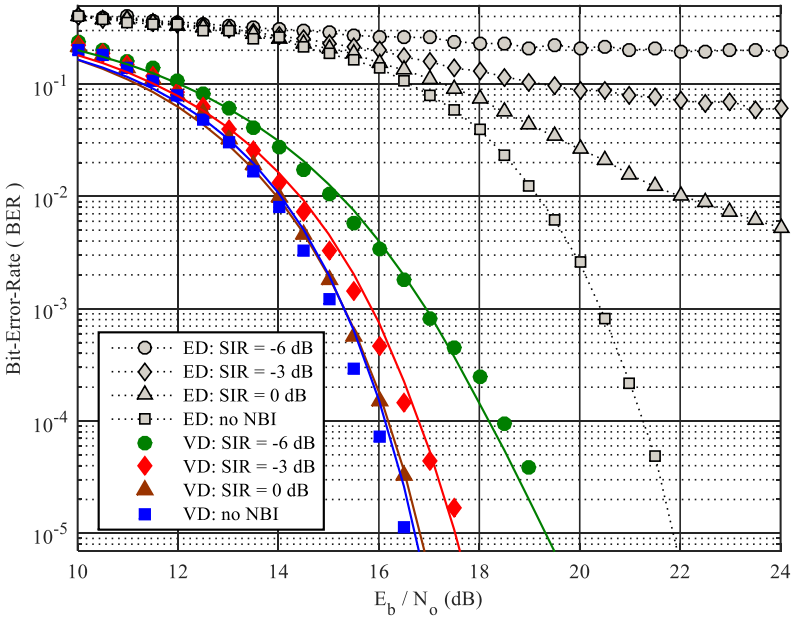

(a) AWGN

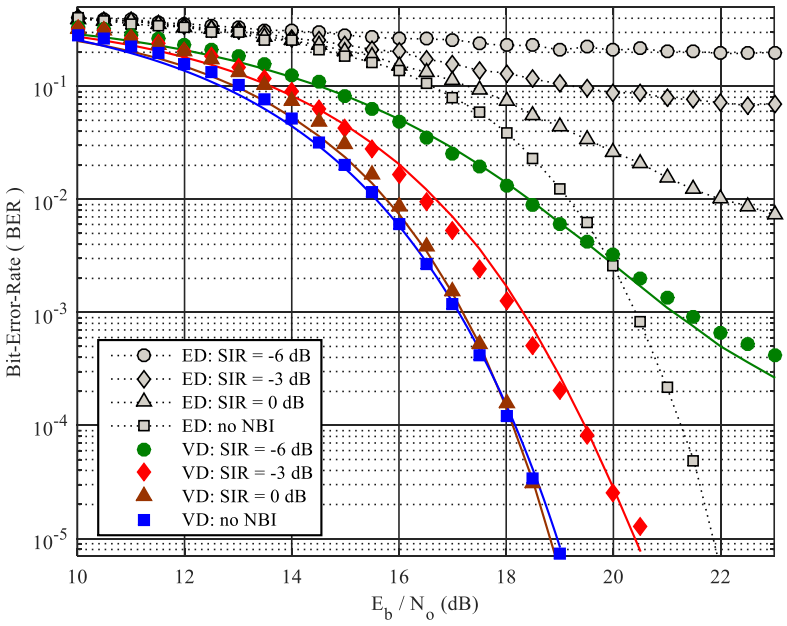

(b) CM1

Figure 19 BER performances of the VD-based and ED-based receivers in AWGN (left) and multipath CM1 (right) channels with different NBIs. The solid lines are the theoretical results of (4.25), and circular and square dots are the simulation results.

Figs. 19, 20, 21 and 22 present the results when NBI is present.

Fig. 19 is obtained when signal-to-interference ratio (SIR) is varied from 0dB, to -3dB and to -6dB. It shows that the BER performance of the conventional ED-based receiver is unacceptably poor, while the VD-based receiver can still achieve decent BER performance even when SIR is lower than 0dB under both the AWGN channels and the CM1 channel conditions.

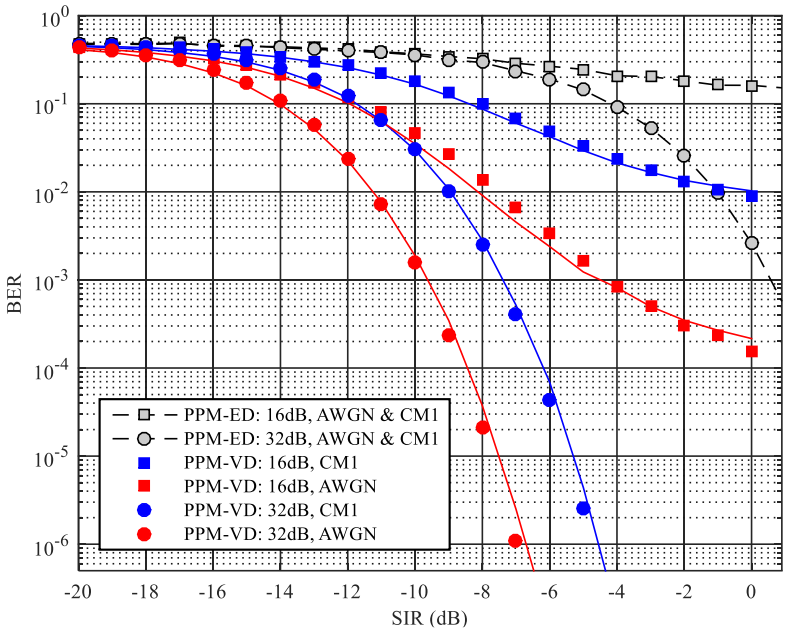

Figure 20 NBI mitigation performances of the VD-based and ED-based receivers in AWGN and multipath CM1 channels. The solid lines are the theoretical results of (4.25), and circular and square dots are the simulations results.

Fig. 20 shows the results when the SIR is changed and E_b/N_0 is fixed at 32dB and 16dB, respectively. As compared with the ED-based receivers at BER of 10^{-3}, the VD-based receivers can achieve a NBI performance improvement of 8dB in CM1 and 10dB in AWGN for E_b/N_0 of 32dB. In other words, the ED-based receiver is vulnerable to NBI,

while the VD-based receiver has an inherent ability to mitigate the destructive effects caused by NBI.

4.5.3 Comparison with the FD-based Receiver

The proposed VD-based receiver was also compared with the FD-based receiver [15]. Fig. 21 and Fig. 22 show the BER results with different receivers. The ideal receiver, the full Rake receiver, was also simulated and its results are shown for reference.

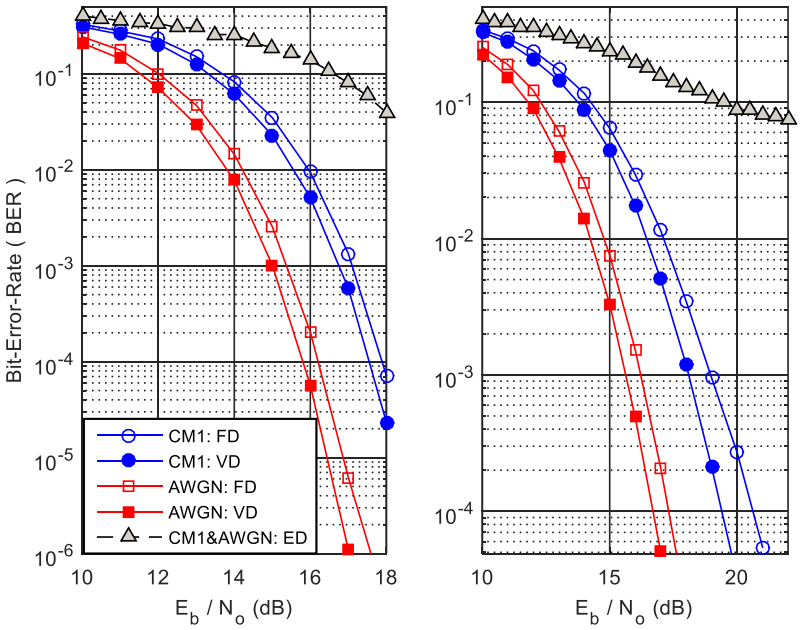

Figure 21 The BERs of the VD-, FD- and ED-based receivers under AWGN and multipath CM1 channel conditions without NBI (left) or with NBI (right). T_I = 200 ns, *SIR*= -3 dB.

From the Fig. 21, we can see that the VD-based receiver has a marginally better performance than the FD-based receiver when NBI does not exist; however, it performs better than the FD-based receiver when an NBI of -3dB is present.

Fig. 22 shows the impact of different interference levels or SIRs. The conventional ED-based receiver has the worst performance and surely the ideal coherent Rake-based receiver has the best performance. In all cases, the proposed VD-based receiver is superior to the FD- and ED- based receivers.

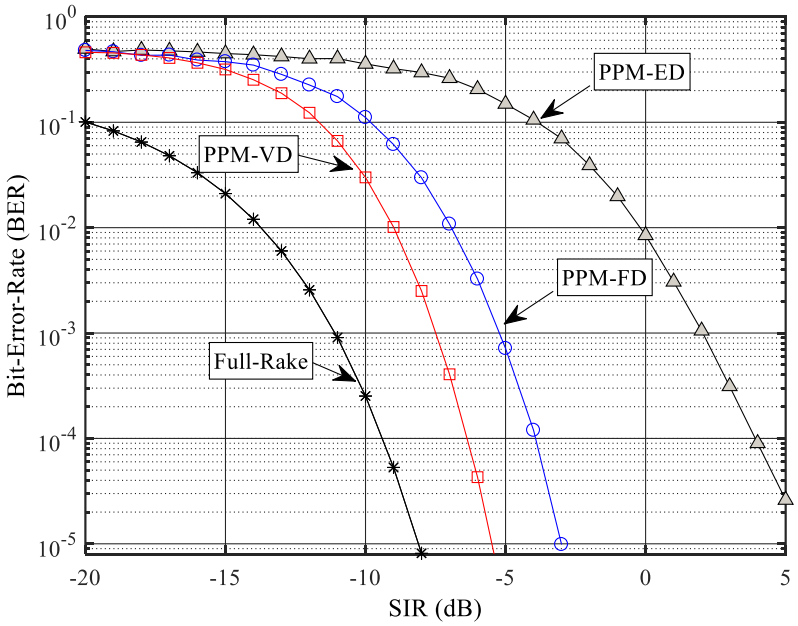

Figure 22 The impact of the NBI on BERs of the VD-, ED-, FD- and Rake-based receivers. *Eb/No* = 32 dB, T_I = 200 ns, BW_I =20M Hz, f_I = 3.326 GHz, under CM1 channel condition.

4.6 CONCLUSION

In this chapter, we present a non-coherent IR-UWB system based on VD technology and then evaluate its performances analytically and empirically. We find and show that the log-normal model is the best-fit model for the VD-based detection. With the log-normal model, the analytical formula for the BER of the VD-based system with and without NBI in both AWGN and CM1 channels has been derived for the first time. Our results show that as compared with the conventional ED-based receiver, the proposed VD- based

receiver can achieve a much better BER performance. In particular, unlike the conventional ED-based receiver which is vulnerable to NBI, the VD-based receiver has an inherent ability to mitigate the destructive effects caused by strong NBI. Therefore, the VD-based receiver is recommended as a preferred detection technology for IR -UWB systems. Finally, our initial results show that the performance of the VD-based receiver can degrade significantly due to multipath effects. Further analysis on the effect of multipath and new techniques to mitigate them deserve further investigation and research.

CHAPTER 5 A UNIFYING GENERALIZED NONLINEAR DETECTIONS FOR IMPULSE RADIO UWB SYSTEMS

In this chapter, based on our published paper [16], [61] and [62], a unified framework, denoted as the Generalized Nonlinear Detector (GND), is developed to encompass existing nonlinear detection technologies as well as further optimize the performance of nonlinear detection for non-coherent IR-UWB receivers. Computer simulations show that independent of absence or presence of NBIs, the GND-based receivers can achieve much better BER performance than the ED based receivers under both AWGN and multipath channels. Furthermore, as compared to the existing nonlinear detection algorithms, the GND algorithm with a well selected value always has the best BER performance and the strongest ability to resist NBIs.

5.1 INTRODUCTION

Using short duration pulses to carry information, IR-UWB technologies have the advantages of low complexity, high achievable data rates, low power consumption, and good time-domain resolution, which make it emerge as a strong candidate for low complexity and low power applications, such as wireless personal area network (WPAN), wireless body area network (WBAN), and wireless sensor network [45-48]. The IR UWB approach has been selected by the IEEE WPAN standard 802.15.4a in 2007 [48], and the IEEE WPAN standard 802.15.6 standard in 2012 [49]. However, the received IR UWB signals may consist of a large amount of resolvable MPCs [50], which makes the design of IR UWB receiver become a challenging work. Using traditional coherent detection approaches, such as the Rake receiver, to process those MPCs often leads to an unacceptably

high system complexity [9]. To capture signal energy from more MPCs with low system complexity, a group of non-coherent ED based transceiver technologies have been proposed, such as, on-off keying (OOK) transceiver [6], PPM-ED transceiver [7], FSR transceiver [8], CSR transceiver [9], and DCSR transceiver [10].

As compared to a coherent receiver, the ED-based receivers are more vulnerable to noise and interferences [18], because the detectors in the ED-based receivers cannot distinguish noise and interferences from the desired UWB signals, thus the energy of noise and interferences is collected and processed as signal energy as well. Meanwhile, due to the wide bandwidth of IR UWB systems, the received IR UWB signals are typically corrupted by not only wideband AWGN but also strong NBIs. Therefore, various advanced signal processing technologies have been developed to mitigate the destructive effects of AWGN and NBIs [15]. For example, to achieve a better performance as well as maintain low system complexity, some recent researches replace the square-law operation in the ED-based receivers with higher order nonlinear operations, such as kurtosis detection [15], fourth-order detection [15] and variance detection [16]. Computers simulations show that those nonlinear detection technologies can considerably mitigate the destructive effects of AWGN and NBIs.

In this chapter, we have developed a unified framework, denoted as generalized nonlinear detection (GND), to encompass the existing nonlinear detection technologies as well as further optimize the performance of nonlinear detection. In the KD, the nonlinear detection output is given by [15]:

$$K = \frac{1}{T_I}\int_0^{T_I} r^4(t)dt - \frac{3}{T_I^2}\left[\int_0^{T_I} r^2(t)dt\right]^2. \tag{5.1}$$

In the FD, the nonlinear detection output is given by [15]:

$$F = \frac{1}{T_I}\int_0^{T_I} r^4(t)dt\,. \tag{5.2}$$

In the VD, the nonlinear detection output is given by [16]:

$$V = \frac{1}{T_I}\int_0^{T_I} r^4(t)dt - \frac{1}{T_I^2}\left[\int_0^{T_I} r^2(t)dt\right]^2. \tag{5.3}$$

In the proposed GND, a common system parameter β is applied to unify those nonlinear detectors into a unified framework:

$$G = \frac{1}{T_I}\int_0^{T_I} r^4(t)dt - \frac{\beta}{T_I^2}\left[\int_0^{T_I} r^2(t)dt\right]^2, \tag{5.4}$$

where β=3 for the KD, β=0 for the FD, and β=1 for the VD. Furthermore, by exploring the effect of β value on the performance of the GND, we found that the optimal value for β is not 0, 1, or 3, but a value around 2.2. Independent of the value of β, unlike the ED-based receivers, which are vulnerable to NBIs, the GND-based receiver has an inherent ability to mitigate the destructive effects caused by strong NBIs.

The organization of the paper is as follows. In Section 5.2, the system structure of a GND-based receiver for a binary pulse position modulated (BPPM) IR-UWB system is described. Section 5.3 presents in detail the comparisons between the GND-based detection algorithm and the ED-based detection algorithm. In section 5.4, through computer simulations, the bit-error rate (BER) performance of the proposed GND-based receiver is thoroughly investigated and compared with the ED-based receiver. Finally, the conclusions of this paper are given in Section 5.5.

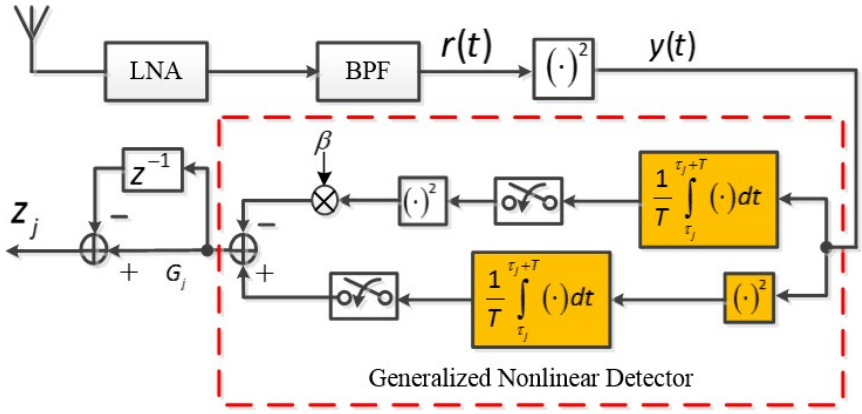

Figure 23 System structure of a GND-based receiver for a BPPM IR-UWB system

5.2 System Configuration of GND-based Receiver

In a GND-based receiver, as shown in Fig. 23, demodulation is based on the signal measured over a specific time interval ($0 < t < T_I$). First, at the RF front end, the received IR-UWB signal is amplified by a low noise amplifier (LNA) and filtered by the BPF to remove out-of-band noise and interferences. Then the filtered signal, denoted by $r(t)$, is sent to a square law device to get the squared IR-UWB signal $y(t)$. Next, the proposed GND is employed to measure the value of G_{j0} over the time interval from $jT_f + \tau_0$ to $jT_f + \tau_0 + T_I$ and that of G_{j1} over the time $jT_f + \tau_0 + T_f/2$ to $jT_f + \tau_0 + T_f/2 + T_I$, where the value of G_{ji} is obtained by:

$$G_{ji} = \frac{1}{T_I} \int_{jT_S+\tau_0+iT_f/2}^{jT_S+\tau_0+iT_f/2+T_I} y^2(t)dt - \frac{\beta}{T_I^2}\left[\int_{jT_S+\tau_0+iT_f/2}^{jT_S+\tau_0+iT_f/2+T_I} y(t)dt\right]^2, \qquad i = 0,1 \tag{5.5}$$

In the above equation, the adjustable parameter β allows us not only to unify the existing nonlinear detectors ($\beta = 3$ for the KD [15], $\beta = 0$ for the FD [15], and $\beta = 1$ for the VD

[35]), but also to optimize the value of β for a better performance. Finally, the j^{th} information bit is recovered with the following rule:

$$\hat{d}_j = \begin{cases} 0, & Z_j^{GND} = G_{j1} - G_{j0} < 0, \\ 1, & Z_j^{GND} = G_{j1} - G_{j0} \geq 0. \end{cases} \tag{5.6}$$

5.3 DETECTION ALGORITHM COMPARISONS

In order to compare the GND-based detection algorithm with the ED-based detection algorithm, without loss of generality, the case of d_j=1 is considered in this section. Thus, for the time interval from $jT_f + \tau_0$ to $jT_f + \tau_0 + T_I$, $r(t)$ is given by:

$$r_{j0}(t) = n_{j0}(t) + i_{j0}(t), \tag{5.7}$$

and after passing a square device, $y(t)$ is given by:

$$y_{j0}(t) = \left[n_{j0}(t) + i_{j0}(t) \right]^2, \tag{5.8}$$

Similarly, for the time interval from $jT_f + \tau_0 + \frac{T_f}{2}$ to$jT_f + \tau_0 + \frac{T_f}{2} + T_I$, $r(t)$ is given by:

$$r_{j1}(t) = q(t) + n_{j1}(t) + i_{j1}(t), \tag{5.9}$$

and $y(t)$ is given by:

$$y_{j1}(t) = q^2(t) + \left[n_{j1}(t) + i_{j1}(t) \right]^2 + 2q(t)\left[n_{j1}(t) + i_{j1}(t) \right]. \tag{5.10}$$

In the above equation, $q^2(t)$ is the UWB term, $\left[n_{j1}(t) + i_{j1}(t)\right]^2$ is the noise/interference term, and $2q(t)\left[n_{j1}(t) + i_{j1}(t)\right]$ is the cross-term between UWB signal and noise/interference. Furthermore, $i_{j1}(t) = 0$ and $i_{j0}(t) = 0$ if no NBI is present.

5.3.1 ED-based Detection Algorithm

In the ED-based detection algorithm, the energy of $r(t)$ is measured as follows:

$$E_{ji} = \int_{jT_S+\tau_0+iT_f/2}^{jT_S+\tau_0+iT_f/2+T_I} y(t)dt, \quad i = 0,1, \tag{5.11}$$

and the *j*th information bit is recovered according to the following rule:

$$\hat{d}_j = \begin{cases} 0, & Z_j^{ED} = E_{j1} - E_{j0} < 0, \\ 1, & Z_j^{ED} = E_{j1} - E_{j0} \geq 0. \end{cases} \tag{5.12}$$

For the case of d_j=1, according to (5.11), (5.13), (5.14), and (5.15), the decision variable, Z_j^{ED}, can be derived as follows:

$$\begin{aligned} Z_j^{ED} = & \int_0^{T_I} q^2(t)dt + 2\int_0^{T_I} q(t)\left(n_{j1}(t) + i_{j1}(t)\right)dt \\ & + \left[\int_0^{T_I}\left(n_{j1}(t) + i_{j1}(t)\right)^2 dt - \int_0^{T_I}\left(n_{j0}(t) + i_{j0}(t)\right)^2 dt\right]. \end{aligned} \tag{5.13}$$

From the above equation, we can conclude that the value of Z_j^{ED} is adversely effected by both the noise/interference term, $\left[\int_0^{T_I}\left(n_{j1}(t) + i_{j1}(t)\right)^2 dt - \int_0^{T_I}\left(n_{j0}(t) + i_{j0}(t)\right)^2 dt\right]$, and the cross-term, $2\int_0^{T_I} q(t)\left(n_{j1}(t) + i_{j1}(t)\right)dt$, which make the BER performance of ED-based receivers poor.

5.3.2 GND-based Detection Algorithm

In the GND-based detection algorithm, the G_{ji} value of $r(t)$ is measured as follows:

$$G_{ji} = \frac{1}{T_I}\int_{jT_S+\tau_0+iT_f/2}^{jT_S+\tau_0+iT_f/2+T_I} r^4(t)dt - \frac{\beta}{T_I^2}\left[\int_{jT_S+\tau_0+iT_f/2}^{jT_S+\tau_0+iT_f/2+T_I} r^2(t)dt\right]^2, \quad i = 0,1 \tag{5.14}$$

For the case of d_j=1, according to (5.7), (5.9), and (5.14), the decision variable, Z_j^{GND}, can be derived as follows:

$$Z_j^{GND} = S_j^{GND} + NI_j^{GND} + C_j^{GND}. \tag{5.15}$$

where S_j^{GND} is the UWB term given by:

$$S_j^{GND} = \frac{1}{T_I}\int_0^{T_I} q^4(t)dt - \frac{\beta}{T_I^2}\left[\int_0^{T_I} q^2(t)dt\right]^2 \tag{5.16}$$

NI_j^{GND} is the noise/interference term given by:

$$NI_j^{GND} = \frac{1}{T_I}\left\{\int_0^{T_I}\left[n_{j1}(t)+i_{j1}(t)\right]^4 dt - \int_0^{T_I}\left[n_{j0}(t)+i_{j0}(t)\right]^4 dt\right\}$$

$$-\frac{\beta}{T_I^2}\left\{\left(\int_0^{T_I}\left[n_{j1}(t)+i_{j1}(t)\right]^2 dt\right)^2 - \left(\int_0^{T_I}\left[n_{j0}(t)+i_{j0}(t)\right]^2 dt\right)^2\right\}, \tag{5.17}$$

and C_j^{GND} is the cross-term term given by:

$$\begin{aligned} C_j^{GND} = {} & \frac{6}{T_I}\int_0^{T_I} q^2(t)\left[n_{j1}(t)+i_{j1}(t)\right]^2 dt + \frac{4}{T_I}\int_0^{T_I} q^3(t)\left[n_{j1}(t)+i_{j1}(t)\right]dt \\ & + \frac{4}{T_I}\int_0^{T_I} q(t)\left[n_{j1}(t)+i_{j1}(t)\right]^3 dt - \frac{4\beta}{T_I^2}\left[\int_0^{T_I} q(t)\left[n_{j1}(t)+i_{j1}(t)\right]dt\right]^2 \\ & - \frac{2\beta}{T_I^2}\int_0^{T_I} q^2(t)dt\int_0^{T_I}\left[n_{j1}(t)+i_{j1}(t)\right]^2 dt \\ & - \frac{4\beta}{T_I^2}\int_0^{T_I} q^2(t)dt\int_0^{T_I} q(t)\left[n_{j1}(t)+i_{j1}(t)\right]dt \\ & - \frac{4\beta}{T_I^2}\int_0^{T_I}\left[n_{j1}(t)+i_{j1}(t)\right]^2 dt\int_0^{T_I} q(t)\left[n_{j1}(t)+i_{j1}(t)\right]dt. \end{aligned} \tag{5.18}$$

Because both $q(t)$ and $\left[n_{j1}(t)+i_{j1}(t)\right]$ have a zero mean, and they are independent with each other, C_j^{GND} can be approximated by

$$C_j^{GND} \approx \frac{6}{T_I}\int_0^{T_I} q^2(t)\left[n_{j1}(t)+i_{j1}(t)\right]^2 dt - \frac{2\beta}{T_I^2}\int_0^{T_I} q^2(t)dt\int_0^{T_I}\left[n_{j1}(t)+i_{j1}(t)\right]^2 dt\,. \tag{5.19}$$

Typically, the value of $\int_0^{T_I} q^2(t)\left[n_{j1}(t)+i_{j1}(t)\right]^2 dt$ is larger than that of $\int_0^{T_I} q^2(t)dt\int_0^{T_I}\left[n_{j1}(t)+i_{j1}(t)\right]^2 dt$, and hence when β is set at a proper value, C_j^{GND} is

a positive value. Thus, unlike the cross-term in the ED-based detection algorithm, which could be a negative value and has an adverse effect on the value of Z_j^{ED}, the cross-term in the GND-based detection algorithm has a positive effect on the value of Z_j^{GND}, and hence the newly proposed GND-based detection algorithm can achieve much better performance than the ED-based detection algorithm, especially when strong AWGN and/or NBI is present.

Furthermore, from (5.19) we can conclude that as the value of β increases from zero, the absolute value of NI_j^{GND} decreases, and hence the adverse effect of NI_j^{GND} on Z_j^{GND} is mitigated. Therefore, although the values of Z_j^{GND} and C_j^{GND} decrease as well when β increases, a well selected value of β can allow the GND-based receiver achieving better BER performance than the FD, the KD, and the VD technologies.

5.4 Parameter Optimization and Performance Evaluation

In order to evaluate the optimal value for β and thoroughly investigate the BER performance and NBI mitigation ability of the GND-based receivers, various computer simulations have been undertaken in both with-NBI and without-NBI scenarios. In the computer simulations, the BPPM IR-UWB modulation scheme is used as an example for the case study. In the BPPM IR-UWB modulation scheme, UWB pulses with a duration of T_p=20ns, a bandwidth of BW=2GHz, and a center frequency of 4.1GHz is used as the transmitted signal. The duration of the BPPM frame is set as T_f=400ns and T_I is fixed at 200ns in the receiver. In addition, an NBI with bandwidth 20MHz and center frequency 3.5GHz is applied. In the computer simulations, it is assumed that a perfect synchronization is achieved.

5.4.1 Parameter Optimization

In order to evaluate the effect of β on the BER performance of the GND-based receivers, various simulations have been undertaken to obtain the BERs of the system as a function of β ranging from 0 to 4, under an AWGN channel and the IEEE802.15.4a CM1 multipath channels [51]. During the simulations, E_b/N_0 is fixed at 15dB for the AWGN channel and 17dB for the CM1 channels and a strong NBI with SIR equal to -3dB is added. From the simulation results shown in Fig. 24, we can conclude that with the value of β increasing, the BERs of the GND-based receivers decrease initially and then increase; more specifically, the optimal value for β appears at around 2.2. In other words, the existing nonlinear detectors (β =0 for the FD, β =1 for the VD, and β =3 for the KD) are far away from an optimal nonlinear detector, and a well selected value can further improve the BER performance of IR-UWB receivers based on nonlinear signal processing technologies.

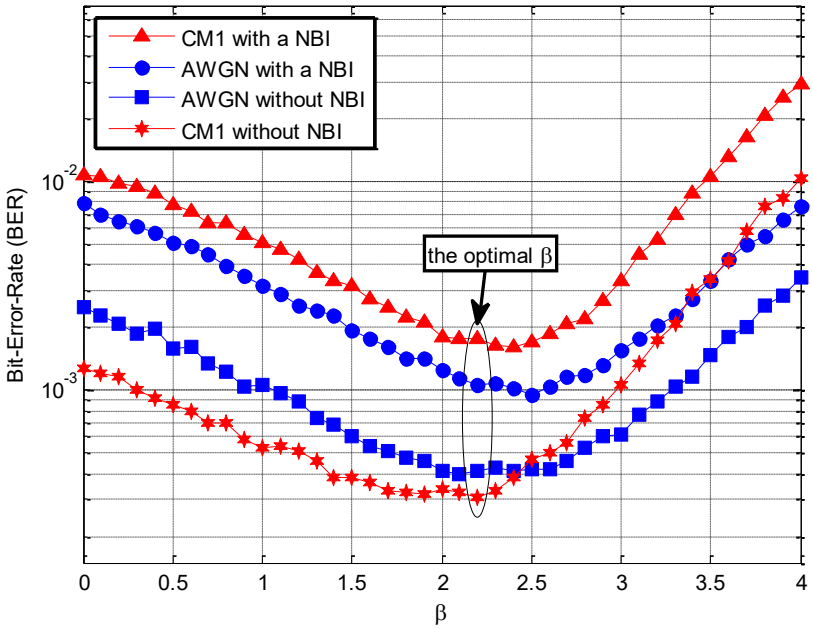

Figure 24 BER performance of the GND-based receivers as a function of β.

5.4.2 In the Absence of NBI

When no NBI was presented, the BER improvement offered by the GND-based receiver was thoroughly investigated under an AWGN channel and the IEEE 802.15.4a CM1 multipath channels, respectively, and the obtained simulation results are shown in Fig. 25. Obviously, under both the AWGN channel and the CM1 multipath channels, all nonlinear detection based receivers can achieve much better BER performance than the ED-based receiver, and the higher the SNR, i.e. E_b/N_0, the greater the performance improvement. Furthermore, the GND-based receiver with a well selected β value always has the best BER performance.

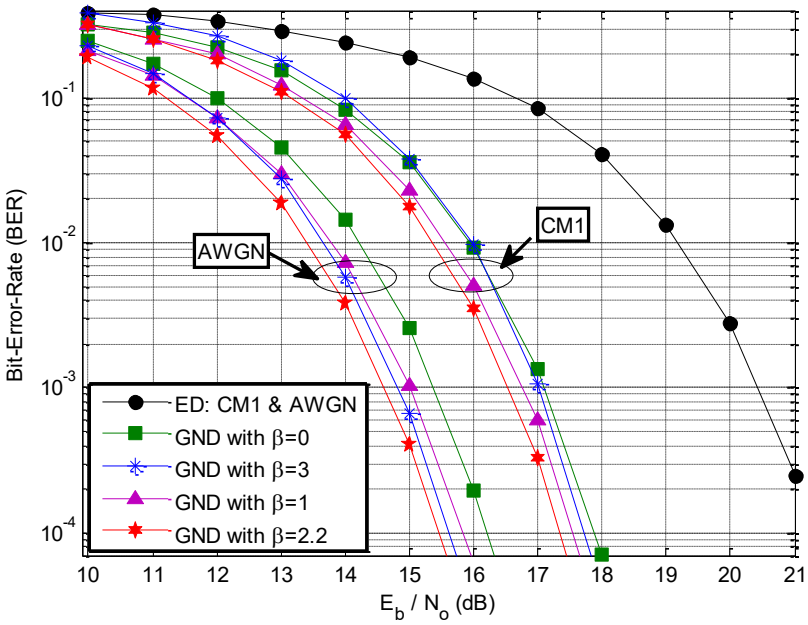

Figure 25 BER performance of the GND- and ED-based receivers under AWGN and CM1 channels without NBI.

5.4.3 In the Presence of NBI

In order to investigate the NBI mitigation ability of the GND-based receivers, more simulations have been undertaken for the scenarios when a strong NBI is present. During the simulations, the NBI is set to have a stronger power than the IR-UWB signals, i.e., $SIR = -3dB$. With the presence of the NBI, the BER performance of the GND-based receivers and that of the ED-based receiver have been investigated as a function of E_b/N_0 and the obtained simulation results are shown in Fig. 26.

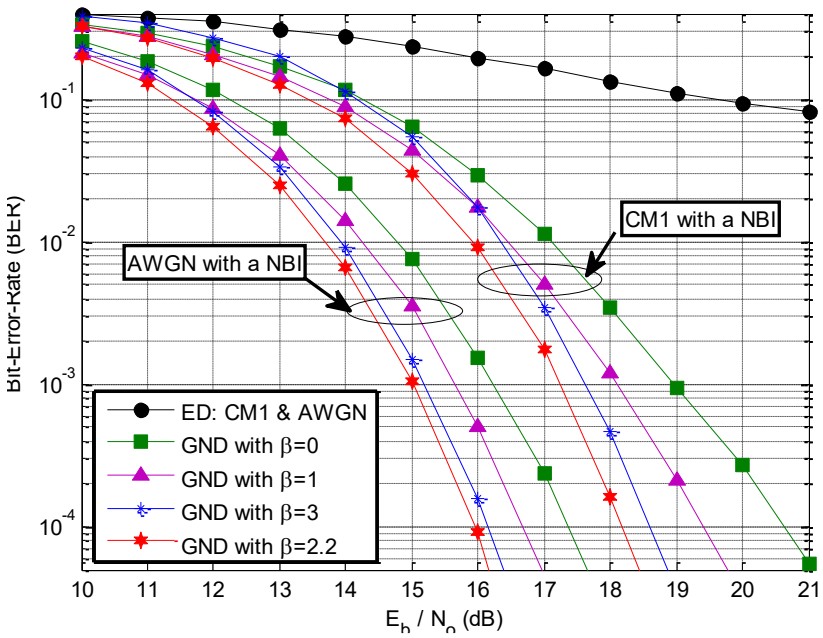

Figure 26 BER performance of the GND- and ED-based receivers under AWGN and CM1 channels with a strong NBI of *SIR*= -3 dB

As shown in Fig. 26, when a strong NBI is present, the BER performance of the ED-based receiver becomes unacceptably poor. Meanwhile, all nonlinear detection based receivers still can achieve decent BER performance under both the AWGN channels and the CM1 channels. Not surprisingly, the GND- based receiver with a well selected value

again has the best BER performance, and the higher SNR, the greater the performance improvement.

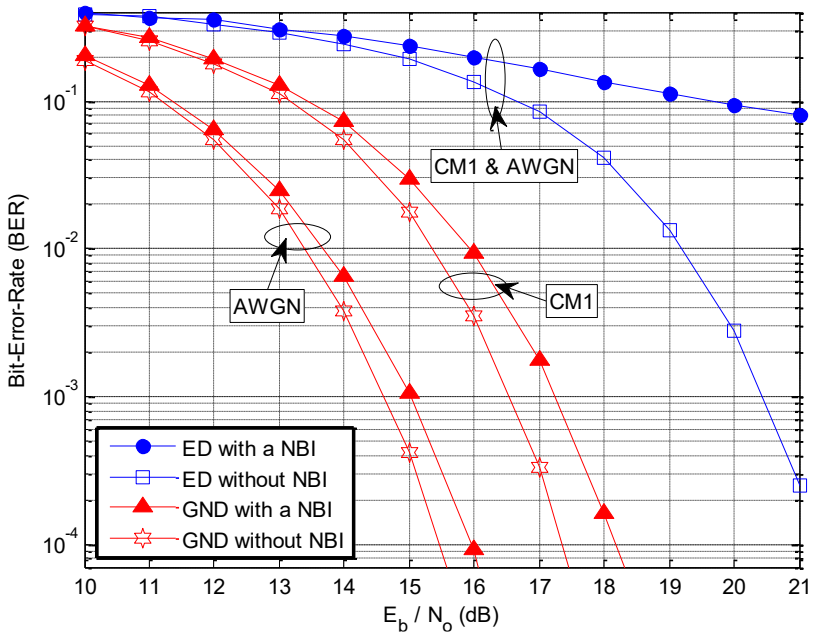

Figure 27 BER performance degradations caused by a strong NBI.

In order to demonstrate the inherent ability of the GND-based receiver on mitigating the destructive effects caused by a strong NBI, the degradations in BER performance caused by a strong NBI are illustrated in Fig. 27 for both the GND-based receiver with β = 2.2 and the ED-based receiver. Obviously, the ED-based receiver does not have the ability to resist a strong NBI and has serious degradations in BER performance when a strong NBI is present. On the contrary, the GND-based receiver shows an excellent ability for mitigating the destructive effects caused by a strong NBI. For example, at $BER = 10^{-3}$, a strong NBI with $SIR = -3dB$ only degrades the performance of the GND-based receiver by less than 0.5dB under an AWGN channel and less than 1dB under the CM1 multipath channels.

5.5 CONCLUSION

In this chapter, a unified framework, denoted as GND, is developed to encompass the existing nonlinear detection technologies as well as further optimize the performance of nonlinear detection for non-coherent IR-UWB receivers. By thoroughly exploring the effect of value on the performance of the GND, we found that the optimal value for β is not 0, 1, or 3, but a value around 2.2. Independent of the value of β, the GND based receiver can achieve a much better BER performance under both AWGN and multipath channels. Furthermore, unlike the conventional ED-based receiver, which is vulnerable to NBI, the GND-based receiver has an inherent ability to mitigate the destructive effects caused by a strong NBI. Therefore, the GND-based receivers can be considered a preferred detection technology for IR-UWB systems.

CHAPTER 6 SQUARE LAW BASED NONLINEAR SIGNAL PROCESSING TECHNIQUES FOR UWB IMPULSE RADIOS

In this chapter, based on our published paper [57] and the reference paper [56], a novel NBI mitigation technique, multiband square law (MSL), is presented for the ED-based IR-UWB receivers. By using a group of band-pass filters, the received signal processed by the MSL device is separated into multiple sub-bands, and then the sub-band with serious NBI will be omitted to improve the NBI mitigation performance. Simulation results show that without any NBI prior knowledge, the proposed MSL based technique can significantly improve the signal-to-interference ratio (SIR) of the received IR-UWB signal and the system performance of the ED-based receivers when one or two NBIs present(s). Furthermore, unlike the Teager-Kaiser operator (TKO) technique, which is difficult to implement in hardware since that the differential operators are carried out in a bandwidth of at least 500MHz, the MSL technique can be implemented with commercially available products and achieve the same performance as the TKO technique [56]. Thus, the MSL technology is an implementable and high effective blind NBI mitigation technology for the ED-based IR-UWB systems.

6.1 INTRODUCTION

The ED-based non-coherent IR-UWB receiver has the potential advantages of low power consumption and low processing complexity, which make it an ideal candidate for low cost, low power consumption and low data rate applications, such as the IEEE 802.15.4a and IEEE 802.15.6 standard wireless personal area networks [45] [46]. This rather new technology is assigned the frequency band of 3.1 GHz to 10.6 GHz by the FCC,

where it is permitted to coexist with the other wireless communication systems without requiring a license. This permission, however, is valid under the condition that the transmitted UWB signal has a very low power spectral density (not higher than -41.3dBm/MHz). Due to the restraint on their transmission power level, the UWB systems unavoidably suffers from the interference caused by the coexisting narrowband systems which transmit at much higher power levels. This NBI can sometimes be so effective that the IR-UWB communication is totally jammed. Therefore, IR-UWB receivers must have a high processing gain to cope with these NBIs.

However, NBI processing in IR-UWB receiver design is a more challenging problem. First, comparing the licensed wideband systems, such as CDMA, the unlicensed IR-UWB extends a much wider frequency band, while transmitting less power. This forces the IR-UWB systems to coexist with a higher number of powerful interferers. Typically, the power of these NBIs can be up to a few tens of dBs [45]. More significantly, in carrier modulated wideband systems, the received signal is down-converted to the baseband and sampled above the Nyquist rate, which allows numerous efficient NBI suppression algorithms based on the digital signal processing techniques. However, in IR-UWB, the desired signal is already in the baseband, sampling the received signal at the Nyquist rate requires an extremely high sampling frequency, which is not possible with the existing technology. In addition to the high sampling rate, the ADC must support a very large dynamic range to resolve the signal from the strong NBIs. Currently, such ADCs are far from being practical [52]. An alternative is to apply notch filtering before the signal detector; however, this method requires a number of narrowband analog filter banks. Since the frequency and power of the narrowband interferers can vary, employing analog filtering adds complexity, cost, and size to the IR-UWB receivers. As a result, many of the NBI suppression

techniques applied to other wideband systems are either not applicable for IR-UWB, or complexities of these methods are too great for the IR-UWB receiver requirements.

Given the low complexity requirements in both hardware and computation, and considering the other limitations such as low-power and low-cost transceiver design, recently, nonlinear signal processing technologies, which can fully utilize the special characteristics of IR-UWB signals, have been explored for the ED-based receivers to improve the system performance and the NBI mitigation abilities. The Teager-Kaiser technique use a nonlinear device TKO and a high pass filter (HPF) to remove an NBI before the IR-UWB signals are detected. As shown in [19], when a signal with a frequency band between f_1 and f_2 is sent into a TKO, the frequency band of the output signal falls in between DC and f_2- f_1. An NBI is then shifted to a frequency band close to DC and hence can be removed easily with a HPF. However, the TKO technology is very difficult to implement in hardware [56]. Therefore, another novel nonlinear signal processing technology, called the square law (SL) technique is proposed by using a SL device with a BPF instead of a TKO with a HPF [56]. Since those techniques do not need any prior knowledge of the NBI, it attracts an increasing attention in recent years [19-20, 53-57].

In our following investigation, we find that the SL technique can work well in just only one NBI exists. However, when two or more NBI exist, the SL technique has a poor NBI mitigation performance, as the crossing component of multiple NBIs cannot be shifted to a low frequency band close to DC by the SL device, this strong component seriously degrades the system performance. To address this problem, in this chapter, a novel nonlinear signal processing technology, MSL, is proposed to improve the NBI mitigation ability of the conventional SL technology when two or more NBI present.

The organization of the chapter is as follows. Sections 6.2, 6.3 and 6.4 describe two new nonlinear processing technologies for the ED -based IR-UWB systems, and section 6.5 presents the proposed MSL technique. Sections 6.6 analyze and verify, through computer simulations, the analytically predicted performances of the proposed receiver. Finally, the conclusions of this chapter are given in section 6.7.

6.2 TEAGER-KAISER TECHNIQUE

The initial attempt to employ a nonlinear signal processing technology in the ED-based IR-UWB receivers was proposed in [19], where a nonlinear device with a HPF, called TKO, are used to remove a NBI before the IR-UWB signals are detected by an OOK receiver. As shown in [20], if the input of the TKO is $x(t)$, the output of the TKO is then:

$$\Psi\left[x(t)\right] = \left[\dot{x}(t)\right] - x(t)\ddot{x}(t) \ , \tag{6.1}$$

where $\dot{x}(t) = \frac{d}{dt}x(t)$ and $\ddot{x}(t) = \frac{d^2}{dt^2}x(t)$ are the first and second order derivate of $x(t)$, respectively. By processing with the TKO, the signal frequency band between f_1 and f_2 is then transferred to a frequency band between DC and $f_2 - f_1$. If a NBI presents in IR-UWB signal, the NBI is then shifted to a frequency band close to DC and hence can be removed easily with a HPF. This feature makes the TKO technology well suitable for processing NBI in IR-UWB signals as it does not need any prior knowledge of the NBI.

6.3 THE SQUARE LAW TECHNIQUE

Although the TKO technology can considerably improve the NBI mitigation ability of the ED based IR UWB receivers, it is very difficult to implement in hardware [18]. To

solve this issue, another similar nonlinear processing operator, denoted the SL operator, was systematically introduced for the ED-based receivers. In the SL operator, it uses a SL device with a BPF instead of a TKO with a HPF to mitigate the NBI effects. With the help of the SL operator, the NBI coexisting with IR-UWB signal can be converted to a low frequency band and then suppressed by a BPF. Since the SL devices are commercial readily available, the implementation of the SL technology will be relatively easy.

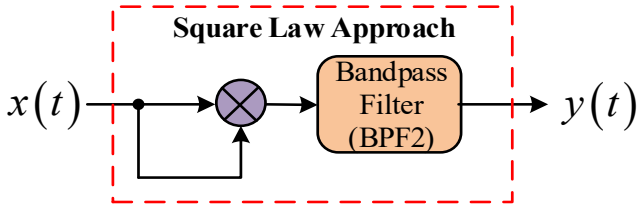

Figure 28 The structure of the SL technology for UWB impulse radios

As shown in Fig. 28, the SL operator, denoted $\psi(\cdot)$, on input signal $x(t)$ can be defined by

$$y(t) = \psi\left[x(t)\right] = x^2(t) * h_2(t) \ , \tag{6.2}$$

where $h_2(t)$ is the impulse response of the cascaded band-pass filter (i.e. BPF2) with a frequency response

$$H_2(f) = \begin{cases} 1, & f_1 \le |f| \le f_2; \\ 0, & \text{others}, \end{cases} \tag{6.3}$$

where f_1 and f_2 are the low and up cut-off frequencies of the filter, respectively.

6.4 Two Propositions for the Square Law Technique

To develop the proposed detector in the next sections, we first define two propositions as follows:

Proposition 1: Suppose the input to a SL operator $x(t)$ is composed of three different components

$$x(t) = x_1(t) + x_2(t) + x_3(t) \triangleq x_1 + x_2 + x_3 \,, \tag{6.4}$$

where x_1, x_2, x_3 is the notation of $x_1(t)$, $x_2(t)$, and $x_3(t)$. By substituting (6.4) to (6.2), the output of the SL operator can be given by

$$\begin{aligned} \psi\left[x(t)\right] &= \psi\left[x_1 + x_2 + x_3\right] \\ &= \psi\left[x_1\right] + \psi\left[x_2\right] + \psi\left[x_3\right] + \psi_c\left[x_1 + x_2 + x_3\right], \end{aligned} \tag{6.5}$$

where the cross-term $\psi_c\left[x_1 + x_2 + x_3\right]$ is defined as

$$\psi_c\left[x_1 + x_2 + x_3\right] = 2\left[x_1x_2 + x_2x_3 + x_1x_3\right] * h_2 \,, \tag{6.6}$$

where h_2 is the notation of $h_2(t)$, and $*$ is a convolution operation.

Proposition **2**: If the input, $x(t)$, is a zero-mean narrowband random process with a power spectral density (PSD)

$$S_x\left(f\right) = \begin{cases} P, & f_c - \dfrac{B_x}{2} \le \left|f\right| \le f_c + \dfrac{B_x}{2}; \\ 0, & \text{others}, \end{cases} \tag{6.7}$$

where B_x and f_c are the bandwidth and center frequency of the random process, respectively. Then the output of SL operator can be given by

$$\psi\left[x(t)\right] = x^2(t) * h_2(t) = 0, \text{ if } f_1 > B_x, \text{ and } f_2 < 2f_c - \frac{B_x}{2}. \tag{6.8}$$

Proof: see Appendix *D*.

The result from proposition 2 can be exploited to mitigate NBI regardless of its center frequency in any location of signal frequency range. Since compared with the center frequency, f_c, of an IR-UWB signal, the NBI bandwidth, B_x, is so small, then applying the BPF2, the NBI can be easily removed by (6.8).

6.5 The Proposed Multiband Square Law Technique

In this section, based on the SL technique discussed in section 6.3 and 6.4, we will present a novel NBI mitigation technique, MSL, for the ED-based IR-UWB systems, and then its NBI mitigation performance analysis. Without loss of generality, we assume a transmission with perfect synchronization of the integration window, no ISI and no IPI.

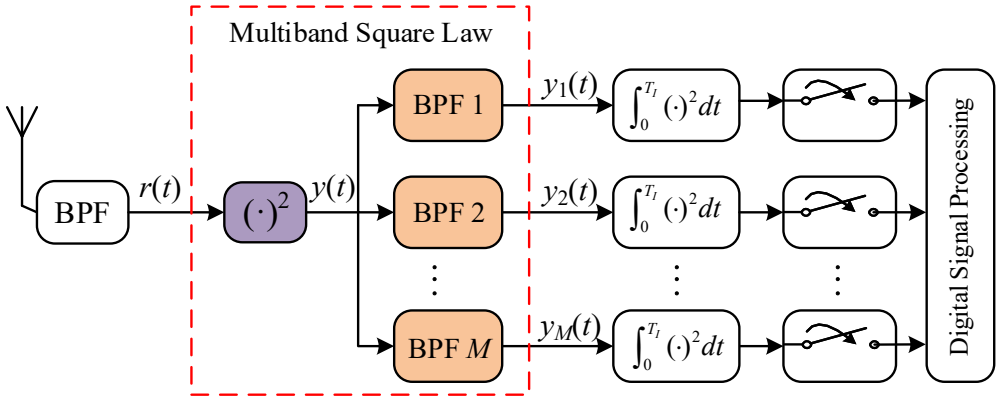

Figure 29 The structure of energy detector based on the MSL technique for UWB impulse radios.

To mitigate NBI in the received IR-UWB signal, as shown in Fig. 29, we proposed an energy detector based on the MSL technique in [57]. As usual, the received IR-UWB signal is amplified by a low noise amplifier and filtered by a band-pass filter (BPF) to remove the out-of-band noise and interferences. Then the filtered signal $r(t)$ is fed to the MSL device to get M separated sub-band-limited signals $y_1(t)$, $y_2(t)$, …, $y_M(t)$. Subsequently, the signal energy over each sub-band is collected by an energy detector with integration time of T_I. Finally, these collected energies are sent to a digital signal processing unit to retrieve user's information bits. Since this technique does not need any prior knowledge of the NBI, it leads to designs of low cost and low complexity ED-based IR-UWB receivers.

For each symbol duration, the demodulation is based on the signal energy collected over a specific time interval ($0 \le t \le T_I$), which is determined by the delay spread of a multipath channel. When the UWB pulse is transmitted, the received signal $r(t)$, after the BPF, can be given by

$$r(t) = p(t) + n(t) + i(t), 0 < t < T_I \ , \tag{6.9}$$

where $n(t)$ is the background noise and $p(t)$ is the received UWB pulse with a bandwidth of B and an energy of E_p given by

$$p(t) = a(t)\cos 2\pi f_c t \ , \tag{6.10}$$

where $a(t)$ is the baseband equivalent of $p(t)$ and f_c is the center frequency of $p(t)$. Typically, B << f_c for a IR-UWB system operating in the 3.1-10.6GHz frequency band. Furthermore, in order to analyze the SIR improvement offered by the MSL technique, the NBI, $i(t)$, is modeled with a wide-sense stationary, zero-mean Gaussian band-pass random process [58] with the following autocorrelation function (ACF)

$$R_i(t) = E\left[i(t+\tau)i(t)\right] = P_I \frac{\sin \pi B_I \tau}{\pi B_I \tau} \cos 2\pi f_I \tau \ , \tag{6.11}$$

and the power spectral density (PSD)

$$S_i(f) = \begin{cases} P_i, & f_i - \dfrac{B_i}{2} \le |f| \le f_i + \dfrac{B_i}{2} \ ; \\ 0, & \text{others} \ , \end{cases} \tag{6.12}$$

where B_i, f_i and P_i are the bandwidth, the center frequency, and amplitude of PSD, respectively.

By sending the filtered signal $r(t)$ to the MSL operator, the output in the m^{th} sub-band, $y_m(t)$, m=1, 2, …, M, according the *proposition* 1, can be expressed by

$$y_m(t)=\begin{cases}\psi(q)+\psi(n)+\psi(i)+\psi_c(q,n,i), & \text{when the NBIs present;}\\ \psi(q)+\psi(n)+\psi_c(q,n), & \text{when no NBI presents;}\end{cases} \tag{6.13}$$

where the $\psi(i)$ is a strong NBI component. According the *proposition* 2, it can be removed by the SL operator,

$$\psi(i)=i^2(t)*h_m(t)=0, \tag{6.14}$$

as the condition of $f_1 > B_i$ and $f_2 = B$ is chosen. Thus, the $y_m(t)$ in (6.13) can be obtained by

$$y_m(t)=\begin{cases}\psi(q)+\psi(n)+\psi_c(q,n,i), & \text{when the NBIs presents;}\\ \psi(q)+\psi(n)+\psi_c(q,n), & \text{when no NBI presents;}\end{cases}. \tag{6.15}$$

It should be noted that, comparing with (5.10), the $y_m(t)$ in (6.15) has no any strong NBI component, *i.e.* $\psi(i)$, hence the SL operator technology can significantly improve the NBI mitigation performance of the ED-based IR-UWB systems.

To evaluate the NBI mitigation performance of the proposed MSL technique, as examples, we will focus on the following two special cases.

6.5.1 NBI Mitigation When One NBI Presents

When one NBI presents in a IR-UWB signal, the proposed MSL technique becomes the SL technique in [56], *i.e.* M=1, as shown in Fig. 28. Typically, the power of the NBI is much higher than that of the background noise; hence, when the NBI is present, the effect of the background noise can be omitted in the SIR improvement analysis for the sake of simplicity. The SIR of $r(t)$ over $0 \le t \le T_I$ is given by

$$SIR_{\text{in}} = E_p \big/ P_I T_I . \tag{6.16}$$

After the SL technique is applied, the squared signal $s(t)$, is written as

$$s(t) = r^2(t) = p^2(t) + i^2(t) + 2p(t)i(t), \quad 0 < t < T_I, \tag{6.17}$$

where we denote $p^2(t)$ as the UWB term, $i^2(t)$ as the NBI term, and $2p(t)i(t)$ as the cross-term.

As shown in Fig. 30, in frequency domain, the UWB term in (6.17) is located in [0, B] and [$2f_c - B, 2f_c - B$] frequency bands, the NBI term is in [0, BI] and [$2f_I - B_I, 2f_I + B_I$], and the cross-term is in [0, $|f_c - f_I| + (B + B_I)/2$] and [$f_c + f_I - (B + B_I)/2$, $fc + f_I + (B + B_I)/2$]. Therefore, when the BPF2 with a pass-band of [f_p, B] is used to filter $s(t)$, the whole NBI term can be removed if $f_p > B_I$, and consequently the filter output, $y(t)$, can have much higher SIR than the original signal, $r(t)$. It should be noted that the SL technique does not require any prior knowledge about the NBI except an estimation on the widest possible bandwidth of the NBI to set f_p at that value [56].

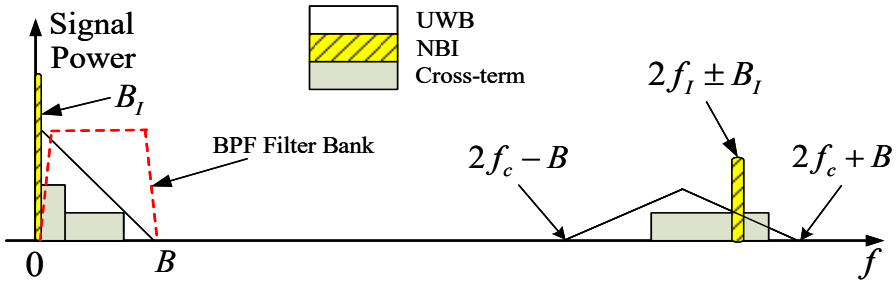

Figure 30 Power spectrum of the received signal after the SL processing when one NBI presents.

The analysis for the exact SIR of $y(t)$ is given in [56]. We assume the BPF2 is an ideal band-pass filter with a frequency response

$$H(f) = \begin{cases} 1, & f_p \le |f| \le B \\ 0, & \text{otherwise} \end{cases}. \tag{6.18}$$

From (6.10) and (6.17), when the SL technology is used, the energy of the UWB term $p^2(t)$ in (6.17) is given by

$$E_p = \frac{1}{2}\int_{f_p}^{B} \left| A(f) * A(f) \right|^2 df \ , \tag{6.19}$$

where $A(f)$ is the Fourier transform (FT) of the $a(t)$ in (6.10). Meanwhile, the average energy, E_i, of the NBI term $i^2(t)$ in (6.17) is derived by

$$E_i = \begin{cases} 0, & f_p \geq B_I, \\ \left(\frac{P_I}{B_I}\right)^2 \left(B_I - f_p\right)^2 T_I, & f_p < B_I. \end{cases} \tag{6.20}$$

Usually, the UWB pulse $p(t)$ and the NBI $i(t)$ are independent, the average energy, $E_{p,i}$, of the cross-term $2p(t)i(t)$ in (6.17) can be approximated by

$$E_{p,i} = \int_{-\infty}^{+\infty} \overline{S}_{p,i}(f) \left| H(f) \right|^2 df \approx P_I \int_{f_p}^{B} \left[\left| A(f-\Delta f) \right|^2 + \left| A(f+\Delta f) \right|^2 \right] df \ , \tag{6.21}$$

where $\Delta f = |f_2 - f_1|$ and $\overline{S}_{p,i}(f)$ is the average energy spectrum of the cross term. Finally, from (6.19), (6.20), and (6.21), the SIR of $y(t)$ over $[0,\ T_I]$ can be derived by [56]

$$SIR_{SL} = \frac{E_p}{E_i + E_{p,i}} = \begin{cases} \dfrac{\frac{1}{2}\int_{f_p}^{B} \left| A(f) * A(f) \right|^2 df}{P_I \int_{f_p}^{B} \left[\left| A(f-\Delta f) \right|^2 + \left| A(f+\Delta f) \right|^2 \right] df}, & f_p \geq B_I, \\ \dfrac{\frac{1}{2}\int_{f_p}^{B} \left| A(f) * A(f) \right|^2 df}{\left(\frac{P_I}{B_I}\right)^2 \left(B_I - f_p\right)^2 T_I + P_I \int_{f_p}^{B} \left[\left| A(f-\Delta f) \right|^2 + \left| A(f+\Delta f) \right|^2 \right] df}, & f_p < B_I. \end{cases} \tag{6.22}$$

For an example, if we consider the following UWB pulse,

$$p(t) = \begin{cases} \sqrt{2BE_p}\, \dfrac{\sin(\pi B t)}{\pi B t} \cos\left(2\pi f_c t\right), & 0 < t < T_p \\ 0, & \text{otherwise.} \end{cases} \tag{6.23}$$

where T_p is the pulse duration time. By substituting (6.23) into (6.22), the output SIR of $y(t)$, after the SL device, is obtained by

$$SIR_{\mathrm{SL}} = \frac{E_p (B - f_p)^3}{3P_I B\left(B - 2f_p\right)}, \quad f_p \geq B_I. \tag{6.24}$$

By comparing (6.25) with (6.16), the SIR improvement offered by the SL technology, denoted as G_{SL}, can be derived by

$$G_{SL} = \frac{SIR_{\mathrm{SL}}}{SIR_{\mathrm{in}}} = \frac{T_I (B - f_p)^3}{3B\left(B - 2f_p\right)} \approx \frac{1}{3} T_I B, \quad B \geq f_p. \tag{6.25}$$

Due to the wideband feature of IR-UWB systems, $T_I B \gg 1$, the SL technology can achieve a significant SIR improvement for the ED-based IR-UWB receivers. For example, when B = 500MHz and T_I = 200ns, the SIR improvement, G_{SL}, is around 15.2dB.

6.5.2 NBI Mitigation When Two NBIs Present

When the received signal is disrupted by two or more strong NBIs, the proposed MSL technique, as shown in Fig. 29, is applied to improve the NBI mitigation performance of the SL technique.

A. The Output Analysis for the SL Technique with Two NBI presents

For the sake of simplicity, in this section, we omit the effect of the background noise (as the powers of the NBIs are much higher than that of the background noise), and consider the case of two NBIs presents as an example.

According to the *proposition 1* and the *proposition 2*, the output signal $y(t)$, after the SL device, is then written by

$$
\begin{aligned}
y(t) &= \psi(p) + \psi(i_1) + \psi(i_2) + \psi_c(p, i_1, i_2) \\
&= \psi(p) + \psi_c(p, i_1, i_2) \\
&= p^2(t) + 2\left[p(t)i_1(t) + p(t)i_2(t) + i_1(t)i_2(t)\right] * h(t),
\end{aligned} \tag{6.26}
$$

where $i_1(t)$ and $i_2(t)$ are the two NBIs with center frequency f_{I_1}, f_{I_2} and bandwidth B_{I_1}, B_{I_2}. The two NBIs are in the frequency band $[f_{I_1,L}, f_{I_1,H}]$ and $[f_{I_2,L}, f_{I_2,H}]$, respectively. When the two NBIs pass through the SL device, a very strong interference component $i_1(t)i_2(t) * h(t)$ is produced in $y(t)$ as shown in (6.26). This strong component seriously degrades the NBI mitigation performance of the SL technique, as it cannot be shifted to a low frequency band close to DC by the SL device.

B. Filter Bank Design and Signal Combining

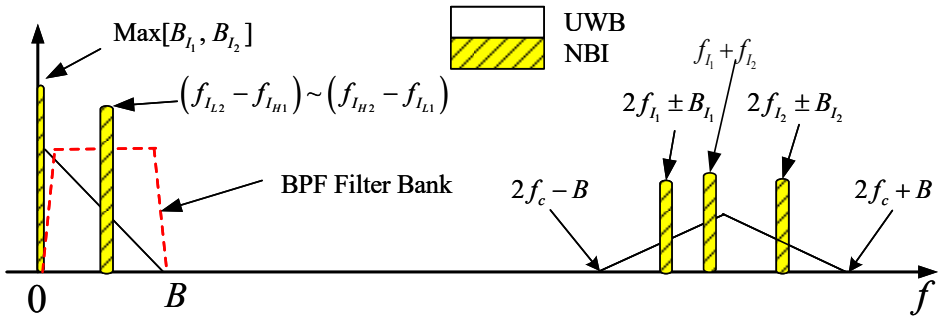

Figure 31 The power spectrum density of the received signal after SL processing when two NBI present.

In the proposed MSL technique, a group of band-pass filters is designed after the square law device to further improve the NBI mitigation performance. As shown in Fig. 31, after passing through the SL device, the two NBI components are re-located at the frequency range of *i*) DC, *ii*) DC to the max value of $[f_{I_1,H} - f_{I_1,L}, f_{I_2,H} - f_{I_2,L}]$, *iii*) $[f_{I_2,L} - f_{I_1,H}, f_{I_2,H} - f_{I_1,L}]$, *iv*)$[2f_{I_1,L}, 2f_{I_1,H}]$, and *v*) $[2f_{I_2,L}, 2f_{I_2,H}]$. If a multiband BPFs with the

passing band of the max of $[f_{I_1,H} - f_{I_1,L}, f_{I_2,H} - f_{I_2,L}]$ to $f_{I_2,L} - f_{I_1,H}$, and $f_{I_2,H} - f_{I_1,L}$ to B is applied, the most energy of NBIs can be removed.

Based on the spectrum analysis above, the filter bank design is required *i*) to remove the band between DC and the max of (B_{I_1}, B_{I_2}), the band of $[f_{I_2,L} - f_{I_1,H}, f_{I_2,H} - f_{I_1,L}]$, and *ii*) the band of $[B, +\infty]$. Generally, the powers of the two strong NBIs are much higher than that of UWB and noise component, thus the terms of the sub-band disrupted by NBIs will have a higher energy than those of other sub-bands. Therefore, to mitigate the NBIs and their cross terms, the sub-band disrupted by NBIs and their cross terms must be detected by comparing the signal energy of each sub-band. Then the signal energy of the disrupted sub-band will be omitted for retrieving information bits.

6.6 Simulation and Discussion

In this section, using an ED-based binary pulse position modulation (BPPM) UWB system as an example, based on the proposed MSL-based receiver architecture for M=3 and M=1 (*i.e.* the SL technique), computer simulations have been carried out to verify the validity of the theoretical analysis on the SIR improvement as well as investigate the NBI mitigation performance offered by the MSL technique.

In the simulations, the transmitted IR-UWB pulses have a waveform defined by (6.10) with B = 499.2MHz and f_c = 3.9936GHz. The duration of a BPPM frame is 400ns, and the time shift to differentiate 1 from 0 is 200ns. Correspondingly T_I is fixed at 200ns in the receiver. In addition, an NBI with bandwidth B_I = 6MHz and center frequency f_I = 3.9GHz is applied. The BPF2 is designed by cascading a high pass filter (HPF) with a low pass

filter (LPF). The cut-off frequency of the LPF is B = 499.2MHz and that of the HPF is f_p = 2MHz or 6MHz. Both the LPF and the HPF are implemented with Butterworth filters.

A. No NBI Presents

Fig. 32 shows the simulation results without NBI present and their comparisons with the SL-based ED and the conventional ED-based detectors. From the Fig. 32 we have the following conclusions: *i*) regardless of Gaussian or multipath channel, the proposed MSL technique can considerably improve both the SNR and the BER performance of IR-UWB system; *ii*) the performance improvement under multipath channel is less than that under Gaussian channel; *iii*) the MSL technique has a inferior performance compared with the SL technique; *iv*) Omitting any one sub-band of the MSL based receiver will lead to a little deterioration on the BER performance, moreover, omitting the frequency band closer to DC cause the more deterioration.

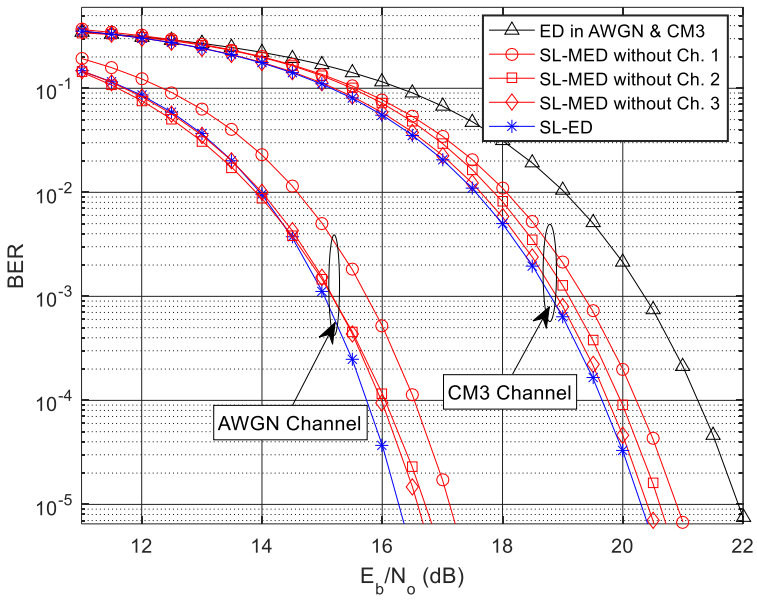

Figure 32 The BER performance of the ED-, SL-, and MSL- based receivers without NBI present.

B. One NBI Presents

As shown in Fig. 33, the SIR improvements offered by the SL and TKO techniques are investigated through theoretical analysis and computer simulations under both AWGN channel and multipath channels [56]. Clearly, for all scenarios, the SL technique can achieve the same NBI mitigation performance as the TKO technique. Furthermore, the SIR improvement under multipath channels is less than that under AWGN channel, as in the multipath channel the FT of UWB pulse in (6.23) is no longer a flat spectrum in AWGN channel, and hence E_p given by (6.19) has a reduced value.

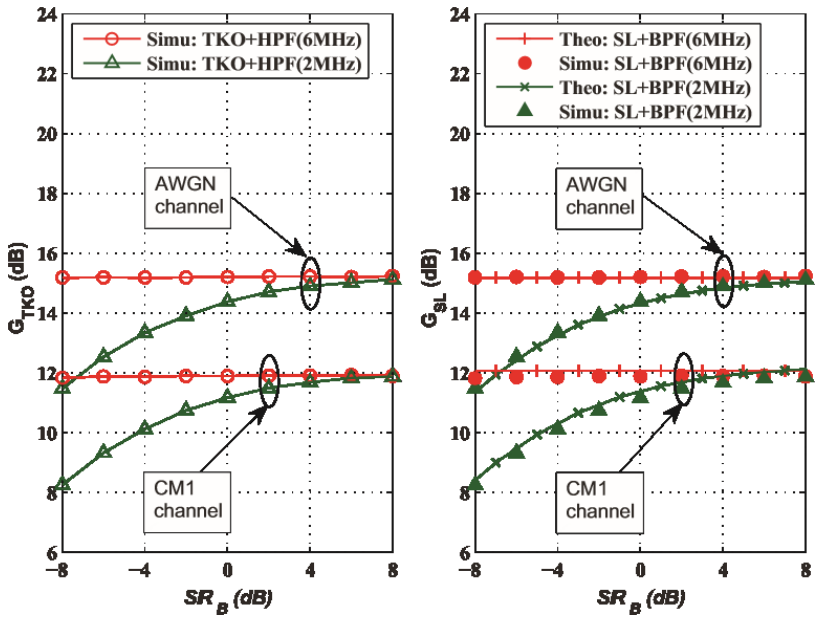

Figure 33 SIR improvement offered by TKO and the MSL techniques for M=1 [56] ©2012 IEEE.

Fig. 34 shows the BER performance offered by the SL and the TKO techniques when a strong NBI presents and the channel SNR fixed at E_b/N_0 = 19dB in both AWGN and CM1 channels. We can see that the SL technique has the same performance as the TKO technique, and they can significantly improve the BER performance of the ED-based UWB receiver

when a strong NBI is present. In particular, at BER= 10^{-3}, the ED-based receiver requires a SIR higher than 5dB, while when the SL technique with f_p = 6MHz is applied, the required SIR is relaxed to −6.8dB under AWGN channel and −2.8dB under the CM1 channels.

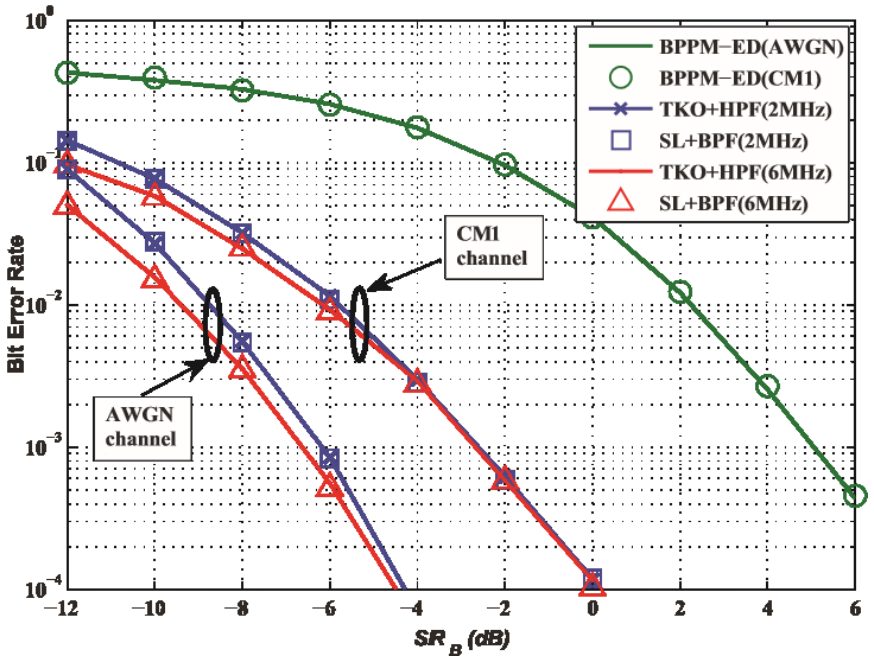

Figure 34 BER performance of the ED-based BPPM receiver employing the SL or TKO technique [56] ©2012 IEEE.

C. *Two NBIs present*

Fig. 35 shows the BER performance improvement offered by the MSL based technique with two strong NBIs present. Clearly, the proposed MSL technique can significantly mitigate the destructive effect of two NBIs on the performance of the ED-based receivers. When two NBIs present, the BER performance of the conventional ED-based receiver is unacceptably poor, and both SL- and MSL- based ED receivers have better performances. Moreover, comparing with the SL based receiver, the proposed MSL based receiver has a

superior performance when two strong NBI presents and a similar performance (less than 0.2dB worse) when one strong NBI presents.

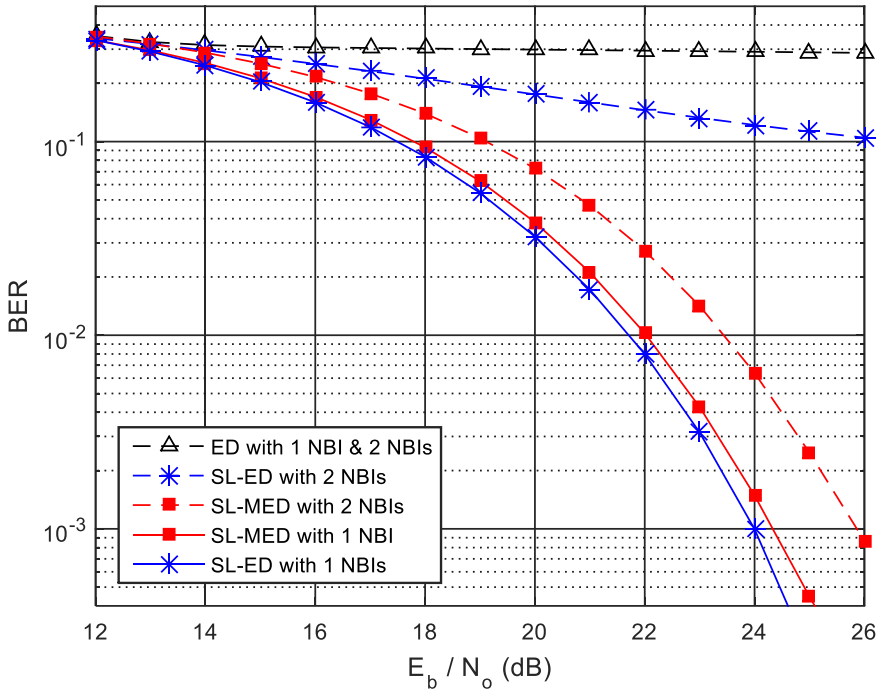

Figure 35 BER performance improvement in a multipath channel with two strong NBIs present for *M*=3. The *SIR* of two strong NBIs are set by -10 dB with a center frequency 3.9 GHz and 4.1GHz, respectively.

6.7 CONCLUSION

In this chapter, a new blind NBI mitigation technique, MSL, is proposed to mitigate destructive effects of an NBI on ED-based UWB receivers. Through theoretical analysis and computer simulations, we find that without requiring any NBI prior knowledge, the SL and the proposed MSL techniques can significantly improve the SIR of the received UWB pulses, and can make the ED-based receivers have a better BER performance in AWGN and multipath channels with/without NBI presents. Furthermore, when comparing with the SL technique, the proposed MSL technique has a better NBI mitigation performance when two or more NBI present and has the similar performance when one NBI or no NBI presents.

As a prior-ED NBI mitigation technique, the SL or MSL technique can be employed jointly with posterior-ED NBI mitigation techniques [59] to further improve the performance of ED-based IR-UWB ranging systems. Therefore, the proposed MSL technique provides an implementable, highly effective and low complexity solution for IR-UWB communications under strong NBI environments.

CHAPTER 7 CONCLUSION AND RECOMMENDATIONS

In this dissertation, nonlinear signal processing techniques have been analyzed and proposed for IR-UWB systems, and future works in this area are provided.

7.1 CONCLUSION

We proposed the use of a nonlinear signal processing technique, VD technology, to replace the conventional square law device to achieve better BER performance. We evaluate its performances analytically and empirically, and find that the log-normal model is the best-fit model for the VD-based detection. With the log-normal model, the analytical formula for the BER of the VD-based system with and without NBI in both AWGN and CM1 channels have been derived. Our results show that as compared with the conventional ED-based receiver, the proposed VD- based receiver can achieve a much better BER performance. It does not require high sampling rates and there is only a slight increase in receiver complexity as compared to conventional ED-based receivers. Our simulation results indicate that the VD based receiver can be a preferred nonlinear detection technology for IR-UWB systems.

For the MSL nonlinear signal processing technologies, we analyzed and verified its NBI mitigation performance, and have shown that without requiring any prior knowledge of the NBI, the MSL technique can significantly improve the SIR of the received UWB pulses, and hence can improve the BER performance of the ED-based UWB receivers. Furthermore, computer simulations show that the proposed MSL technique has the same NBI mitigation performance as the TKO technique and is easy to implement in hardware, therefore, the proposed MSL technique is an implementable and highly effective blind NBI

mitigation technique for ED-based IR-UWB receivers that demand low complexity and low power consumption.

7.2 Recommendations for Future Work

The use of nonlinear signal processing technologies presents a potentially new horizon for research and development of the ED based impulse radio UWB systems. However, nonlinear signal processing technologies also offer a number of challenges to be addressed and opportunities to explore for commercial applications. These challenges and opportunities are recommended as indicated below.

(i) Theoretical analysis for SL technology

Our initial theoretical analysis of the SL technology focused on frequency spectra or SNR. Some important analysis, for example BER performance, has to be completed with computer simulation. In addition, further understanding of the related operational principles and physics are still needed, in order to design the optimal systems.

(ii) The combination of SL technique with other NBI mitigation techniques

The proposed SL technique is a highly effective blind NBI mitigation technique for ED-based IR-UWB receivers that are of low complexity and low power consumption. It may be employed jointly with other NBI mitigation techniques to further improve the performance of ED-based IR-UWB ranging systems.

(iii) Multipath effects mitigation techniques for VD- based receivers

Our initial results in chapter 4 show that the performance of the VD-based receiver can degrade significantly due to multipath effects; further analysis on the effect of

multipath and new techniques to mitigate them deserve further investigation and research.

(iv) High order nonlinear signal processing technologies

Based on our work so far, high order nonlinear detectors may be explored for impulse radio UWB communications. For example, the four-order detector and kurtosis detector. Our initial study found that the high order variance detector may have a better BER performance. Further work to exploit these high order nonlinear signal processing technologies should be carried out.

BIBLIOGRAPHY

[1] A. F. Molisch, "Ultrawideband propagation channels-theory, measurement, and modeling," *IEEE Transactions on Vehicular Technology*, vol. 54, no. 5, pp. 1528-1545, 2005.

[2] Federal Communications Commission, "In the matter of revision of part 15 of the commission's rules regarding ultra-wideband transmission systems," *First Report and Order*, ET Docket 98-153, 2002.

[3] LAN/MAN Standards Committee, "Part 15.4: wireless medium access control (MAC) and physical layer (PHY) specifications for low-rate wireless personal area networks (LR-WPANs)," *IEEE Computer Society*, 2007.

[4] IEEE Standards Association, IEEE standard for local and metropolitan area networks-part 15.4: Low-rate wireless personal area networks physical layer specifications for low-data-rate, wireless, smart metering utility networks, 2012.

[5] M. Z. Win and R. A. Scholtz, "On the energy capture of ultrawide bandwidth signals in dense multipath environments," *IEEE Communications Letters*, vol. 2, no. 9, pp. 245-247, 1998.

[6] Y. Liuqing and G. B. Giannakis, "Ultra-wideband communications: an idea whose time has come," *IEEE Signal Processing Magazine*, vol. 21, no. 6, pp. 26-54, 2004.

[7] L. Stoica, A. Rabbachin, H. O. Repo, T. S. Tiuraniemi, and I. Oppermann, "An ultrawideband system architecture for tag based wireless sensor networks," *IEEE Transactions on Vehicular Technology*, vol. 54, no. 5, pp. 1632-1645, 2005.

[8] D. L. Goeckel and Q. Zhang, "Slightly frequency-shifted reference ultra-wideband radio," *IEEE Transactions on Communications*, vol. 55, no. 3, pp.508-519, 2007.

[9] H. Nie and Z. Chen, "Performance analysis of code-shifted reference UWB radio," *IEEE Radio and Wireless Symposium*, pp. 396–399, 2009.

[10] H. Nie and Z. Chen, "Differential code-shifted reference ultra-wideband (UWB) radio," *IEEE Vehicular Technology Conference*, pp.1-5, 2008.

[11] C. Steiner and A. Wittneben, "On the interference robustness of ultra-wideband energy detection receivers," *IEEE International Conference on Ultra-Wideband*, pp. 721-726, 2007.

[12] A. Rabbachin, T. Q. S. Quek, P. C. Pinto, I. Oppermann, and M. Z. Win, "Noncoherent UWB communication in the presence of multiple narrowband interferers," *IEEE Transactions on Wireless Communications*, vol. 9, no. 11, pp. 3365–3379, 2010.

[13] L.B. Milstein, "Interference rejection techniques in spread spectrum communications," *Proceedings of the IEEE*, vol. 76, pp. 657-671, Jun 1988.

[14] H. Shaman and J. S. Hong, "Ultra-wideband bandpass filter with embedded band notch structures," *IEEE Microwave and Wireless Components Letters*, vol. 17, pp. 193-195, March 2007.

[15] M. G. Khan, B. Sallberg, J. Nordberg, and I. Claesson, "Non-coherent detection of impulse radio uwb signals based on fourth order statistics," *IEEE International Conference on Ultra-Wideband*, pp. 824–828, 2009.

[16] **©2014 IEEE. Reprinted, with permission, from A. Yang, H. Nie, Z. Xu, and Z. Chen, "Variance detection for non-coherent impulse radio UWB receivers," International *Conference on Computing, Networking and Communications*, pp. 529–533, 2014.**

[17] J. F. Kaiser, "On a simple algorithm to calculate the 'energy' of a signal," International *Conference on Acoustics, Speech, and Signal Processing,* pp. 381-384 vol.1, 1990.

[18] H. Nie, Z. Chen, and Z. Xu, "Nonlinear signal processing technologies for energy detection based impulse radio UWB transceivers," *IEEE International Conference on Ultra-Wideband*, pp. 202-206, 2012.

[19] H. U. Dehner, H. Jakel, D. Burgkhardt, and F. K. Jondral, "The teager-kaiser energy operator in presence of multiple narrowband interference," *IEEE Communications Letters*, vol. 14, pp. 716-718, 2010.

[20] H. U. Dehner, H. Jkel, and F. K. Jondral, "On the modified teager-kaiser energy operator regarding narrowband interference," *Wireless Telecommunications Symposium,* pp. 1-5, 2011.

[21] V. Lottici, A. D'Andrea, and U. Mengali, "Channel estimation for ultrawideband communications," *IEEE Journal on Selected Areas in Communications*, vol. 20, pp. 1638–1645, 2002.

[22] M. R. Casu, G. Durisi, and S. Benedetto, "On the implementation of a transmitted-reference uwb receiver," *European Signal Processing Conference*, pp.1-4, Sept 2005.

[23] Q. Zhang and D. L. Goeckel, "Multi-differential slightly frequency-shifted reference ultra-wideband (UWB) radio," *Annual Conference on Information Sciences and Systems*, pp. 615-620, 2006.

[24] A. A. D'Amico, U. Mengali, and E. A. de Reyna, "Energy detection UWB receivers with multiple energy measurements," *IEEE Transactions on Wireless Communications*, vol. 6, pp. 2652-2659, 2007.

[25] Y. Ying, M. Ghogho, and A. Swami, "Block-coded modulation and noncoherent detection for impulse radio UWB," *IEEE Signal Processing Letters*, vol. 15, pp. 112-115, 2008.

[26] A. Gerosa, S. Solda, A. Bevilacqua, D. Vogrig, and A. Neviani, "An energy detector for noncoherent impulse-radio uwb receivers," *IEEE Transactions on Circuits and Systems I: Regular Papers*, vol. 56, pp. 1030-1040, 2009.

[27] Y. Chen, "Improved energy detector for random signals in gaussian noise," *IEEE Transactions on Wireless Communications*, vol. 9, pp. 558-563, 2010.

[28] Xianda Zhang, Zheng Bao. Communication Signal Processing. Beijing: National Defense Industry Press, 2000.

[29] M. Sahin, I. Guvenc and H. Arslan, "Optimization of energy detector receivers for UWB systems," *IEEE Vehicular Technology Conference*, vol. 2, pp. 1386-1390, 2005.
[30] M. Weisenhorn and W. Hirt, "Robust noncoherent receiver exploiting UWB channel properties," *IEEE Conference on UWB Systems and Technologies*, pp.156-160, 2004.
[31] Z. Xu, A. Yang, H. Qian, H. Nie, Z. Chen and L. Yu, "Narrowband interference mitigations capacity of differential code-shifted-reference UWB systems," *IEEE International Conference on Ultra-Wideband*, Nanjing, pp.1-4, 2010.
[32] Hyvarinen, J. Karhunen and E. Oja, Independent Component Analysis, John Wiley & Sons, Inc, 2001.
[33] **©2016 IEEE. Reprinted, with permission, from A. Yang, Z. Xu, H. Nie and Z. Chen, "On the Variance-Based Detection for Impulse Radio UWB Systems," *IEEE Transactions on Wireless Communications*, vol. 15, no. 12, pp. 8249-8259, Dec. 2016.**
[34] M. M. El-Gamal, S. Shaaban and M. H. Aly, "New trends towards speedy IR-UWB techniques," *IEEE Radio Science Conference*, pp. 1-8, 2011
[35] C. Carbonelli, U. Mengali and U. Mitra, "Synchronization and channel estimation for UWB signal," *IEEE Global Telecommunications Conference*, vol. 2, pp. 764-768, Dec. 2003.
[36] G. R. Aiello and G. D. Rogerson, "Ultra-wideband wireless systems," *IEEE Microwave Magazine,* vol. 4, no. 2, pp. 36-47. 2003.
[37] D. L. Goeckel and Qu Zhang, "Slightly frequency-shifted reference ultra-wideband radio: TR-UWB without the delay element," *IEEE Military Communications Conference*, vol. 5, pp. 3029-3035, 2005.
[38] H. Nie and Z. Chen, "Code-shifted reference ultra-wideband (UWB) radio," *IEEE Communication Networks and Services Research Conference*, pp. 385-389, 2008.
[39] H. Nie and Z. Chen, "Performance evaluations for differential code-shifted reference ultra-wideband radio," *IEEE Ultra-Wideband International Conference*. pp. 274-278, 2009.
[40] C. Steiner and A. Wittneben, "On the interference robustness of ultra-wideband energy detection receivers," *IEEE Ultra-Wideband International Conference*. pp. 721-726, 2007.
[41] J. Taghipour, V. Tabataba Vakili and D. Abbasi-Moghadam, "Comparison of Kurtosis and Fourth Power Detectors with Applications to IR-UWB OOK Systems," *International Journal of Communications, Network and System Sciences*, vol. 5, no. 1, pp. 43-49, 2012.
[42] Y. Chen, "Improved energy detector for random signals in Gaussian noise," *IEEE Transactions on Wireless Communications*, vol. 9, no. 2, pp.558 -563, 2010.
[43] E. Karapistoli, F. Pavlidou, I. Gragopoulos and I. Tsetsinas, "An overview of the IEEE 802.15.4a Standard," *IEEE Communications Magazine*, vol. 48, no. 1, pp. 47-53, 2010.
[44] T. Kvalseth, "Some informational properties of the lognormal distribution," *IEEE Transactions on Information Theory*, vol.28, no. 6, pp. 963-966, 1982.

[45] H. Cao, V. Leung, C. Chow, and H. Chan, "Enabling technologies for wireless body area networks: A survey and outlook," *IEEE Communications Magazine*, vol. 47, no12, pp. 84–93, 2009.

[46] IEEE Computer Society, IEEE Standard 802.15.4-2011: IEEE Standard for Local and Metropolitan area networks Part 15.4: Low Rate Wireless Personal Area Networks, *IEEE Standard 802.15.4-2011* (*Revision of IEEE Std. 802.15.4-2006*), NY, US.

[47] C. Park and T. S. Rappaport, "Short range wireless communications for Next Generation Networks: UWB, 60 GHz millimeter wave WPAN, and ZigBee," *IEEE Wireless Communications*, vol. 14, no.4, pp. 70–78, 2007.

[48] J. Zhang, P. V. Orlik, Z. Sahinoglu, A. F. Molisch, and P. Kinney, "UWB systems for wireless sensor networks," *Proceedings of the IEEE*, vol. 97, no.2, pp. 313-331, 2009.

[49] IEEE Computer Society, IEEE Standard 802.15.6: IEEE Std. for Local and Metropolitan area networks-Part 15.6: Wireless Body Area Networks, *IEEE Standard 802.15.6-2012*, NY, USA.

[50] A. F. Molisch, "Ultrawideband propagation channels-Theory, measurement, and modeling," *IEEE Transactions on Vehicular Technology*, vol. 54, no.5, pp. 1528-1545, 2005.

[51] A. F. Molisch, K. Balakrishnan, D. Cassioli, C.-C. Chong, S. Emami, A. Fort, J. Karedal, J. Kunisch, H. Schantz, U. Schuster, and K. Siwiak*, IEEE 802.15.4a Channel Model-Final Report*, *IEEE 802.15.4a*, 2004.

[52] H. Yin, Z. Wang, L. Ke and J. Wang, "Monobit digital receivers: design, performance, and application to impulse radio," *IEEE Transactions on Communications*, vol. 58, no. 6, pp. 1695-1704, 2010.

[53] J. F. Kaiser, "On a simple algorithm to calculate the energy of a signal," *International Conference on Acoustics, Speech, and Signal Processing,* pp. 381-384, 1990.

[54] P. Maragos, J. F. Kaiser, and T. F. Quatieri, "On amplitude and frequency demodulation using energy operators," *IEEE Transactions on Signal Processing*, vol. 41, no. 4, pp. 1532-1550, 1993

[55] W. Godycki, R. Dokania, X. Wang, and A. Apsel, "A high-speed, onchip implementation of Teager Kaiser Operator for in-band interference rejection," *IEEE Asian Solid State Circuits Conference*, pp. 1-4, 2010.

[56] **©2012 IEEE. Reprinted, with permission, from Z. Xu, H. Nie, Z. Chen, H. Khani and L. Yu, "Nonlinear blind narrowband interference mitigation for energy detection based UWB receivers." *IEEE Communications Letters*, vol. 16, no. 10, pp. 1596-1599, 2012.**

[57] **©2016 IEEE. Reprinted, with permission, from Z. Xu, A. Yang, Z. D. Chen, and H. Nie, "Multichannel energy detection UWB receivers based on nonlinear square law technology." *IEEE International Conference on Ubiquitous Wireless Broadband,* pp. 1-4, 2016.**

[58] H. Benaroya, S. M. Han, and M. Nagurka, *Probability Models in Engineering and Science*. Boca Raton, FL, USA: CRC Press, 2005.

[59] D. Dardari, A. Conti, U. Ferner, A. Giorgetti, and M. Z. Win, “Ranging with ultrawide bandwidth signals in multipath environments,” *Proceedings of the IEEE*, vol. 97, no. 2, pp. 404-426, 2009.

[60] J.V., Michalowicz, J.M., Nichols, F., Bucholtz, C.C., Olson, "An Isserlis’ theorem for mixed Gaussian variables: application to the auto-bispectral density", *Journal of Statistical Physics*. vol. 136, no. 1, pp. 89-102, 2009.

[61] **©2014 IEEE. Reprinted, with permission, from A. Yang, Z. Xu, H. Nie and Z. Chen, "A unified framework for nonlinear detections of impulse radio UWB systems," *IEEE 25th Annual International Symposium on Personal, Indoor, and Mobile Radio Communication*, Washington DC, pp. 913-917, 2014.**

[62] **©2013 IEEE. Reprinted, with permission, from A. Yang, H. Nie, Z. Xu and Z. Chen, "Modified kurtosis detection for UWB impulse radios," *IEEE Radio and Wireless Symposium*, Austin, TX, pp. 136-138, 2013.**

APPENDIX A Proof of the Approximation of G_j^{VD}

In this appendix, the approximation of the expectation of G_j^{VD} in (4.21) is derived. From (4.19) and section 4.2, we have known

$$E\left[G_j^{VD}\right] = E\left[\ln\left(V_{j1}\right)\right] - E\left[\ln\left(V_{j0}\right)\right], \tag{A.1}$$

and V_{ji} obeys the log-normal distribution with a location parameter

$$\alpha = E\left[\ln\left(V_{ji}\right)\right] = \ln\left(E\left[V_{ji}\right]\right) - \frac{1}{2}\ln\left(1 + \frac{Var\left[V_{ji}\right]}{E^2\left[V_{ji}\right]}\right). \tag{A.2}$$

Suppose $x = \frac{Var\left[V_{ji}\right]}{E^2\left[V_{ji}\right]}$, by applying the Taylor series expansion, we have

$$\ln\left(1+x\right) = \sum_{n\geq 0}\frac{\left(-1\right)^n x^{n+1}}{n+1} = x - \frac{1}{2}x^2 + \frac{1}{3}x^3 - \ldots, \tag{A.3}$$

Taking the first order approximation, we get

$$E\left[\ln\left(V_{ji}\right)\right] \approx \ln\left(E\left[V_{ji}\right]\right) - \frac{1}{2}\cdot\frac{Var\left[V_{ji}\right]}{E^2\left[V_{ji}\right]}. \tag{A.4}$$

Substituting (A.4) to (A.1), we obtain

$$E\left[G_j^{VD}\right] \approx \left[\ln\left(E\left[V_{j1}\right]\right) - \ln\left(E\left[V_{j0}\right]\right)\right] + \frac{1}{2}\left[\frac{Var\left[V_{j0}\right]}{E^2\left[V_{j0}\right]} - \frac{Var\left[V_{j1}\right]}{E^2\left[V_{j1}\right]}\right]. \tag{A.5}$$

Since the term $\frac{1}{2}\left[\frac{Var\left[V_{j0}\right]}{E^2\left[V_{j0}\right]} - \frac{Var\left[V_{j1}\right]}{E^2\left[V_{j1}\right]}\right]$, denoted as term (2), in (A.5) is much smaller than the term $\ln\left(E\left[V_{j1}\right]\right) - \ln\left(E\left[V_{j0}\right]\right)$, denoted as term (1), (as shown in Fig. 36), (A.5) can be approximated as

$$E\left[G_j^{VD}\right] \approx \ln\left(E\left[V_{j1}\right]\right) - \ln\left(E\left[V_{j0}\right]\right). \tag{A.6}$$

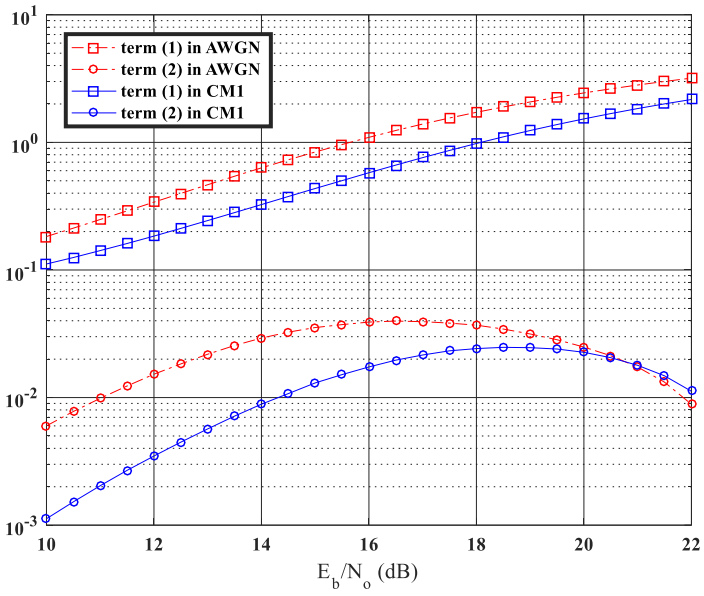

Figure 36 The values of the first and second terms in (A.5) with both AWGN and multipath CM1 channels.

APPENDIX B Derivation of the Approximation of $E[V_{ji}]$

In this appendix, the expectations of r_{jik}^4, w_{jik}^4, $r_{jik}^2 r_{jik}^2$, $w_{jik}^2 w_{jil}^2$, and $r_{jik}^2 w_{jil}^2$ in (4.28) are derived. Variable r_{jik} is if a zero mean with normal distribution. By using Isserlis' theorem [60], these expectations can be derived as follows:

$$E\left\{\sum_{k=0}^{M-1} r_{jik}^4\right\} = \sum_{k=0}^{M-1}\left[E^2\left\{r_{jik}^2\right\} + E^2\left\{r_{jik}^2\right\} + E^2\left\{r_{jik}^2\right\}\right] = 3M\cdot\sigma_{ri}^4, \tag{B.1}$$

where $\sigma_{ri}^2 = E\left\{r_{jik}^2\right\}$, $i = 0,1$ is the variance of r_{jik} in the j^{th} frame;

$$E\left\{\sum_{k=0}^{M-1}\sum_{l=0}^{M-1} r_{jik}^2 r_{jil}^2\right\} = \sum_{k=0}^{M-1} E\left\{r_{jik}^4\right\} + \sum_{k=0}^{M-1}\sum_{l=0,l\neq k}^{M-1} E\left\{r_{jik}^2 r_{jil}^2\right\}. \tag{B.2}$$

Assume that the variable r_{jik}^2 and r_{jil}^2 are independent (to simplify the analysis). Then $E\{r_{jik}^2 r_{jil}^2\} = E\{r_{jik}^2\}\ E\{r_{jil}^2\} = \sigma_{ri}^4$ if $k \neq l$. Then

$$E\left\{\sum_{k=0}^{M-1}\sum_{l=0}^{M-1} r_{jik}^2 r_{jil}^2\right\} = \left(M^2 + 2M\right)\sigma_{ri}^4\ . \tag{B.3}$$

Similarly, the expectations of variables w_{jik}^4, $w_{jik}^2 w_{jil}^2$, and $r_{jik}^2 w_{jil}^2$ can be found as:

$$E\left\{\sum_{k=M}^{N-1} w_{jik}^4\right\} = \sum_{k=M}^{N-1} E\left\{w_{jik}^4\right\} = 3\left(N-M\right)\sigma_w^4, \tag{B.4}$$

$$E\left\{\sum_{k=M}^{N-1}\sum_{l=M}^{N-1} w_i^2 w_j^2\right\} = \left(M^2 + N^2 - 2NM + 2N - 2M\right)\sigma_w^4, \tag{B.5}$$

and

$$E\left\{\sum_{k=0}^{M-1}\sum_{l=M}^{N-1} r_{jik}^2 w_{jil}^2\right\} = M\left(N-M\right)\sigma_{ri}^2\sigma_w^2, \tag{B.6}$$

where $\sigma_w^2 = E\left\{w_{jik}^2\right\}$, $i = 0,1$ is the variance of w_{jik} in the j^{th} frame.

APPENDIX C Derivation of the Approximation of $E[V_{ji}^2]$

In this appendix, $E\{V_{ji}^2\}$ in (4.31) are derived. The first term in (4.31) can be expanded as

$$\frac{1}{N^2}E\left\{\left(\sum_{k=0}^{M-1}r_{jik}^4+\sum_{k=M}^{N-1}w_{jik}^4\right)^2\right\}=\frac{1}{N^2}E\left\{\sum_{k=0}^{M-1}\sum_{l=0}^{M-1}r_{jik}^4r_{jil}^4\right\}+\frac{1}{N^2}E\left\{\sum_{k=M}^{N-1}\sum_{l=M}^{N-1}w_{jik}^4w_{jil}^4\right\}+\frac{2}{N^2}E\left\{\sum_{k=0}^{M-1}\sum_{l=M}^{N-1}r_{jik}^4w_{jil}^4\right\}, \tag{C.1}$$

the second term can be expanded as

$$\begin{aligned}\frac{1}{N^4}E\left\{\left(\sum_{k=0}^{M-1}r_{jik}^2+\sum_{k=M}^{N-1}w_{jik}^2\right)^4\right\}&=\frac{1}{N^4}E\left\{\sum_{k=0}^{M-1}\sum_{l=0}^{M-1}\sum_{m=0}^{M-1}\sum_{n=0}^{M-1}r_{jik}^2r_{jil}^2r_{jim}^2r_{jin}^2\right\}\\&+\frac{1}{N^4}E\left\{\sum_{k=M}^{N-1}\sum_{l=M}^{N-1}\sum_{m=M}^{N-1}\sum_{n=M}^{N-1}w_{jik}^2w_{jil}^2w_{jim}^2w_{jin}^2\right\}\\&+\frac{4}{N^4}E\left\{\sum_{k=0}^{M-1}\sum_{l=0}^{M-1}\sum_{m=0}^{M-1}\sum_{n=M}^{N-1}r_{jik}^2r_{jil}^2r_{jim}^2w_{jin}^2\right\}\\&+\frac{6}{N^4}E\left\{\sum_{k=0}^{M-1}\sum_{l=0}^{M-1}\sum_{m=M}^{N-1}\sum_{n=M}^{N-1}r_{jik}^2r_{jil}^2w_{jim}^2w_{jin}^2\right\}\\&+\frac{4}{N^4}E\left\{\sum_{k=0}^{M-1}\sum_{l=M}^{N-1}\sum_{m=M}^{N-1}\sum_{n=M}^{N-1}r_{jik}^2w_{jil}^2w_{jim}^2w_{jin}^2\right\},\end{aligned} \tag{C.2}$$

and the last term as

$$\begin{aligned}-\frac{2}{N^3}E\left\{\left(\sum_{k=0}^{M-1}r_{jik}^4+\sum_{k=M}^{N-1}w_{jik}^4\right)\left(\sum_{k=0}^{M-1}r_{jik}^2+\sum_{k=M}^{N-1}w_{jik}^2\right)^2\right\}&=-\frac{2}{N^3}E\left\{\sum_{k=0}^{M-1}\sum_{l=0}^{M-1}\sum_{m=0}^{M-1}r_{jik}^4r_{jil}^2r_{jim}^2\right\}\\&-\frac{2}{N^3}E\left\{\sum_{k=0}^{M-1}\sum_{l=M}^{N-1}\sum_{m=M}^{N-1}r_{jik}^4w_{jil}^2w_{jim}^2\right\}-\frac{4}{N^3}E\left\{\sum_{k=0}^{M-1}\sum_{l=0}^{M-1}\sum_{m=M}^{N-1}r_{jik}^4r_{jil}^2w_{jim}^2\right\}\\&-\frac{2}{N^3}E\left\{\sum_{k=M}^{N-1}\sum_{l=0}^{M-1}\sum_{m=0}^{M-1}w_{jik}^4r_{jil}^2r_{jim}^2\right\}-\frac{2}{N^3}E\left\{\sum_{k=M}^{N-1}\sum_{l=0}^{M-1}\sum_{m=0}^{M-1}w_{jik}^4w_{jil}^2w_{jim}^2\right\}\\&-\frac{4}{N^3}E\left\{\sum_{k=M}^{N-1}\sum_{l=0}^{M-1}\sum_{m=M}^{N-1}w_{jik}^4r_{jil}^2w_{jim}^2\right\}\quad.\end{aligned} \tag{C.3}$$

In order to evaluate (C.1), (C.2), and (C.3), the following equations or identities are used:

$$
\begin{aligned}
E\left\{\sum_{k=0}^{M-1}\sum_{l=0}^{M-1}\xi_k^4\xi_l^4\right\} &= \sum_{k=0}^{M-1}\sum_{l=0,k\neq l}^{M-1}E\left\{\xi_k^4\xi_l^4\right\}+\sum_{k=0}^{M-1}E\left\{\xi_k^8\right\} \\
&= \sum_{k=0}^{M-1}\sum_{l=0,k\neq l}^{M-1}E\left\{\xi_k^4\right\}E\left\{\xi_l^4\right\}+\sum_{k=0}^{M-1}E\left\{\xi_k^8\right\} \\
&= \left(9M^2+96M\right)\sigma_\xi^8,
\end{aligned}
\tag{C.4}
$$

$$
\begin{aligned}
E\left\{\sum_{k=0}^{M-1}\sum_{l=0}^{M-1}\sum_{m=0}^{M-1}\xi_k^4\xi_l^2\xi_m^2\right\} &= E\left\{\sum_{k=0}^{M-1}\xi_k^8\right\}+2E\left\{\sum_{l=0}^{M-1}\sum_{m=0,l\neq m}^{M-1}\xi_l^6\xi_m^2\right\} \\
&\quad + E\left\{\sum_{k=0}^{M-1}\sum_{l=0,k\neq l}^{M-1}\xi_k^4\xi_l^4\right\}+E\left\{\sum_{k=0}^{M-1}\sum_{\substack{l=0\\k\neq l}}^{M-1}\sum_{\substack{m=0\\m\neq l\\m\neq k}}^{M-1}\xi_k^4\xi_l^2\xi_m^2\right\} \\
&= \left(3M^3+30M^2+72M\right)\sigma_\xi^8,
\end{aligned}
\tag{C.5}
$$

$$
\begin{aligned}
E\left\{\sum_{k=0}^{M-1}\sum_{l=0}^{M-1}\sum_{m=0}^{M-1}\sum_{n=0}^{M-1}\xi_k^2\xi_l^2\xi_m^2\xi_n^2\right\} &= \sum_{k=0}^{M-1}E\left\{\xi_k^8\right\}+4E\left\{\sum_{k=0}^{M-1}\sum_{\substack{l=0,\\l\neq k}}^{M-1}\xi_k^6\xi_l^2\right\}+3E\left\{\sum_{k=0}^{M-1}\sum_{\substack{l=0,\\l\neq k}}^{M-1}\xi_k^4\xi_l^4\right\} \\
&\quad + 6\sum_{k=0}^{M-1}\sum_{\substack{l=0,\\l\neq k}}^{M-1}\sum_{\substack{m=0\\m\neq l\\m\neq k}}^{M-1}E\left\{\xi_k^2\xi_l^2\xi_m^4\right\}+E\left\{\sum_{k=0}^{M-1}\sum_{\substack{l=0,\\l\neq k}}^{M-1}\sum_{\substack{m=0,\\m\neq l,\\m\neq k}}^{M-1}\sum_{\substack{n=0,\\n\neq k,\\n\neq l,\\n\neq m}}^{M-1}\xi_k^2\xi_l^2\xi_m^2\xi_n^2\right\} \\
&= \left(M^4+12M^3+44M^2+48M\right)\sigma_\xi^8,
\end{aligned}
\tag{C.6}
$$

where $\{\xi_k\}$ are zero-mean independent normal random variables, and $\sigma_\xi^2 = E\left\{\xi_k^2\right\}$ is the variance of ξ_k. Following the identities of (C.4) - (C.6) and Appendix II, the equations of (C.1) - (C.3) can be obtained.

APPENDIX D Proof of Proposition 2

In this appendix, the proposition 2 in section 6.4 is derived.

By substituting the zero-mean Gaussian narrowband random process, $x(t)$, with a PSD in (6.7), to (6.2), the output signal, after the SL device, $y(t)$, can be written by

$$y(t) = x^2(t) * h_2(t), \tag{D.1}$$

where $h_2(t)$ is the impulse response of the cascaded bandpass filter in (6.3).

In frequency domain, the power spectrum density (PSD) of $y(t)$ in (D.1) is given by

$$S_y(f) = |H_2(f)|^2 S_{x^2}(f). \tag{D.2}$$

where $H_2(f)$ is frequency response of bandpass filter $h_2(t)$, and $S_{x^2}(f)$ is the PSD of $x^2(t)$ expressed by

$$\begin{aligned} S_{x^2}(f) &= \left[R_x(0)\right]^2 \delta(f) + S_x(f) * S_x(f) \\ &+ \frac{1}{2} S_x(f) * S_x(f) * \left[\delta\left(f + 2f_c\right) + \delta\left(f - 2f_c\right)\right], \end{aligned} \tag{D.3}$$

where $R_x(0)$ is the value at $\tau = 0$ of the autocorrelation function, $R_x(\tau)$ of $x(t)$ given by

$$R_x(\tau) = E\left[x(t+\tau)x(t)\right] = P\frac{sin(\pi B_x \tau)}{\pi B_x \tau}\cos(2\pi f_c \tau)\ , \tag{D.4}$$

where P, f_c, and B_x are, the power, the center frequency, and the bandwidth of $x(t)$, respectively.

In order to get the output signal $y(t)$ in (D.1), the $H_2(f)$ is rewritten as

$$H_2(f) = \begin{cases} 1, & f_1 \le |f| \le f_2; \\ 0, & \text{others}, \end{cases} \tag{D.5}$$

where f_1 and f_2 are the low and up cut-off frequencies of the filter, respectively.

By substituting (D.5) and (D.3) to (D.2), $S_y(f)$ is obtained by

$$S_y(f) = 0, \text{ if } f_1 > B_x, \text{ and } f_2 < 2f_c - \frac{B_x}{2}. \tag{D.6}$$

It is should be noted that (D.6) can be held as the PSD in (D.3) is located out of the filter in (D.5) once filter parameters $f_1 > B_x$, and $f_2 < 2f_c - \frac{B_x}{2}$ are chosen.

APPENDIX E LIST OF MY PUBLICATIONS

[1] A. Yang, Z. Xu, H. Nie and Z. Chen, "On the Variance-Based Detection for Impulse Radio UWB Systems," *IEEE Transactions on Wireless Communications*, vol. 15, no. 12, pp. 8249-8259, Dec. 2016.

[2] A. Yang, H. Nie, Z. Xu and Z. Chen, "Variance detection for non-coherent impulse radio UWB receivers," *International Conference on Computing, Networking and Communications, Honolulu*, HI, pp. 529-533, 2014.

[3] A. Yang, Z. Xu, H. Nie and Z. Chen, "A unified framework for nonlinear detections of impulse radio UWB systems," *IEEE 25th Annual International Symposium on Personal, Indoor, and Mobile Radio Communication*, Washington DC, pp. 913-917, 2014.

[4] A. Yang, H, Nie, Z. Xu and Z. Chen. "Modified Kurtosis Detector for Impulse Radio UWB Signals," *IEEE Radio and Wireless Symposium*, Austin, TX, pp. 136-138, 2013.

[5] A. Yang, H. Qian, H. Nie, Z. Chen and L. Yu, "A random pulse phase jitter technique for suppression of frequency spikes associated with UWB pulse position modulation," *IEEE International Conference on Ultra-Wideband*, Nanjing, pp. 1-4, 2010.

[6] Z. Xu, A. Yang, Z. David Chen and H. Nie, "Multichannel energy detection UWB receivers based on nonlinear square law technology," *IEEE International Conference on Ubiquitous Wireless Broadband*, Nanjing, pp. 1-4, 2017.

[7] Z. Xu, A. Yang, H. Qian, H. Nie, Z. Chen and L. Yu, "Narrowband interference mitigations capacity of differential code-shifted-reference UWB systems," *IEEE International Conference on Ultra-Wideband*, Nanjing, pp. 1-4, 2010.

[8] Z. Xu, H. Nie, Z. Chen, H. Khani and A. Yang, "Blind narrowband interference mitigation using filter bank for energy detection based UWB receivers," *IEEE Radio and Wireless Symposium*, Austin, TX, 2013, pp. 139-141, 2013.

[9] Z. Xu, H. Qian, A. Yang and L. Yu "Differential Code Shifted Reference UWB Receiver Based on Teager-Kaiser Operator," *Chinese Journal of Sensors and Actuators*, vol. 25, No. 5, pp. 707-711, 2012.

[10] Z. Xu, L. Yu and A. Yang, "Power Spectrum Smoothing Technique for Impulse Ultra-Wideband Based on Phase Jitter," *Journal of Fuzhou University (Natural Science Edition)*, vol. 40, No. 2, pp. 193-197, 2012.

[11] X. Yu, X. Cai, J. Shi, A. Yang and Z. Chen, "A Robust 2D Segmented Digital Predistortion for Dual-Band Power Amplifiers" *IEEE Microwave and Wireless Components Letters*, Aug. 2017, Submitted.

APPENDIX F COPYRIGHT PERMISSIONS

From: Aidong Yang
Sent: August 10, 2017 16:39
To: pubs-permissions@ieee.org
Cc: Zhizhang Chen
Subject: Copyright Permission for Thesis Reuse

Aug. 10th, 2017

IEEE Author Relations and Content Discoverability
IEEE Product Design
445 Hoes Lane
Piscataway, NJ 08854

Dear IEEE,

I am preparing my Ph.D. thesis for submission to the Faculty of Graduate Studies at Dalhousie University, Halifax, Nova Scotia, Canada. I am seeking your permission to include a manuscript version of the following paper(s) as a chapter in the thesis:

[1] A. Yang, Z. Xu, H. Nie and Z. Chen, "On the Variance-Based Detection for Impulse Radio UWB Systems," in IEEE Transactions on Wireless Communications, vol. 15, no. 12, pp. 8249-8259, Dec. 2016.
[2] A. Yang, H. Nie, Z. Xu and Z. Chen, "Variance detection for non-coherent impulse radio UWB receivers," in International Conference on Computing, Networking and Communications, Honolulu, HI, pp. 529-533, 2014.
[3] A. Yang, Z. Xu, H. Nie and Z. Chen, "A unified framework for nonlinear detections of impulse radio UWB systems," in IEEE 25th Annual International Symposium on Personal, Indoor, and Mobile Radio Communication, Washington DC, pp. 913-917, 2014.
[4] A. Yang, H. Nie, Z. Xu and Z. Chen, "Modified kurtosis detection for UWB impulse radios," in IEEE Radio and Wireless Symposium, Austin, TX, pp. 136-138, 2013.
[5] Z. Xu, H. Nie, Z. Chen, H. Khani and L. Yu, "Nonlinear Blind Narrowband Interference Mitigation for Energy Detection Based UWB Receivers," in IEEE Communications Letters, vol. 16, no. 10, pp. 1596-1599, October 2012.
[6] Z. Xu, A. Yang, Z. David Chen and H. Nie, "Multichannel energy detection UWB receivers based on nonlinear square law technology," in IEEE International Conference on Ubiquitous Wireless Broadband, Nanjing, pp. 1-4, 2016.

Canadian graduate theses are reproduced by the Library and Archives of Canada (formerly National Library of Canada) through a non-exclusive, world-wide license to reproduce, loan, distribute, or sell theses. I am also seeking your permission for the material described above to be reproduced and distributed by the LAC(NLC). Further details about the LAC(NLC) thesis program are available on the LAC(NLC) website (www.nlc-bnc.ca).

Full publication details and a copy of this permission letter will be included in the thesis.

Yours sincerely,
Aidong Yang

Aidong Yang, Ph.D. Candidate
Electrical and Computer Engineering
Faculty of Engineering, Dalhousie University
Email: aidong.yang@dal.ca

From: Pubs Permissions
Sent: August 10, 2017 16:39
To: Aidong Yang
Subject: Re: Copyright Permission for Thesis Reuse

Permission to reuse IEEE content, including use in a thesis or dissertation must be done through the Copyright Clearance Center's RightsLink service, using IEEE Xplore.

1. Please locate the content beginning at http://ieeexplore.ieee.org/Xplore/home.jsp

2. Once on the abstract page of the article, please locate the "Request Permission" link in the left navigation panel

3. You can also find the copyright symbol directly on the article Table of Content

4. If you find there are none of these links, you should open the free front pages of the content to determine if there is another rights holder, as this is an indication IEEE is not the intellectual property rights holder, and we cannot grant permission for reuse

5. If the links are there, please do choose one of them and this will take you to the permission application page

If you do experience difficulty. please contact customer service at customercare@copyright.com or M.E. Brennan at me.brennan@ieee.org.

From: Krista Thom
Sent: August 11, 2017 09:46
To: Aidong Yang
Cc: pubs-permissions@ieee.org; Zhizhang Chen
Subject: Re: Copyright Permission for Thesis Reuse

Dear Mr. Yang,

The IEEE does not require individuals working on a thesis to obtain a formal reuse license however, you must follow the requirements listed below:

Textual Material

Using short quotes or referring to the work within these papers, users must give full credit to the original source (author, paper, publication) followed by the IEEE copyright line **© [Year of publication] IEEE.**

In the case of illustrations or tabular material, we require that the copyright line **© [Year of original publication] IEEE** appear prominently with each reprinted figure and/or table.

If a substantial portion of the original paper is to be used, and if you are not the senior author, you must also obtain the senior author's approval.

Full-Text Article

If you are using the entire IEEE copyright owned article, the following IEEE copyright/credit notice should be placed prominently in the references: **© [year of original publication] IEEE. Reprinted, with permission, from [author names, paper title, IEEE publication title, and month/year of publication]**

Only the *accepted* version of an IEEE copyrighted paper can be used when posting the paper or your thesis on-line. *You may not use the final published version.*

In placing the thesis on the author's university website, please display the following message in a prominent place on the website: **In reference to IEEE copyrighted material which is used with permission in this thesis, the IEEE does not endorse any of [university/educational entity's name goes here]'s products or services. Internal or personal use of this material is permitted. If interested in reprinting/republishing IEEE copyrighted material for advertising or promotional purposes or for creating new collective works for resale or redistribution, please go to http://www.ieee.org/publications_standards/publications/rights/rights_link.html to learn how to obtain a License from RightsLink.**

Cheers,

Krista